Matter Wave Optical Techniques for Probing Many-body Targets

by

Scott Nicholas Sanders

A.B., Chemistry and Physics
Harvard University, 2001

Submitted to the Department of Physics
in partial fulfillment of the requirements for the degree of

Doctor of Philosophy in Physics

at the

MASSACHUSETTS INSTITUTE OF TECHNOLOGY

February 2010

Author .....
Department of Physics
January 23, 2010

Certified by .....
Eric J. Heller
Professor
Thesis Supervisor

Certified by .....
David E. Pritchard
Professor
Thesis Supervisor

Accepted by .....
Thomas Greytak
Chairman, Department Committee on Graduate Theses

to my family

Matter Wave Optical Techniques for Probing Many-body Targets

by

Scott Nicholas Sanders

Submitted to the Department of Physics
on January 23, 2010, in partial fulfillment of the
requirements for the degree of
Doctor of Philosophy in Physics

Abstract

This thesis reports on our investigation of the uses of matter waves to probe many-body targets. We begin by discussing decoherence in an atom interferometer, in which a free gas acts as a refractive medium for a matter wave. The correlations that develop between the probe and the gas reduce the contrast of the interference pattern that forms when the arms of the interferometer recombine. This is due to the availability of partial which-way information left in the disturbed state of the gas. We show that the coherent part of the probe is completely unscattered, though it is phase shifted. This recoil free process leaves both the probe atom and the gas in an unchanged state, but allows for the acquisition of a phase shift. Our work elucidates the actual microscopic, many-body, quantum mechanical scattering mechanism that determines the phase shift and the decoherence of a matter wave passing through a free gas.

In the second part of this thesis, we turn our attention to another complex, many-body system, comprised of ultracold atoms in an optical lattice. We investigate non-destructive techniques for probing the superfluid to Mott insulator transition by studying the scattering cross section of the cold atoms for matter waves. We show that the angular cross section of the target lattice for a matter wave depends strongly on the many-body phase of the atoms in the lattice. Finally, we discuss an interferometric technique for probing the local number fluctuations of atoms in the lattice.

Thesis Supervisor: Eric J. Heller
Title: Professor

Thesis Supervisor: David E. Pritchard
Title: Professor

Acknowledgements

I thank Prof. Heller for his guidance and insight in helping me to bring this thesis to fruition. Working with Rick has been an inspiration, and I have enjoyed learning from his patient instruction. I am also grateful to my colleagues in the Heller group for their discussions and our time together, and to Ms. Judy Morrison for her faithful and caring support in making my time with the Heller group a logistical reality.

I am especially indebted to Dr. Florian Mintert for his tireless assistance and support, which was essential to this project. I have enjoyed collaborating with him over the past years, and more importantly, I have enjoyed his friendship.

Finally, I am thankful to my parents and my brother for their love and the encouragement to pursue my dreams.

Contents

1 Introduction **17**

2 Multiple Scattering from a Free Gas **23**

2.1 Introduction 23

2.2 Review of Free Space Scattering 23

2.2.1 Lippmann-Schwinger Equation 23

2.2.2 The T-matrix and the Born approximation 24

2.2.3 Free Space Time Independent Green's Function 26

2.2.4 Scattering Amplitude and the T-matrix 29

2.2.5 Real and Imaginary parts of G_0^+ 31

2.2.6 S-Matrix Formalism 32

2.2.7 Time dependent derivation of S-matrix 36

2.3 Scattering from a Pseudopotential 38

2.3.1 Regularized Green's Function Method 39

2.3.2 T-matrix for a Delta Potential 41

2.4 Multiple Scattering 42

2.4.1 Fermi treatment of index of refraction 42

2.4.2 Lax Multiple Scattering and the Coherent Wave Equation 43

2.4.3 Expansion of Multiple Scattering in Number of Target Interactions . 47

3 Matter Wave Interferometry **53**

3.1 Mach-Zender Interferometer 53

3.1.1 Configuration of the Interferometer 53

3.1.2 Decoherence in an Interferometer 54

3.2 Decoherence due to a Free Gas 58

3.2.1 Introduction to the Free Gas as a Decohering Environment 58
3.2.2 Paradox of Free Space Scattering without Decoherence 60
3.2.3 Multiple Scattering Due to a Free Gas 62
3.2.4 Calculation of the S-matrix 66
3.2.5 Approximation of the Many-body T-Matrix 68
3.2.6 Dependence of the Phase Shift and Decoherence on the Interaction Potential Strength 72
3.2.7 Low Energy Projectile: Pseudopotential 73

4 Ultracold atoms in an Optical Lattice 77

4.1 Physics of the Optical Lattice 77
4.1.1 AC Stark Shift and the Lattice Potential 77
4.2 Solutions of the Schrödinger Equation in the Optical Lattice 81
4.2.1 Bloch Waves: Single Particle Eigenstates of the Lattice 81
4.2.2 Wannier Functions: States at a Particular Lattice Site 83
4.2.3 Exact Eigenfunctions of the Optical Lattice Hamiltonian 84
4.2.4 Approximations of the Exact Optical Lattice Eigenfunctions 87
4.3 Bose Hubbard Model 90
4.4 Quantum Many-body Phases in the Optical Lattice 92
4.4.1 Superfluid Phase 92
4.4.2 Mott insulator Phase 94
4.4.3 Superfluid Fraction 95
4.4.4 Condensate Fraction 98

5 Probing an Optical Lattice with Matter Wave Scattering and Interferometry 101

5.1 Scattering from a Single Target 101
5.2 Single Target Cross Section: Limiting Cases of Low and High Probe Energy 103
5.3 Single Target Cross Section: Arbitrary Probe Energy 106
5.4 The Van Hove Formalism and Multiple Scattering 112
5.5 Scattering Cross Section of a BEC in an Optical Lattice 116
5.6 Scattering from the Superfluid: High Probe Energy 119
5.6.1 Exact Ground State 119

5.6.2 Coherent State 122
5.7 Inelastic Scattering Cross Sections at Arbitrary Probe Energy 123
5.7.1 Superfluid 124
5.7.2 Mott Insulator 129
5.7.3 Transition Between Superfluid and Mott Insulator 130
5.8 Interference of Focused Beams Scattered from an Optical Lattice 132

List of Figures

3-1 A Mach-Zender atom interferometer. Equally spaced diffraction gratings create two separated arms. The recombination of the arms at the position of the screen leads to an interference pattern. The frequency of the interference fringes is determined by the grating spacing. If the arms of the interferometer experience different interactions, the difference in the accumulated quantum mechanical phase shift in the two arms appears as a shift in the phase of the interference fringes. 54

3-2 The second grating in the Mach-Zender interferometer. The separated paths of the probe wave function are depicted by dashed gray lines. The upper arm interacts with a detector, which evolves due to interactions with the probe. The lower arm is the first-order diffracted beam from the grating. An interference pattern forms at the position of the screen. 55

3-3 A Mach-Zender interferometer with the gas cell serving as a which-way detector. The atom beam is coherently split into the two arms of the interferometer by the leftmost diffraction grating. The initial state of the gas is $|D\rangle$, which evolves into $|D_1\rangle$ or $|D_2\rangle$ depending on whether an atom from the beam passes through the cell. An interference pattern forms on the screen at right where the arms overlap. 63

3-4 Details of the gas cell appearing in Fig. 3-3. The cell has length, l, and is embedded in a waveguide. The j^{th} slab, running from $z = (j-1)w$ to $z = jw$, is illustrated. The waveguide in which the projectile is confined is an infinite tube with a square cross section of dimensions, $a \times a$. 65

4-1 Model of a two level atom with resonance frequency, ω_0, interacting with a light field of frequency, ω_L. The Rabi frequency, proportional to the intensity of the light, is Ω, and the detuning is Δ. Here we have shown the case in which the light is red detuned from the resonance ($\Delta < 0$), which causes the atom to be attracted to the anti-nodes of the laser. 80

4-2 Band diagrams for the optical lattice. The energy of the Bloch waves in the first Brillouin zone are shown for the first few bands of the lattice as a function of the quasimomentum for lattice depths, $V_0 = 0, 5, 10,$ and, 15. The black dots in the lowest band indicate the discrete quasimomenta permitted by the Born von-Karman boundary conditions for a lattice with $N_L = 8$ sites. The light gray line shows the lattice depth. 85

4-3 (a)-(c) Bloch waves at quasimomenta, $k = 0, k_L/2,$ and k_L in a lattice of depth, $V_0 = 5E_r$. (d) Profiles of the Bloch wave amplitude squared for the corresponding choices of the quasimomentum. 86

4-4 The Wannier function of the lowest band for lattice depths, $V_0 = 2E_r, 5E_r, 10E_r,$ and $15E_r$. A scaled plot of the optical lattice is shown in light gray. For shallow lattices, the Wannier function has pronounced lobes. At a depth, $V_0 = 15E_r$, the Wannier function closely resembles the Gaussian ground state of a harmonic well. 87

4-5 The Wannier function for the lowest band of the lattice (blue) and the ground state of the Harmonic approximation (red) are shown for a lattice with 8 sites and depths of $2E_r$ and $15E_r$. 88

4-6 The Bloch wave for the $q = -3k_L/4$ mode of the lowest band of the lattice (blue) plotted alongside the reconstruction using the Gaussian approximation of the Wannier function. The wave functions are determined for a lattice with 8 sites and a depth, $V_0/E_r = 15$. 89

5-1 The lowest four energy bands of the optical lattice. The flat line is the depth of the lattice. The dots on the lowest band are the acceptable modes for a lattice with 8 sites and periodic boundary conditions. All quantities on the y-axis are in units of the recoil energy. The band structure is for a lattice of depth $5E_r$. 107

5-2 The band width of the lowest band divided by the gap to the first band. As the lattice becomes deeper, the lowest band flattens, and the band width becomes smaller. At the same time, the gap to the first excited band widens. 108

5-3 This plot shows the weight of the contribution to the cross section of each quasimomentum in the lowest band of a lattice of depth $V_0 = 15E_r$. Two different incident probe energies are shown. An incident probe with one-fifth the energy of the lowest band width (red) can only excite the lowest three modes. A probe with ten times the energy of the lowest band width (blue) excites all of the modes with nearly equal weights. 108

5-4 Diagram of the scattering configuration. The one-dimensional optical lattice, with a single target atom, is arranged perpendicular to the incident probe wave vector. A detector is placed in the far-field to measure the scattering cross section at the angle, θ. 109

5-5 The probabilities of scattering into several modes (q/k_L) of the lattice ($V_0 = 15E_r$) are shown as a function of the momentum transferred to the lattice, κ_x. The probability is peaked when the momentum transferred to the lattice equals the quasimomentum of the specified mode, or is separated from it by a reciprocal lattice vector. The energy diagram of the lowest band of the lattice is superimposed on the probability to indicate the location of the modes. . 110

5-6 All of the conditional scattering probabilities for a lattice of depth $V_0 = 15E_r$ are plotted together. Summing these would give the cross section due to uniform weighting of the possible inelastic scattering channels. The envelope apparent in this plot indicates the overall shape of the cross section in that case. 111

5-7 The total inelastic scattering cross section, $\frac{1}{a_s^2}\frac{d\sigma}{d\Omega}(\theta)$, for a single particle in a lattice of depth $V_0 = 15E_r$. The cross section is shown for several incident probe energies, specified in units of the band width of the lattice. 112

5-8 The analytic results for the superfluid (light gray) and Mott insulator (dark gray) differential cross sections for a sample lattice in 1D with 15 atoms and 15 sites. These are shown on a log scale in order to draw attention to the absence of inelastic scattering from the Mott insulator. The cross section is for a probe with energy $6E_r$ and a lattice depth of $V_o/E_r = 15$. 128

5-9 Diagram of the scattering configuration. The one-dimensional optical lattice, with N_L sites and N atoms, is arranged perpendicular to the incident probe wave vector. A detector is placed in the far-field to measure the scattering cross section at the angle, θ. 128

5-10 Cross sections for a probe with initial energy $(\hbar k_o)^2/(2m) = E_r$, a lattice of depth $V_o = 15E_r$, with 4 atoms and 4 sites, and $J = 0.002$. The values of U/J shown are: 0, 4, 8, and 16. The superfluid inelastic background $(U/J = 0)$ scales as N. The analytic result for the Mott insulator $(U/J \to \infty)$ background (filled in dark gray) is strongly suppressed. The inset shows the numerical cross section at the vertical dashed line as a function of U/J. . . 131

5-11 Diagram of the interference configuration. The probe matter wave is coherently split into two arms. The individual arms strike a one-dimensional lattice at the positions indicated. Downstream of the lattice, the arms overlap, and an interference pattern is formed. 132

Chapter 1

Introduction

Decoherence in an atom interferometer

An atom interferometer exploits the ability of an atom to exist in a superposition of states. An atomic wave function can be spatially separated into two wave packets and made to travel along different paths. When the packets recombine, interference fringes can be observed in the spatial position of the atom. The relative quantum phase that develops between the two arms of the interferometer is imprinted in the interference pattern as a shift of the fringes. In this way, the interferometer reveals a record of the different interactions experienced along the separate paths. This behavior has been harnessed experimentally to demonstrate that a gas of atoms can act as a refractive medium for a matter wave [1], much the same as a piece of glass refracts a light wave.

Long before the advent of atom interferometers, Enrico Fermi argued that a slow neutron passing through a medium of scattering centers would be refracted and acquire a phase shift [2]. In fact, multiple scattering theory has shown that even a discrete collection of randomly distributed scattering centers can act as a refractive medium for a matter wave [3], as in refraction of an atom by a free gas. Placing a free gas in only one arm of an interferometer causes a differential phase shift of the atomic matter wave between the separated wave packets and permits measurement of the index of refraction of the gas for a matter wave. In analyzing interference, however, we are naturally led to ask, what is the effect of the atom on the free gas? Complementarity requires that the free gas not retain any record of its interaction with the probe. The deflection of even a single gas atom would constitute which-path information, and ought to eliminate the possibility of interference.

In this thesis, I present a microscopic analysis of the many-body scattering problem, which takes into account the quantum mechanical degrees of freedom of the targets, in order to treat the decoherence in an atom interferometer due to interactions with a free gas. We have shown the mechanism by which an atom can interact strongly enough with a gas of atoms to acquire a phase shift that is large compared to π, and yet with high probability leave the state of the free gas entirely untouched.

Non-destructive probe of the quantum many-body phase in an optical lattice

In the second part of this thesis, we extend our investigation of matter wave probes and consider what we can learn about a complex, many-body target through atom scattering and interferometry. We turn our attention to the scattering of matter waves from cold atoms in an optical lattice. A Bose Einstein condensate (BEC) of neutral atoms can be made to feel a periodic lattice potential due to the AC Stark shift of a far off-resonant standing wave of light. The atoms of the BEC in the optical lattice were shown to be very well-described by the Bose-Hubbard model, in which repulsively interacting bosons hop between the sites of the lattice [4].

The Bose-Hubbard Hamiltonian exhibits a quantum phase transition that depends on the relative strength of its kinetic and interaction terms. Weakly interacting atoms will delocalize and occupy the single-particle ground state of the lattice. This many-body state is a pure superfluid that exhibits long-range off-diagonal order in the single-particle density matrix. When the repulsive interactions dominate, the atoms are forced to retreat into separate wells of the lattice and find a new ground state in which each atom is localized at a site. There is an energy cost equal to the interaction strength associated with shifting an atom from site to site in this state. A corresponding gap opens in the many-body spectrum of this so-called Mott insulator phase. Experimental observations of the quantum phase of atoms in a lattice have been made by taking time of flight images. Here, the atoms are released from both trapping and lattice potentials, and allowed to expand ballistically, prior to being imaged with light [5]. The correlation properties of the ground state are evident in the interference patterns that form, and the system is necessarily destroyed in the process.

We have determined the scattering cross sections of the degenerate Bose gas in an optical

lattice in the weakly and strongly interacting regimes. Each target can be treated as an s-wave scatterer, in which the scattered probe wave function is a spherical wave, so that the features in the scattering cross section are due to the structure of the target. Inelastic scattering of the probe depends on the many-body target spectrum, and the cross sections we determine display unambiguous indicators of the quantum phase, without requiring the destruction of the lattice. Numerical calculations of the cross section were performed for the intermediate points in the phase transition. We also show that interference of matter waves focused at different points in the lattice depend on density correlations, which are well-known indicators of the many-body phase.

Overview

- The second chapter lays the groundwork of the scattering formalism that we will employ extensively and extend in the following chapters. The logic of the progression is to being with the simplest situation, scattering from a potential, and deal subsequently with multiple scattering from a collection of potential centers.

- The third chapter introduces the problem of decoherence in an atom interferometer. We treat decoherence due to the presence of a free gas from microscopic analysis of the multiple scattering problem, introducing the degrees of freedom of the gas in order to determine the effect of correlations between the probe and the gas environment on the visibility of interference fringes.

- The fourth chapter begins the second part of the thesis, in which we redirect our attention to the uses of matter waves to probe the quantum phase transition between a superfluid and a Mott insulator. This chapter introduces the physics of cold atoms in an optical lattice, including the origin of the lattice potential, the Bose Hubbard model and the properties of the superfluid and Mott insulator phases.

- The fifth chapter deals in detail with scattering from atoms in an optical lattice. First, we consider scattering from single-particle states in the lattice before moving to the many-body case. We show that there is a clear dependence of the cross section on the quantum phase in the lattice. Finally we examine the interference of multiple coherent beams after scattering from the atoms in the lattice and show that the interference

patterns depend on the target's correlation properties.

Publications of the PhD work

- *Coherent scattering from a free gas.*

  S.N. Sanders, F. Mintert and E.J. Heller,

  Physical Review A **79**, 023610, (2009).

- *Matter Wave Scattering from Ultracold Atoms in an Optical Lattice.*

  S.N. Sanders, F. Mintert and E.J. Heller,

  Submitted for publication; preprint available at **cond-mat/0910.1873**.

Chapter 2

Multiple Scattering from a Free Gas

2.1 Introduction

2.2 Review of Free Space Scattering

2.2.1 Lippmann-Schwinger Equation

We will make extensive use of formal scattering theory in treating the interaction of a probe particle with a target comprised of many individual particles. Here we begin by reviewing the fundamentals of formal scattering theory. At the most basic level, the scattering problem can be treated as a time independent eigenvalue equation [6]. We will subsequently return to this problem beginning from the time dependent Schrödinger equation to confirm more rigorously the result we obtain here.

We assume that we know a solution, $|\phi\rangle$, to the time independent Schrödinger equation,

$$H_0 |\phi\rangle = E |\phi\rangle . \tag{2.1}$$

We would like to find a solution of the same energy to the Schrödinger equation in which a scattering potential, V, is present,

$$(H_0 + V) |\psi\rangle = E |\psi\rangle . \tag{2.2}$$

$|\psi\rangle$ is the state of the quantum mechanical particle due to scattering from the potential, V. It is illuminating to reorganize the terms in these equations so that the scattering potential appears as a source,

$$(E - H_0)\,|\phi\rangle = 0 \tag{2.3}$$

$$(E - H_0)\,|\psi\rangle = V\,|\psi\rangle\,. \tag{2.4}$$

The eigenvalue equation for the scattering state, $|\psi\rangle$, may be formally solved by dividing by the operator, $(E - H_0)$. That is to say, we are acting on both sides of the equation with the inverse of $(E - H_0)$. This inversion introduces the possibility of singular situations in which we have zero in the denominator. We will address this situation and the implications it has for the scattering solution below. The formal solution is

$$|\psi\rangle = \frac{1}{E - H_0} V\,|\psi\rangle\,. \tag{2.5}$$

It is immediately apparent that any solution of $(E - H_0)\,|\phi\rangle = 0$ can be added to $|\psi\rangle$, and the result will also be a solution of Eq. (2.4).

$$|\psi\rangle = |\phi\rangle + \frac{1}{E - H_0} V\,|\psi\rangle\,. \tag{2.6}$$

This we can see by acting on both sides with the operator $(E - H_0)$. $|\phi\rangle$ can be any eigenstate of the unperturbed Hamiltonian, H_0, which has energy, E. Within that degenerate subspace of the Hilbert space of H_0, the choice is arbitrary. In the context of a scattering interaction, however, our choice is constrained by the need to match the solution when there is no scatterer present ($V = 0$). We then require that the scattered state, $|\psi\rangle$, be the same as the unscattered incident state, $|\phi\rangle$. The choice of $|\phi\rangle$ is somewhat like a boundary condition, and we take $|\phi\rangle$ to represent the initial state of the particle before scattering. The solution for the scattered state in Eq. (2.6) is known as the Lippmann-Schwinger equation, and is the foundation of time independent scattering theory.

2.2.2 The T-matrix and the Born approximation

The form of the Lippmann-Schwinger equation presents a difficulty, as the quantity for which we wish to solve appears on both sides of the equation. We may address this formally by

introducing a new operator, T, which we define such that

$$V\left|\psi\right\rangle = T\left|\phi\right\rangle. \tag{2.7}$$

It follows by inserting the expression for $|\psi\rangle$ on the left that we must also have the operator relationship,

$$T = V + V\frac{1}{E - H_0}T. \tag{2.8}$$

This operator equation is equivalent to the Lippmann-Schwinger equation. Solving for T immediately solves the scattering problem for $|\psi\rangle$. When we represent T in the eigenbasis of the unperturbed Hamiltonian, H_0, we refer to it as the T-matrix.

Either the Lippmann-Schwinger equation or Eq. (2.8) may be used to develop expansions of the scattered state in orders of the interaction potential, V. Consider the result of substituting the solution of $|\psi\rangle$ or T recursively into the right hand side of these expressions. To simplify the notation for the expressions we obtain, we name the Green's operator, G_0,

$$G_0 = \frac{1}{E - H_0}. \tag{2.9}$$

Then we obtain

$$\left|\psi\right\rangle = \sum_{n=0}^{\infty}\left(G_0V\right)^n\left|\phi\right\rangle, \tag{2.10}$$

or equivalently,

$$T = V\sum_{n=0}^{\infty}\left(G_0V\right)^n. \tag{2.11}$$

Truncating the series at $n = 1$ gives the so-called first Born approximation,

$$\left|\psi\right\rangle \approx \left|\phi\right\rangle + G_0V\left|\phi\right\rangle, \tag{2.12}$$

$$T \approx V. \tag{2.13}$$

The Born approximation will be useful to us later when we wish to consider cases of a weakly interacting projectile and target.

2.2.3 Free Space Time Independent Green's Function

In order to evaluate any scattering solutions, it is imperative that we first determine the form of the operator, G_0, in some representation. We are usually interested in the spatial wave function of a scattered particle, $\langle \boldsymbol{r}|\psi\rangle = \psi(\boldsymbol{r})$. Also, the potentials we will treat are invariably diagonal in position space, so that $V\left|\boldsymbol{r}\right\rangle = V(\boldsymbol{r})\left|\boldsymbol{r}\right\rangle$. It is convenient therefore to expand the Lippmann-Schwinger equation as

$$\psi(\boldsymbol{r}) = \phi(\boldsymbol{r}) + \int d^3r' \ \langle \boldsymbol{r}|\, G_0 \left|\boldsymbol{r}'\right\rangle V(\boldsymbol{r}')\psi(\boldsymbol{r}'), \tag{2.14}$$

where the integral is to be taken over all space. The matrix element of the operator G_0 that appears in the integral is the free space, time independent Green's function,

$$G_0(\boldsymbol{r},\boldsymbol{r}';E) = \langle \boldsymbol{r}|\, G_0 \left|\boldsymbol{r}'\right\rangle = \langle \boldsymbol{r}|\, \frac{1}{E-H_0}\left|\boldsymbol{r}'\right\rangle. \tag{2.15}$$

In order to avoid the possibility of a zero in the denominator, we will add a small imaginary term to the denominator.

$$G_0^{\pm} = \lim_{\varepsilon\to 0} \frac{1}{E - H_0 \pm i\varepsilon} \tag{2.16}$$

The effect of the sign of this additional term on the form of the Green's function is non-trivial, however the physical constraints of the scattering process will provide a ready interpretation of the meaning of the sign on ε. Let us proceed for now, and return to this when we have determined the functional form of the Green's function. We can evaluate this quantity by inserting a complete set of plane wave states that are designated by a wave vector, $|\boldsymbol{k}\rangle$, such that

$$\langle \boldsymbol{r}|\boldsymbol{k}\rangle = \frac{1}{(2\pi)^{3/2}} e^{i\boldsymbol{k}\cdot\boldsymbol{r}}. \tag{2.17}$$

Let us work this out for the G_0^+ case,

$$G_0^+(\boldsymbol{r},\boldsymbol{r}';E) = \int d^3k' \ \langle \boldsymbol{r}|\boldsymbol{k}'\rangle \langle \boldsymbol{k}'| \ \frac{1}{E-H_0+i\varepsilon}\left|\boldsymbol{r}'\right\rangle \tag{2.18}$$

$$= \frac{1}{(2\pi)^3}\int d^3k' \ \frac{e^{i\boldsymbol{k}'\cdot(\boldsymbol{r}-\boldsymbol{r}')}}{E-\hbar^2k'^2/(2m)+i\varepsilon} \tag{2.19}$$

Arranging the axes of the $\boldsymbol{k}'$ coordinate system so that $\boldsymbol{k}' \cdot (\boldsymbol{r} - \boldsymbol{r}') = k' \, |\boldsymbol{r} - \boldsymbol{r}'| \cos(\theta)$ allows us to perform the angular integrals,

$$G_0^+(\boldsymbol{r}, \boldsymbol{r}'; E) = \frac{1}{(2\pi)^2} \int_0^\infty dk' \, k'^2 \frac{1}{ik' \, |\boldsymbol{r} - \boldsymbol{r}'|} \frac{e^{ik'|\boldsymbol{r}-\boldsymbol{r}'|} - e^{-ik'|\boldsymbol{r}-\boldsymbol{r}'|}}{E - \hbar^2 k'^2/(2m) + i\varepsilon} \tag{2.20}$$

Notice that the integrand is an even function in k', so that an additional factor of one-half allows us to extend the integration from $-\infty$ to $+\infty$. It is most convenient to divide the integral into two terms and perform each separately.

$$G_0^+(\boldsymbol{r}, \boldsymbol{r}'; E) = \frac{-i}{8\pi^2} \frac{1}{|\boldsymbol{r} - \boldsymbol{r}'|} \left(I_1 - I_2 \right), \tag{2.21}$$

where

$$I_1 = \int_{-\infty}^{+\infty} dk' \, k' \frac{e^{ik'|\boldsymbol{r}-\boldsymbol{r}'|}}{E - \frac{\hbar^2 k'^2}{2m} + i\varepsilon} \tag{2.22}$$

$$I_2 = \int_{-\infty}^{+\infty} dk' \, k' \frac{e^{-ik'|\boldsymbol{r}-\boldsymbol{r}'|}}{E - \frac{\hbar^2 k'^2}{2m} + i\varepsilon} \tag{2.23}$$

$$\tag{2.24}$$

These integrals can be performed by extending the integral into the complex plane. The appropriate contour for I_1 should be closed in the upper half-plane, and the contour for I_2 should be closed in the lower half-plane. Let us introduce the wave number, k, corresponding to the energy of the scattered particle,

$$E = \frac{\hbar^2 k^2}{2m}. \tag{2.25}$$

There are two singular points in these integrals, at

$$k' = \pm \sqrt{k^2 + i \frac{2m\varepsilon}{\hbar^2}}. \tag{2.26}$$

The positive value is a point lying in the upper half-plane. The negative value lies in the lower half-plane. In converting I_1 to a contour integral, we need only find the residue at $k' = +\sqrt{k^2 + i\frac{2m\varepsilon}{\hbar^2}}$. This we do by multiplying by $k' - \sqrt{k^2 + i\frac{2m\varepsilon}{\hbar^2}}$ and then setting $k' = +k$. Note that after we have determined the residue, we could allow ε to go to zero in the resulting expression. The value of the contour integral, which is equal to the value of

I_1, is then given by the residue theorem as

$$I_1 = \frac{-2\pi i m}{\hbar^2} e^{ik|\boldsymbol{r}-\boldsymbol{r}'|}. \tag{2.27}$$

I_2 can be found in a similar way, closing the the contour in the lower half-plane. The only singular point in this contour lies at $k' = -\sqrt{k^2 + i\frac{2m\varepsilon}{\hbar^2}}$. We can find the residue in the same fashion as we did above, giving as a result for the contour integral, and hence, I_2,

$$I_2 = \frac{2\pi i m}{\hbar^2} e^{ik|\boldsymbol{r}-\boldsymbol{r}'|}. \tag{2.28}$$

Putting these parts together in Eq. (2.21) gives us our result for the free space Green's function,

$$G(\boldsymbol{r}, \boldsymbol{r}'; E) = \frac{-m}{2\pi\hbar^2} \frac{e^{ik|\boldsymbol{r}-\boldsymbol{r}'|}}{|\boldsymbol{r} - \boldsymbol{r}'|}. \tag{2.29}$$

With this choice of sign on $i\varepsilon$, the Green's function is an outgoing spherical wave, emanating from the point, $\boldsymbol{r}'$. This solution is appropriate for scattering, in which we have an incoming plane wave and an outgoing scattered wave. Had we chosen $-i\varepsilon$, we would have found an incoming spherical wave.

Inserting the Green's function into Eq. (2.14) shows that the scattered wave is comprised of the incident wave plus a spherical wave emanating from every point in space, weighted by the strength of the potential and the amplitude of the scattered wave itself at that point. This is more easily understood in the Born approximation, in which we replace $\psi(\boldsymbol{r}')$, the total scattering solution, with $\phi(\boldsymbol{r}')$, the unscattered, incident wave, in the integrand on the left-hand side of Eq. (2.14). Then we see that the amplitude of the incident wave and the strength of the interaction at the point, $\boldsymbol{r}'$, determine the weight of the spherical wave emanating from that point. What we have discarded in making the Born approximation is the possibility that the spherical wave scattered at one point is subsequently scattered at another point. One could imagine a process in which the scattered wave is self-consistently solved by realizing that the incident wave being scattered at a particular point is actually comprised of the incoming wave plus the scattering from all other points in space. This approach is formalized in the Foldy-Lax method [3, 7] when dealing with multiple scattering centers, which we discuss in Sec. 2.4.2.

2.2.4 Scattering Amplitude and the T-matrix

Let us substitute the Green's function in Eq. (2.29) into Eq. (2.14) for the wave function of the scattered particle,

$$\psi(\boldsymbol{r}) = \phi(\boldsymbol{r}) + \frac{-m}{2\pi\hbar^2}\int d^3r'\,\frac{e^{ik|\boldsymbol{r}-\boldsymbol{r}'|}}{|\boldsymbol{r}-\boldsymbol{r}'|}V(\boldsymbol{r}')\psi(\boldsymbol{r}'). \tag{2.30}$$

This is an exact expression for the scattered wave function due to the potential $V(\boldsymbol{r}')$. We will occasionally use some simplifications of this expression. In the first Born approximation, we may replace $\psi(\boldsymbol{r}')$ on the right-hand side with the incident wave, $\phi(\boldsymbol{r}')$. Furthermore, note that the values of $\boldsymbol{r}'$ that contribute to the integral are those for which the potential is non-negligible, whereas $\boldsymbol{r}$ is the position at which an observation of the scattered wave is to be made. We will invariably be interested in far field scattering, in which the width of the potential is small compared to the distance to the observation point. That condition allows us to expand the integrand under the assumption that $|\boldsymbol{r}'| \ll |\boldsymbol{r}|$. Expanding the Green's function in this situation gives,

$$G(\boldsymbol{r},\boldsymbol{r}';E) = \frac{-m}{2\pi\hbar^2}\frac{e^{ik|\boldsymbol{r}-\boldsymbol{r}'|}}{|\boldsymbol{r}-\boldsymbol{r}'|} \approx \frac{-m}{2\pi\hbar^2}\frac{e^{ikr}}{r}e^{-i\boldsymbol{k}'\cdot\boldsymbol{r}'}, \tag{2.31}$$

where $\boldsymbol{k}' = k\hat{r}$. In the first Born approximation in the far field, the scattered wave function takes the form,

$$\psi(\boldsymbol{r}) = \phi(\boldsymbol{r}) - \frac{m}{2\pi\hbar^2}\frac{e^{ikr}}{r}\int d^3r'\,e^{-i\boldsymbol{k}'\cdot\boldsymbol{r}'}V(\boldsymbol{r}')\phi(\boldsymbol{r}'). \tag{2.32}$$

The scattering solution consists of the unscattered incident wave, plus a scattered part, which is an outgoing spherical wave with angular modulation that depends on the integral in the second term. Had we chosen the opposite sign for the small imaginary part, $i\varepsilon$, that we added to the denominator of the Green's function in Eq. (2.15), we would have found instead an incoming spherical wave. Had we not made any changes to the denominator, we would have recovered both an incoming and an outgoing spherical wave. While those solutions are mathematically acceptable, scattering dictates that only the outgoing spherical wave is physically relevant. An eigenstate of the free particle Hamiltonian is a plane wave, which we may use as the incident particle wave function,

$$\phi(\boldsymbol{r}) = \frac{1}{(2\pi)^{3/2}}e^{i\boldsymbol{k}\cdot\boldsymbol{r}}. \tag{2.33}$$

The scattered wave function then becomes

$$\psi(\boldsymbol{r}) = \frac{1}{(2\pi)^{3/2}} \left(e^{i\boldsymbol{k}\cdot\boldsymbol{r}} - \frac{m}{2\pi\hbar^2} \frac{e^{ikr}}{r} \int d^3r' \, e^{i(\boldsymbol{k}-\boldsymbol{k}')\cdot\boldsymbol{r}'} V(\boldsymbol{r}') \right). \tag{2.34}$$

In this approximation, the scattered wave takes the form of the typical phenomenological ansatz [8],

$$\psi(\boldsymbol{r}) = \frac{1}{(2\pi)^{3/2}} \left(e^{i\boldsymbol{k}\cdot\boldsymbol{r}} + f(\boldsymbol{k} \to \boldsymbol{k}') \frac{e^{ikr}}{r} \right), \tag{2.35}$$

where $f(\boldsymbol{k} \to \boldsymbol{k}')$ is the scattering amplitude. Due to energy conservation, $|\boldsymbol{k}'| = |\boldsymbol{k}|$, and the scattering amplitude depends only on the angle of scattering. In the first Born approximation, this scattering amplitude is given by the Fourier transform of the potential,

$$f(\boldsymbol{k} \to \boldsymbol{k}') = \frac{-m}{2\pi\hbar^2} \int d^3r' \, e^{i(\boldsymbol{k}-\boldsymbol{k}')\cdot\boldsymbol{r}'} V(\boldsymbol{r}'). \tag{2.36}$$

The scattering amplitude is closely related to the T-matrix we introduced above. We will determine this relationship here. Recall that the scattered particle state is given by

$$|\psi\rangle = |\boldsymbol{k}\rangle + G_0^+ T \, |\boldsymbol{k}\rangle \,, \tag{2.37}$$

when the incident particle is in the plane wave state, $|\boldsymbol{k}\rangle$. Projecting from the left on both sides with $\langle \boldsymbol{r}|$ gives

$$\psi(\boldsymbol{r}) = \frac{1}{(2\pi)^{3/2}} \left(e^{i\boldsymbol{k}\cdot\boldsymbol{r}} - \frac{(2\pi)^2 m}{\hbar^2} \left\langle \boldsymbol{k}' \right| T \, |\boldsymbol{k}\rangle \, \frac{e^{ikr}}{r} \right). \tag{2.38}$$

Comparing this expression with the scattering ansatz in Eq. (2.35), we can read off the relationship between the T-matrix element, $T_{\boldsymbol{k}',\boldsymbol{k}}$ and the scattering amplitude, $f(\boldsymbol{k} \to \boldsymbol{k}')$,

$$T_{\boldsymbol{k}',\boldsymbol{k}} = -\frac{\hbar^2}{(2\pi)^2 m} f(\boldsymbol{k} \to \boldsymbol{k}'). \tag{2.39}$$

This result holds for the delta function normalization of plane waves that we used above, $\langle \boldsymbol{k}|\boldsymbol{k}'\rangle = \delta^{(3)}(\boldsymbol{k} - \boldsymbol{k}')$. In the case in which the plane waves are normalized to an equilateral box of volume, L^3, we would have found [9]

$$T_{\boldsymbol{k}',\boldsymbol{k}} = -\frac{2\pi\hbar^2}{mL^3} f(\boldsymbol{k} \to \boldsymbol{k}'). \tag{2.40}$$

We will use this relationship to translate between the T-matrix and the scattering amplitude in the more complex situation of multiple scattering from a free gas that we treat in Sec. 3.2.6. This need arises in that situation because the multiple scattering problem is more easily approached in the formal language of the T-matrix, but we will ultimately prefer to relate the scattering solutions to the familiar scattering amplitude due to a single target.

2.2.5 Real and Imaginary parts of G_0^+

In chapter 3, we will study the index of refraction of a free gas for a matter wave. The real part of this quantity determines the phase shift of a matter wave passing through a gas, and the imaginary part determines the attenuation of the matter wave. Determining these components of the complex index of refraction will ultimately require that we be able to determine the real and imaginary parts of the operator expression for G_0^+. The utility of this decomposition makes it worth reviewing carefully how it is accomplished. We proceed by analogy with the expansion of the equivalent algebraic expression

$$\lim_{\varepsilon\to 0}\frac{1}{x+i\varepsilon}=\lim_{\varepsilon\to 0}\frac{x}{x^2+\varepsilon^2}-i\lim_{\varepsilon\to 0}\frac{\varepsilon}{x^2+\varepsilon^2}. \tag{2.41}$$

The second term is a common form of the Dirac delta function, [10]

$$\lim_{\varepsilon\to 0}\frac{\varepsilon}{x^2+\varepsilon^2}=\pi\delta(x). \tag{2.42}$$

The first term is also a distribution, which will be evaluated only as part of the kernel of an integral. For an arbitrary function, $f(x)$, we consider

$$\int_{-\infty}^{+\infty}dx\,\lim_{\varepsilon\to 0}\frac{x}{x^2+\varepsilon^2}f(x)=\lim_{\varepsilon\to 0}\lim_{\eta\to 0}\left(\int_{-\infty}^{-\eta}dx+\int_{-\eta}^{+\eta}dx+\int_{+\eta}^{+\infty}dx\right)\frac{x}{x^2+\varepsilon^2}f(x). \tag{2.43}$$

We have broken the integral into three regions. The central region surrounds the potentially troublesome point $x=0$, in which the quantity we are examining appears to be singular. There we find

$$\lim_{\eta\to 0}\int_{-\eta}^{+\eta}dx\,\frac{x}{x^2+\varepsilon^2}f(x)=f(0)\lim_{\eta\to 0}\int_{-\eta}^{+\eta}dx\,\frac{x}{x^2+\varepsilon^2}=0. \tag{2.44}$$

The last equality is due to the fact that we have an odd integrand and an even interval of integration. So we can say

$$\int_{-\infty}^{+\infty} dx \lim_{\varepsilon\to 0} \frac{x}{x^2+\varepsilon^2} f(x) = \lim_{\eta\to 0} \left(\int_{-\infty}^{-\eta} dx + \int_{+\eta}^{+\infty} dx \right) \frac{1}{x} f(x) = \mathrm{P}\frac{1}{x}. \tag{2.45}$$

P designates the principal part. We have found therefore,

$$\lim_{\varepsilon\to 0} \frac{1}{x+i\varepsilon} = \mathrm{P}\frac{1}{x} - i\pi\delta(x). \tag{2.46}$$

For our operator expression, we have

$$G_0^+ = \lim_{\varepsilon\to 0} \frac{1}{E-H_0+i\varepsilon} = \mathrm{P}\frac{1}{E-H_0} - i\pi\delta(E-H_0). \tag{2.47}$$

This expression gives us the decomposition of the operator, G_0^+, into terms which have exclusively real and exclusively imaginary matrix elements.

2.2.6 S-Matrix Formalism

So far we have approached the scattering problem by treating it as a time independent eigenvalue problem. That method led us to the Lippmann-Schwinger equation, and to solutions for the wave function of a particle scattered from a potential in free space. This approach will at times be insufficient, as for example in the case of scattering from a pseudopotential that we discuss below. Furthermore, some scenarios that we wish to discuss will be awkward without introducing time dependence at some level, such as if we wish to know the asymptotic effect of scattering on a particle long after the scattering interaction has ceased. In order to address these issues, we will review here a more rigorous framework for understanding scattering processes, in which we consider the dynamics of scattering of any number of particles [11]. In so doing, we will recover the results we showed above, and we will introduce the S-matrix, which will be an essential quantity for understanding the many body scattering that we discuss below.

We will consider the scattering of $N+1$ wave packets, where one particle is the probe particle, and the other N particles are targets. As before, we assume that, without interactions, the Hamiltonian, H_0, describes $N+1$ free particles. An eigenstate of H_0 is

$|q\rangle = |\boldsymbol{q}_0, \ldots, \boldsymbol{q}_N\rangle$, in which particle, i, is in a plane wave state with wave vector, $\boldsymbol{q}_i$.

$$H_0 |q\rangle = E_q |q\rangle . \tag{2.48}$$

We can construct an $N+1$ particle wave packet out of eigenstates of H_0,

$$|X\rangle = \int d^3q_0 \cdots d^3q_N \; a_0(\boldsymbol{q}_0 - \boldsymbol{p}_0) \cdots a_N(\boldsymbol{q}_N - \boldsymbol{p}_N) \, |\boldsymbol{q}_0, \ldots, \boldsymbol{q}_N\rangle . \tag{2.49}$$

Each $a_i(\boldsymbol{q}_i - \boldsymbol{p}_i)$ is an envelope in momentum space centered at $\boldsymbol{p}_i$. We will express this more compactly as

$$|X\rangle = \int d^{3(N+1)}q \; A(q) \, |q\rangle . \tag{2.50}$$

The full Hamiltonian, including interparticle interactions, is

$$H = H_0 + V, \tag{2.51}$$

where V accounts for interactions between particles. We will assume that the interaction is sufficiently local, and the wave packets of the particles sufficiently narrow compared to the spacing of their centers, that the particles are initially non-interacting. Without interactions, the wave packet evolves so that

$$|\phi(t_0)\rangle = e^{-iH_0 t_0/\hbar} |X\rangle . \tag{2.52}$$

We label the time when the particles encounter each other and interactions become important, t_0. For $t > t_0$, the state of the $N+1$ particle system is

$$|\psi(t)\rangle = e^{-iH(t-t_0)/\hbar} e^{-iH_0 t_0/\hbar} |X\rangle . \tag{2.53}$$

At $t = t_0$, we have the enforced boundary condition $|\psi(t_0)\rangle = |\phi(t_0)\rangle$. $|\psi(t)\rangle$ is the solution to the scattering problem. The interpretation of Eq. (2.53) is made easier by expressing it in terms of the interaction picture time-evolution operator, $U(t, t_0)$,

$$U(t, t_0) = e^{iH_0 t/\hbar} e^{-iH(t-t_0)/\hbar} e^{-iH_0 t_0/\hbar}. \tag{2.54}$$

The state of the wave packets after scattering, in terms of the propagator, $U(t, t_0)$, is

$$|\psi(t)\rangle = e^{-iH_0 t/\hbar} U(t,0) U(0,t_0) |X\rangle = e^{-iH_0 t/\hbar} U(t,0) \left|\Gamma^+\right\rangle , \tag{2.55}$$

where $|\Gamma^+\rangle$ is the state of the system at time $t = 0$.

$$\left|\Gamma^+\right\rangle = U(0,t_0) |X\rangle . \tag{2.56}$$

We will show first that $|\Gamma^+\rangle$ is determined by the Lippmann-Schwinger equation (Eq. (2.6)) that we derived formally in Section 2.2.1. The propagator $U(0, t_0)$ can be expressed in integral form as [12]

$$U(0,t_0) = 1 - i \int_{t_0}^{0} dt' \, U(0,t') V(t') \tag{2.57}$$

$$= 1 - i \int_{t_0}^{0} dt' \, e^{iHt'/\hbar} V e^{-iH_0 t'/\hbar} . \tag{2.58}$$

In the first line, $V(t') = e^{iH_0 t'/\hbar} V e^{-iH_0 t'/\hbar}$ is the interaction picture representation of V. $|\Gamma^+\rangle$ is given by

$$\left|\Gamma^+\right\rangle = |X\rangle - i \int_{t_0}^{0} dt' \, e^{iHt'/\hbar} V e^{-iH_0 t'/\hbar} |X\rangle \tag{2.59}$$

$$= |X\rangle - i \int d^{N+1} q \int_{t_0}^{0} dt' \, e^{-i(E_q - H)t'/\hbar} V A(q) |q\rangle . \tag{2.60}$$

Under the conditions we stated above, in which the scattering particles do not interact prior to time, t_0, the integrand in Eq. (2.57) vanishes for times earlier than t_0. In this situation, we may take $t_0 \to -\infty$ without affecting our result. We may then carry out the integral over t' in the usual way by inserting a factor of $e^{\varepsilon t'}$ and taking a limit as $\varepsilon \to 0$. The result is

$$\left|\Gamma^+\right\rangle = \int d^{N+1} q \, A(q) \left(|q\rangle + \lim_{\varepsilon \to 0} \frac{1}{E_q - H + i\varepsilon} V |q\rangle \right) . \tag{2.61}$$

The appearance of H in the denominator of this equation can be replaced with H_0 by using the identity, [13]

$$\frac{1}{E_q - H + i\varepsilon} V = \frac{1}{E_q - H_0 + i\varepsilon} T. \tag{2.62}$$

Let us introduce the scattered channel, $\left|\psi_q^+\right\rangle$, that corresponds to the incident channel, $|q\rangle$.

The relationship between these is the Lippmann-Schwinger equation that we introduced previously,

$$\left|\psi_q^+\right\rangle = |q\rangle + \frac{1}{E_q - H_0 + i\varepsilon} T\,|q\rangle\,. \tag{2.63}$$

$\left|\psi_q^+\right\rangle$ is an eigenstate of H with eigenvalue E_q, and the scattered wave is simply a wave packet constructed from the scattering channels,

$$\left|\Gamma^+\right\rangle = \int d^{3(N+1)}q\, A(q)\left|\psi_q^+\right\rangle. \tag{2.64}$$

Returning to Eq. (2.55) for the scattered wave at time, t, we may consider large times, long after the scattering event has happened and the particles involved are far apart and no longer interact. In that case, the propagator $U(t,0)U(0,t_0) = U(t,t_0)$ becomes

$$S = \lim_{t\to\infty} U(t,-t). \tag{2.65}$$

S is the operator which in momentum space representation is the S-matrix. Acting on the initial state with S leads to

$$\begin{aligned} S\,|X\rangle &= \lim_{t\to\infty} U(t,0)\left|\Gamma^+\right\rangle && (2.66)\\ &= \int d^{3(N+1)}q\ A(q)\ \lim_{t\to\infty} e^{-i(E_q-H_0)t/\hbar}\left|\psi_q^+\right\rangle && (2.67)\\ &= \int d^{3(N+1)}q\ A(q)\ \left(|q\rangle + \lim_{t\to\infty}\frac{e^{-i(E_q-H_0)t/\hbar}}{E_q - H_0 + i\varepsilon} T\,|q\rangle\right). && (2.68) \end{aligned}$$

Taking the large t limit, we can simplify Eq. (2.66) using [14]

$$\lim_{t\to\infty}\frac{e^{-i(E_q-H_0)t/\hbar}}{E_q - H_0 + i\varepsilon} = -2\pi i\delta(E_q - H_0). \tag{2.69}$$

The result is

$$S\,|X\rangle = \int d^{3(N+1)}q\ A(q)\ (1 - 2\pi i\delta(E_q - H_0)T)\,|q\rangle\,. \tag{2.70}$$

Each incoming channel, $|q\rangle$, is mapped onto the outgoing channel, $(1 - 2\pi i\,\delta(E_q - H_0)\,T)\,|q\rangle$. Using this result, we obtain the scattered state at large times

$$|\psi(t)\rangle = e^{-iH_0t/\hbar}\int d^{3(N+1)}q\ A(q)\ (1 - 2\pi i\,\delta(E_q - H_0)\,T)\,|q\rangle\,. \tag{2.71}$$

The result for the S-matrix is time independent, as is the mapping of each incoming channel onto each outgoing channel. We are often interested in the effect of a target on a wave packet which is sufficiently broad compared to the size of the scattering target that it is reasonable to treat the incident wave as a plane wave. We therefore will typically use S to refer to the individual mapping,

$$S = 1 - 2\pi i\, \delta(E_q - H_0)\, T. \tag{2.72}$$

This operator will be essential to our investigations of the effect of many-body systems on a probe particle, in which interactions between the probe and the target have long ceased at the time at which a measurement is made on the probe wave function. The measurement may be of the scattering cross section, determined by the flux of probe particles into a particular solid angle, or it may be the interference pattern formed in an atom interferometer when the probe overlaps with the other arm of the interferometer.

2.2.7 Time dependent derivation of S-matrix

We have illustrated the origin of the S-matrix in a very general way by considering the collision of many wave packets. Here we will take a different approach to deriving this quantity that follows the formal derivation of the Lippmann-Schwinger equation due to Sakurai [15]. In that derivation, the potential is treated as a time-varying quantity that is slowly turned on for times less than zero. At time zero, the state of the particle is given by the Lippmann-Schwinger equation. We may continue this procedure by considering a potential which is slowly turned on prior to time zero, and then slowly turned off afterward. The time dependent Schrödinger equation will then give us an expression for the asymptotic behavior of the state of the particle at large times ($t \to \infty$). The relationship between the initial state and the final state of the particle will provide us the form of the S-matrix.

Consider the potential $V(t)$ which is slowly turned on and then off,

$$V(t) = \begin{cases} V e^{\varepsilon t/\hbar} & t < 0, \\ V e^{-\varepsilon t/\hbar} & t \geq 0. \end{cases} \tag{2.73}$$

We will eventually consider the limit in which $\varepsilon \to 0$. The full Hamiltonian is $H = H_0 + V(t)$. The state of the system at time, t, is determined by the time dependent Schrödinger

equation,

$$i\hbar\frac{\partial}{\partial t}\left|\psi;t\right\rangle = \left(H_0 + V(t)\right)\left|\psi;t\right\rangle . \tag{2.74}$$

We may solve this equation using the Green's function $G_0^+(t,t')$ for the operator $i\hbar\frac{\partial}{\partial t} - H_0$. The Green's function is defined by

$$\left(i\hbar\frac{\partial}{\partial t} - H_0\right) G_0^+(t,t') \equiv \delta(t-t'). \tag{2.75}$$

The solution of this equation is,

$$G_0^+(t,t') = -\frac{i}{\hbar}\theta(t-t')e^{-iH_0(t-t')/\hbar}. \tag{2.76}$$

A solution of Eq. (2.74) in terms of this Green's function is

$$\left|\psi;t\right\rangle = \left|\phi;t\right\rangle + \int_{-\infty}^{+\infty} dt'\; G_0^+(t,t')V(t')\left|\psi;t'\right\rangle . \tag{2.77}$$

$\left|\phi;t\right\rangle$ is any state which satisfies $\left(i\hbar\frac{\partial}{\partial t} - H_0\right)\left|\phi;t\right\rangle = 0$. That is, $\left|\phi;t\right\rangle$ is a solution of the time dependent Schrödinger equation neglecting the potential. For the scattering problem, this is the initial state, prior to scattering. We are also seeking a solution that conserves energy, so we require that the initial and final state of the system have the same energy,

$$H\left|\psi;t\right\rangle = E\left|\psi;t\right\rangle , \text{ and} \tag{2.78}$$

$$H_0\left|\phi;t\right\rangle = E\left|\phi;t\right\rangle . \tag{2.79}$$

It follows that

$$\left|\psi;t\right\rangle = e^{-iEt/\hbar}\left|\psi\right\rangle , \text{ and} \tag{2.80}$$

$$\left|\phi;t\right\rangle = e^{-iEt/\hbar}\left|\phi\right\rangle , \tag{2.81}$$

where $\left|\psi\right\rangle$ and $\left|\phi\right\rangle$ are stationary states of H and H_0, respectively. Let us expand the solution for $\left|\psi;t\right\rangle$ in Eq. (2.77) using the definitions of $V(t')$ in Eq. (2.73) and the Green's function given in Eq. (2.75). This gives a relationship between the stationary states, $\left|\psi\right\rangle$

and $|\phi\rangle$, valid for times $t > 0$.

$$|\psi\rangle = |\phi\rangle - \frac{i}{\hbar} e^{i(E-H_0)t/\hbar} \left(\int_{-\infty}^{0} dt' \; e^{-i(E-H_0+i\varepsilon)t'/\hbar} + \int_{0}^{t} dt' \; e^{-i(E-H_0-i\varepsilon)t'/\hbar} \right) V |\psi\rangle \,. \quad (2.82)$$

Carrying out the integrals over t' yields

$$|\psi\rangle = |\phi\rangle + e^{i(E-H_0)t/\hbar} \left(\frac{1}{E - H_0 + i\varepsilon} + \frac{e^{-i(E-H_0-i\varepsilon)t/\hbar} - 1}{E - H_0 - i\varepsilon} \right) V |\psi\rangle \quad (2.83)$$

$$= |\phi\rangle - 2\pi i \, \delta(E - H_0) V |\psi\rangle + \frac{e^{-\varepsilon t/\hbar}}{E - H_0 - i\varepsilon} V |\psi\rangle \,. \quad (2.84)$$

Taking the limit as $t \to \infty$ and $\varepsilon \to 0$, and using $V |\psi\rangle = T |\phi\rangle$ gives

$$\lim_{\varepsilon \to 0} \lim_{t \to \infty} |\psi\rangle = (1 - 2\pi i \, \delta(E - H_0) T) |\phi\rangle \,. \quad (2.85)$$

This is the relationship between $|\psi\rangle$, the scattered state, and $|\phi\rangle$, the initial state, which is valid long after the scattering interaction has taken place. This relationship, which we showed previously in Eq. (2.72), allows us to map incoming and outgoing channels in the asymptotic limit in which the interaction has ceased and the scattered state becomes time independent.

2.3 Scattering from a Pseudopotential

Two particles scattering with a classical impact parameter, b, have a relative angular momentum, $l = bk$, where k is the relative wave number. If the interaction between the particles is negligible outside of a range, d, then for impact parameters, $b \gg d$, we expect little scattering to occur. Equivalently, for relative angular momenta, $l \gg kd$, we may neglect scattering. It follows that for low energy scattering, in which $k \to 0$, we need only consider $l = 0$. A more detailed quantum mechanical derivation of this result is given in [16]. Expanding the scattered wave function in partial waves is particularly simple in this case, as we must retain only the 0^{th} partial wave. This so called s-wave, in relative coordinates, is

$$\psi^{(l=0)}(\boldsymbol{r}) \propto \frac{e^{ikr}}{r}. \quad (2.86)$$

An interaction potential with zero range, called a contact potential, is represented by the pseudopotential, $V(\boldsymbol{r}) = V_0\,\delta(\boldsymbol{r})$. Not surprisingly, the exact solution for scattering from this potential has only an s-wave contribution and takes the form of Eq. (2.86). In situations where the energy of the scattering particles is low, such as scattering between ultracold atoms, we can make use of the pseudopotential, regardless of the actual interaction potential, so long as we choose the constant of proportionality in Eq. (2.86), the scattering length, appropriately.

2.3.1 Regularized Green's Function Method

What follows is the solution of the pseudopotential scattering problem. We appeal to the general scattering solution given in Eq. (2.14). In order to use this expression, we require the Green's function. The expression for this function given in Eq. (2.29) presents a problem in that it diverges when $\boldsymbol{r} = \boldsymbol{r}'$. Determining the value of the Green's function when $\boldsymbol{r} = \boldsymbol{r}'$ requires a more careful derivation. We follow the regularized Green's function method discussed in [17]. The time independent Green's function may be recovered by returning to a time dependent picture of the scattering.

The time dependent propagator in free space is $K_o(\boldsymbol{r}, t; \boldsymbol{r}', t')$, defined by

$$K_o(\boldsymbol{r}, t; \boldsymbol{r}', t') = \langle \boldsymbol{r}|\, e^{-iH(t-t')/\hbar}\, |\boldsymbol{r}'\rangle = \left(\frac{m}{2\pi\hbar i t}\right)^{3/2} \exp\left[\frac{im|\boldsymbol{r}-\boldsymbol{r}'|^2}{2\hbar t}\right]. \tag{2.87}$$

A Green's function for the time independent Schrödinger equation in free space is given by

$$G_0(\boldsymbol{r}, \boldsymbol{r}'; z) = \int_0^\infty dt\, e^{-zt} K_o(\boldsymbol{r}, t; \boldsymbol{r}', 0). \tag{2.88}$$

To obtain a result that is regular when $\boldsymbol{r} = \boldsymbol{r}' = 0$, we take this limit before doing the integral over t,

$$G_0(0, 0; z) = \int_0^\infty dt\, e^{-zt} K_o(0, t; 0, 0). \tag{2.89}$$

If we choose z to be

$$z = -i\frac{E}{\hbar} + \varepsilon = e^{-i\frac{\pi}{2}}\frac{\hbar k^2}{2m} + \varepsilon, \tag{2.90}$$

then $G(\boldsymbol{r}, \boldsymbol{r}')$ satisfies the following differential equation

$$(E - H_0 + i\hbar\varepsilon)\left(\frac{-i}{\hbar}\right) G(\boldsymbol{r}, \boldsymbol{r}'; E) = \delta^{(3)}(\boldsymbol{r} - \boldsymbol{r}'). \tag{2.91}$$

$-\frac{i}{\hbar}G(\boldsymbol{r},\boldsymbol{r}')$ is a Green's function for the time independent Schrödinger equation in the limit $\varepsilon \to 0$. Notice that this definition of G differs from Eq. (2.29) by the factor $-i/\hbar$. A solution of

$$(H_0 + V(\boldsymbol{r}))\psi(\boldsymbol{r}) = E\psi(\boldsymbol{r}) \tag{2.92}$$

is given in Eq. (2.14), which we repeat here,

$$\psi(\boldsymbol{r}) = \phi(\boldsymbol{r}) - \frac{i}{\hbar}\int d^3r'\, G(\boldsymbol{r},\boldsymbol{r}')V(\boldsymbol{r}')\psi(\boldsymbol{r}'). \tag{2.93}$$

Performing the integral in Eq. (2.88) gives the result we found in Eq. (2.29),

$$G(\boldsymbol{r},\boldsymbol{r}') = -\frac{im}{2\pi\hbar}\frac{e^{ik|\boldsymbol{r}-\boldsymbol{r}'|}}{|\boldsymbol{r}-\boldsymbol{r}'|}. \tag{2.94}$$

Performing the integral in Eq. (2.89) gives

$$G(0,0) = \frac{mk}{2\pi\hbar}. \tag{2.95}$$

We have effectively avoided the divergence by taking $\boldsymbol{r} = \boldsymbol{r}'$ before taking the Fourier transform of the time dependent propagator. If $V(\boldsymbol{r})$ is a delta function potential

$$V(\boldsymbol{r}) = V_o\,\delta(\boldsymbol{r}), \tag{2.96}$$

then we can insert it into Eq. (2.93) and take the integral over the primed coordinates, giving an expression for $\psi(\boldsymbol{r})$ in terms of $\psi(0)$. Algebraically solving for $\psi(0)$ gives a solution of Eq. (2.92),

$$\psi(\boldsymbol{r}) = e^{i\boldsymbol{k}\cdot\boldsymbol{r}} - \frac{i}{\hbar}G(\boldsymbol{r},0)V_o\psi(0) \tag{2.97}$$

$$\psi(\boldsymbol{r}) = e^{i\boldsymbol{k}\cdot\boldsymbol{r}} - \frac{i}{\hbar}V_o\frac{G(\boldsymbol{r},0)}{1+\frac{i}{\hbar}V_oG_0(0,0)} \tag{2.98}$$

We can write Eq. (2.98) in the form of the Fermi ansatz, [2]

$$\psi(\boldsymbol{r}) = e^{i\boldsymbol{k}\cdot\boldsymbol{r}} + C_o\frac{e^{ikr}}{r}, \tag{2.99}$$

where C_o is given by

$$C_o = \frac{-mV_o/(2\pi\hbar^2)}{1 + i\frac{mV_o}{2\pi\hbar^2}k}. \tag{2.100}$$

The scattering length, $a_s = -\lim_{k\to 0} f(\theta, \phi)$, is $a_s = mV_0/(2\pi\hbar^2)$. As we anticipated, the pseudopotential shows only s-wave scattering.

2.3.2 T-matrix for a Delta Potential

In the previous section, we found the solution to scattering from a pseudopotential. In treating the problem of multiple targets that are each well-described by a contact potential, it will be necessary to know the T-matrix for this potential. We will use the results we determined in the previous section for the free space Green's function. Adjusting to make our terminology consistent with Eq. (2.29), we have

$$G(\boldsymbol{r}, \boldsymbol{r}') = \frac{-m}{2\pi\hbar^2}\frac{e^{ik|\boldsymbol{r}-\boldsymbol{r}'|}}{|\boldsymbol{r}-\boldsymbol{r}'|}, \tag{2.101}$$

$$G(\boldsymbol{r}', \boldsymbol{r}') = \frac{-imk}{2\pi\hbar^2}. \tag{2.102}$$

An incident wave, $\varphi(\boldsymbol{r})$, scattered from a potential, $V(\boldsymbol{r})$, gives the Lippmann-Schwinger equation solution,

$$\psi(\boldsymbol{r}) = \phi(\boldsymbol{r}) + \int d^3r'\; G(\boldsymbol{r}, \boldsymbol{r}')\, V(\boldsymbol{r}')\, \psi(\boldsymbol{r}'). \tag{2.103}$$

The scattering potential is

$$V(\boldsymbol{r}) = \frac{2\pi\hbar^2}{m} a_s\, \delta(\boldsymbol{r} - \boldsymbol{r}_i). \tag{2.104}$$

This potential has a scattering length, a_s, and is centered at $\boldsymbol{r}_i$. Inserting this potential into Eq. (2.103), we obtain the solution for the scattered wave,

$$\psi(\boldsymbol{r}) = \varphi(\boldsymbol{r}) + s(k)\, G(\boldsymbol{r}, \boldsymbol{r}_i)\, \varphi(\boldsymbol{r}_i), \tag{2.105}$$

$$s(k) = \frac{2\pi\hbar^2}{m}\frac{a}{1 + iak}. \tag{2.106}$$

In Sec. 2.2.2, we introduced the Lippmann-Schwinger equation in terms of the T-matrix. This was given by

$$|\psi\rangle = |\varphi\rangle + GT\,|\varphi\rangle\,. \tag{2.107}$$

The wave function for the scattered wave in terms of T is then given by,

$$\psi(\boldsymbol{r}) = \varphi(\boldsymbol{r}) + \int d^3r'\, G(\boldsymbol{r}, \boldsymbol{r}')\, \langle \boldsymbol{r}' | \, T \, | \varphi \rangle \,. \tag{2.108}$$

A comparison of Eq. (2.108) and Eq. (2.105) shows immediately that T is given by [18]

$$T = s(k) \, |\boldsymbol{r}_i\rangle \langle \boldsymbol{r}_i| \,. \tag{2.109}$$

This expression for the T-matrix for a single contact potential scatterer can be used to treat the problem of many such scatterers, which we address in the next section.

2.4 Multiple Scattering

2.4.1 Fermi treatment of index of refraction

The problem of an atom passing through a dilute gas bears resemblance to slow neutron scattering from a medium, which was addressed in an approximate way by Fermi [2]. He showed that a thin, infinite slab filled with a continuous, uniform medium of scattering centers behaves like a material with an index of refraction for a matter wave. Formal multiple scattering techniques should replicate that result, which we review here. We treat a slab of width, w, uniformly filled with s-wave scatterers of density, n. In that we keep only the s-wave contribution to the scattering, the scattered waves will be spherical waves, with a uniform scattering amplitude, that we call C_0. We will ignore the effect of secondary scattering, in which the wave emanating from one point in the slab scatters again from another point in the slab. Working in cylindrical coordinates, it is convenient to place the z-axis normal to the slab. For a sufficiently thin slab, we can treat all of the points in the slab as being at $z \approx 0$. Under these assumptions, we may immediately write an expression for the scattered wave function,

$$\psi(z) = e^{ikz} + 2\pi n w C_0 \int_0^\infty d\rho \, \rho \frac{e^{ikr}}{r}, \tag{2.110}$$

where $r = \sqrt{\rho^2 + z^2}$ is the distance from the point of scattering to a point a distance z beyond the slab along the axis, $\rho = 0$. The scattered wave function does not depend on ρ due to the translation symmetry of the slab perpendicular to the z-axis. Likewise it is

independent of the cylindrical angle because of the rotational symmetry about the z-axis. Changing the variable of the integration to r gives the simple expression,

$$\psi(z) = e^{ikz} + 2\pi n w C_0 \int_z^\infty dr\, e^{ikr} \tag{2.111}$$

$$= e^{ikz} + 2\pi n w C_0 \lim_{\epsilon \to 0} \int_z^\infty dr\, e^{ikr} e^{-\epsilon r} \tag{2.112}$$

$$= \left(1 - \frac{2\pi n w C_0}{ik}\right) e^{ikz}. \tag{2.113}$$

We can compare this to the result expected of a wave passing through a medium with an index of refraction, n_r,

$$\psi(z) = e^{in_r k w} e^{ik(z-w)} \approx (1 + ik(n_r - 1)w)\, e^{ikz}. \tag{2.114}$$

The expansion is valid when the index of refraction does not deviate too far from 1 and when the slab is sufficiently thin, so that the additional phase accumulated due to the presence of the slab is small. Equating the results of these two methods leads us to conclude that the medium has an index of refraction given by

$$n_r - 1 = \frac{2\pi n C_0}{k^2}. \tag{2.115}$$

This quantity is not dependent on the specific width of the slab, w. We can therefore consider it to be valid in the limit where w vanishes.

2.4.2 Lax Multiple Scattering and the Coherent Wave Equation

In analyzing the problem of the effect of a free, thermal gas on a plane matter wave, it is useful first to review the general multiple scattering theory that pertains to scattering from potentials located at various scattering centers. In this theory, the targets do not carry degrees of freedom, and therefore can not cause decoherence of the probe matter wave; however, this theory elucidates the origin of the index of refraction of the free gas for a matter wave. Here, we will follow the development due to Lax [3]. The scattering situation is constructed such that there is an incident matter wave, $\phi(\boldsymbol{r})$, which interacts with the generic potential $\sum_{j=1}^{N} V(\boldsymbol{r} - \boldsymbol{r}_j)$. We may then introduce the scattered wave due to scattering from the target at the position $\boldsymbol{r}_j$, which we designate, $F(\boldsymbol{r}, \boldsymbol{r}_j)$. The wave

that is incident on the j^{th} target is $\psi^j(\boldsymbol{r})$, and is due to scattering from all of the other centers of $\phi(\boldsymbol{r})$. The total scattered wave due to all the scattering centers is designated, $\psi(\boldsymbol{r})$. We may then write a set of self-consistent equations for these quantities. The total scattered wave is given by the sum of the incident wave, and the scattered waves from all of the individual targets,

$$\psi(\boldsymbol{r}) = \phi(\boldsymbol{r}) + \sum_j F(\boldsymbol{r}, \boldsymbol{r}_j). \tag{2.116}$$

The wave which is incident upon the j^{th} scatterer is the total scattered wave with the component due to the j^{th} scatter removed,

$$\psi^j(\boldsymbol{r}) = \psi(\boldsymbol{r}) - F(\boldsymbol{r}, \boldsymbol{r}_j). \tag{2.117}$$

Using T-matrix notation, in which the T-matrix associated with scattering from the j^{th} target is $T(\boldsymbol{r}_j)$, the scattered wave from an individual target is

$$F(\boldsymbol{r}, \boldsymbol{r}_j) = \frac{1}{E - H_0} T(\boldsymbol{r}_j)\psi^j(\boldsymbol{r}), \tag{2.118}$$

where E is the energy of the incident matter wave and H_0 is a free particle Hamiltonian.

In the case of a statistically large number of scattering centers, we will not seek to solve these equations for $\psi(\boldsymbol{r})$ by specifying the positions of each scattering center. Instead, we will describe their locations probabilistically. The probability of finding the scatterers at the positions $\boldsymbol{r}_1, \ldots, \boldsymbol{r}_N$ is $p(\boldsymbol{r}_1, \ldots, \boldsymbol{r}_N)d^N r$. Given this distribution, we can compute $\langle\psi(\boldsymbol{r})\rangle$ as an average over the positions of the targets. Other properties of the target may be similarly averaged, such as momentum, mass, spin, etc. Assuming we have the specific solutions for a given distribution of scatterers, $\psi(\boldsymbol{r}; \boldsymbol{r}_1, \ldots, \boldsymbol{r}_N)$, the averaged wave function is

$$\begin{aligned}\langle\psi(\boldsymbol{r})\rangle &= \int d^N r\, p(\boldsymbol{r}_1, \ldots, \boldsymbol{r}_N)\psi(\boldsymbol{r}; \boldsymbol{r}_1, \ldots, \boldsymbol{r}_N) \\ &= \int dr_1\, p_1(\boldsymbol{r}_1) \int dr_2 \cdots dr_N\, \psi(\boldsymbol{r}; \boldsymbol{r}_1, \ldots, \boldsymbol{r}_N) p(\boldsymbol{r}_1 | \boldsymbol{r}_2, \ldots, \boldsymbol{r}_N).\end{aligned} \tag{2.119}$$

The quantity that appears on the right of this expression gives the scattered wave function averaged over all but one set of target coordinates. This quantity we note in shorthand by

$$\langle\psi(\boldsymbol{r})\rangle_1 = \int dr_2 \cdots dr_N\, \psi(\boldsymbol{r}; \boldsymbol{r}_1, \ldots, \boldsymbol{r}_N) p(\boldsymbol{r}_1 | \boldsymbol{r}_2, \ldots, \boldsymbol{r}_N). \tag{2.120}$$

We can construct analogous quantities for the wave incident upon a particular target,

$$\left\langle \psi^j(\boldsymbol{r}) \right\rangle = \int dr_j \, p(\boldsymbol{r}_j) \left\langle \psi^j(\boldsymbol{r}) \right\rangle_j . \tag{2.121}$$

Taking the average of the scattered wave function on both sides of the Lippmann-Schwinger equation gives

$$\begin{aligned} \langle \psi(\boldsymbol{r}) \rangle &= \phi(\boldsymbol{r}) + \sum_j \frac{1}{E - H_0} \int d^3 r_1 \cdots d^3 r_N \, p(\boldsymbol{r}_1, \ldots \boldsymbol{r}_N) T(\boldsymbol{r}_j) \psi^j(\boldsymbol{r}) \\ &= \phi(\boldsymbol{r}) + \sum_j \frac{1}{E - H_0} \int d^3 r_j \, p(\boldsymbol{r}_j) T(\boldsymbol{r}_j) \left\langle \psi^j(\boldsymbol{r}) \right\rangle_j . \end{aligned} \tag{2.122}$$

The total scattered wave function on the left hand side and the wave function incident upon the j^{th} scatterer on the right hand side differ by the average of the scattered wave produced by a single scatterer. For uncorrelated scatterers that are randomly distributed, we expect that the contribution due to a single scatterer is negligible, so that these quantities are approximately equal,

$$\langle \psi(\boldsymbol{r}) \rangle \approx \left\langle \psi^j(\boldsymbol{r}) \right\rangle_j . \tag{2.123}$$

When we make this replacement in Eq. (2.122), the sum over scatterers may be replaced by the number, N, of scatterers. The density of scatterers is $n(\boldsymbol{r}) = Np(\boldsymbol{r})$. What remains is an average of the T-operator of the form

$$\bar{T} = \int d^3 r_j \, n(\boldsymbol{r}_j) T(\boldsymbol{r}_j). \tag{2.124}$$

The resulting equation for the average scattered wave function simplifies considerably,

$$\langle \psi(\boldsymbol{r}) \rangle = \phi(\boldsymbol{r}) + \frac{1}{E - H_0} \bar{T} \langle \psi(\boldsymbol{r}) \rangle . \tag{2.125}$$

The average wave function $\langle \psi(\boldsymbol{r}) \rangle$ is therefore a solution of

$$(E - H_0 - \bar{T}) \langle \psi(\boldsymbol{r}) \rangle = 0. \tag{2.126}$$

A free gas, such as we investigate in Chapter 3, has a uniform distribution of scatterers. We may compute $\bar{T}$ for this case, in which we set $n(\boldsymbol{r}) = \bar{n}$. It will be convenient to relate

the momentum space matrix elements of $T(\boldsymbol{r}_j)$ to those of $T(0)$. In a space with volume V, the state with wave vector $\boldsymbol{k}_a$ has the wave function, $\phi_a(\boldsymbol{r}) = 1/\sqrt{V}\exp(i\boldsymbol{k}_a \cdot \boldsymbol{r})$. Using the solution for the T operator given in Eq. (2.109), we see that

$$T_{ba}(\boldsymbol{r}_j) = \langle \boldsymbol{k}_b | \, s(k) \, | \boldsymbol{r}_j \rangle \, \langle \boldsymbol{r}_j | \boldsymbol{k}_a \rangle = \frac{s(k)}{V} e^{-i(\boldsymbol{k}_b - \boldsymbol{k}_a)\cdot \boldsymbol{r}_j}. \tag{2.127}$$

Similarly, we find $T_{ba}(0) = \frac{s(k)}{V}$. Combining these equations gives

$$T_{ba}(0) = e^{i(\boldsymbol{k}_b - \boldsymbol{k}_a)\cdot \boldsymbol{r}_j} T_{ba}(\boldsymbol{r}_j). \tag{2.128}$$

This relation allows us to compute the matrix element of the averaged T-matrix, $\bar{T}_{ba}$,

$$\bar{T}_{ba} = \bar{n} T_{ba}(0) \int d^3 r \, e^{i(\boldsymbol{k}_a - \boldsymbol{k}_b)\cdot \boldsymbol{r}} = \bar{n} T_{aa}(0) \delta_{ab}. \tag{2.129}$$

For a medium with a uniform density, the averaged T operator is diagonal in momentum space. The solutions of Eq. (2.126) are plane waves, therefore. We can relate the diagonal T matrix element $T_{aa}(0)$ to the scattering amplitude $f(k_a, \theta)$ for scattering of an incident plane wave with wave number k_a through an angle θ. These are related by

$$T_{aa}(0) = \frac{-4\pi\hbar^2}{2m} f(k_a, 0), \tag{2.130}$$

where the mass of the projectile is m. Substituting this relation into Eq. (2.126), we obtain

$$\left(\nabla^2 + k_a^2 + 4\pi\bar{n} f(k_a, 0)\right) \langle \psi(\boldsymbol{r}) \rangle = 0. \tag{2.131}$$

The averaged scattered wave is, therefore, a plane wave propagating in the uniform medium of scatterers with a shifted wave number, k', given by

$$k'^2 = k_a^2 + 4\pi\bar{n} f(k_a, 0). \tag{2.132}$$

From this expression, we can immediately read off an index of refraction, n_r, which relates the incoming wave number to the wave number in the uniform sample by $k' = n_r k_a$.

$$n_r = \sqrt{1 + 4\pi\bar{n}\frac{f(k_a, 0)}{k_a^2}}. \tag{2.133}$$

For weak scattering, when the scattering amplitude is small or the density of scatterers is low, such that the second term under the square root is small compared to 1, the index of refraction can be expanded as

$$n_r \approx 1 + 2\pi\bar{n}\frac{f(k_a, 0)}{k_a^2}. \tag{2.134}$$

This is precisely equivalent to the Fermi result in Eq. (2.115). In this multiple scattering formulation, however, we have not begun by assuming a medium of scatterers, but rather we have considered a discrete collection of scatterers, which acts as a refractive medium when the distribution of scatterer locations is uniform. In the Fermi formulation, multiple scattering was neglected explicitly, which has the effect of assuming that the probe is weakly interacting with a dilute target.

2.4.3 Expansion of Multiple Scattering in Number of Target Interactions

In analyzing multiple scattering, it is occasionally useful to be able to expand a scattered wave into terms corresponding to a number of sequential scattering events. We may do so in the multiple scattering formalism above by expanding the wave incident upon the j^{th} scatterer as,

$$\psi^{j(i+1)}(\boldsymbol{r}) = \phi(\boldsymbol{r}) + \sum_{s\neq j}(E - H_0)^{-1}T(\boldsymbol{r}_s)\psi^{s(i)}(\boldsymbol{r}), \tag{2.135}$$

with the 0^{th} term $\psi^{j(0)}(\boldsymbol{r})$ being the initial wave, $\phi(\boldsymbol{r})$, that is incident on the collection of scatterers before any scattering has taken place. Let us consider the consequences of this expansion for a collection of delta potential scatterers. Plugging the expression for $\psi^{j(1)}(\boldsymbol{r})$ into the expression for the total scattered wave given in Eq. (2.116) leads to

$$\psi(\boldsymbol{r}) \approx \phi(\boldsymbol{r}) + \sum_j \frac{1}{E - H_0}T(\boldsymbol{r}_j)\phi(\boldsymbol{r}) + \sum_j\sum_{s\neq j}\frac{1}{E - H_0}T(\boldsymbol{r}_j)\frac{1}{E - H_0}T(\boldsymbol{r}_s)\phi(\boldsymbol{r}). \tag{2.136}$$

We may read off an expression for the quantity $(E - H_0)^{-1}T(\boldsymbol{r}_j)\phi(\boldsymbol{r})$ from the result in Eq. (2.109) for scattering from a pseudopotential of the form given in Eq. (2.104). Taking $\phi(\boldsymbol{r})$ to be a plane wave,

$$\phi(\boldsymbol{r}) = \frac{1}{(2\pi)^{3/2}}e^{i\boldsymbol{k}\cdot\boldsymbol{r}}, \tag{2.137}$$

we obtain

$$(E - H_0)^{-1} T(\boldsymbol{r}_j)\phi(\boldsymbol{r}) = -\frac{a_s}{(2\pi)^{3/2}}\, e^{i\boldsymbol{k}\cdot\boldsymbol{r}_j} \frac{e^{ik|\boldsymbol{r}-\boldsymbol{r}_j|}}{|\boldsymbol{r}-\boldsymbol{r}_j|}. \tag{2.138}$$

The meaning of this expression is that the first scattering of a plane wave from a pseudopotential results in an outgoing spherical wave emanating from the location, $\boldsymbol{r}_s$, of the scattering center. This result is sufficient to evaluate the first two terms in Eq. (2.136). That is, including only a single scattering event from a collection of scattering centers modeled by a pseudopotential interaction, the total scattered wave due to an incident plane wave is

$$\psi(\boldsymbol{r}) = \frac{1}{(2\pi)^{3/2}} \left(e^{i\boldsymbol{k}\cdot r} - a_s \sum_j e^{i\boldsymbol{k}\cdot\boldsymbol{r}_j} \frac{e^{ik|\boldsymbol{r}-\boldsymbol{r}_j|}}{|\boldsymbol{r}-\boldsymbol{r}_j|} \right). \tag{2.139}$$

We may also calculate the scattered wave including double scattering. This requires that we evaluate

$$\langle \boldsymbol{r}| \frac{1}{E - H_0} T(\boldsymbol{r}_j) |\psi_s\rangle = \frac{1}{E - H_0} T(\boldsymbol{r}_j) \frac{1}{E - H_0} T(\boldsymbol{r}_s)\phi(\boldsymbol{r}) \tag{2.140}$$

We have re-expressed the scattered wave using Dirac notation for convenience in carrying out the calculation. We can separate the quantity on the left into manageable pieces as follows,

$$\langle \boldsymbol{r}| \frac{1}{E - H_0} T(\boldsymbol{r}_j) |\psi_s\rangle = \int d^3r' d^3\tilde{k}\ \langle \boldsymbol{r}| \frac{1}{E - H_0} \left|\boldsymbol{r}'\right\rangle \left\langle \boldsymbol{r}'\right| T(\boldsymbol{r}_j) |\tilde{\boldsymbol{k}}\rangle \langle \tilde{\boldsymbol{k}}|\psi_s\rangle. \tag{2.141}$$

The quantity, $\langle \boldsymbol{r}| \frac{1}{E-H_0} |\boldsymbol{r}'\rangle$ is the usual free space time independent Green's function. We need to determine $\langle \boldsymbol{r}'| T(\boldsymbol{r}_j)|\tilde{\boldsymbol{k}}\rangle$ and $\langle \tilde{k}|\psi_s\rangle$. The momentum space representation of the singly scattered state is given by the Fourier transform of a spherical wave,

$$\langle \tilde{\boldsymbol{k}}|\psi_s\rangle = -\frac{a_s}{(2\pi)^{3/2}} \int d^3r \frac{1}{(2\pi)^{3/2}} e^{-i\tilde{\boldsymbol{k}}\cdot\boldsymbol{r}} e^{i\boldsymbol{k}\cdot\boldsymbol{r}_s} \frac{e^{ik|\boldsymbol{r}-\boldsymbol{r}_s|}}{|\boldsymbol{r}-\boldsymbol{r}_s|} \tag{2.142}$$

$$= -\frac{1}{(2\pi)^3} a_s\, e^{i(\boldsymbol{k}-\tilde{\boldsymbol{k}})\cdot\boldsymbol{r}_s} \frac{4\pi}{\tilde{k}^2 - k^2}. \tag{2.143}$$

We may determine the quantity $\langle \boldsymbol{r}'| T(\boldsymbol{r}_j)|\tilde{\boldsymbol{k}}\rangle$ most easily by recalling the result from Eq. 2.128,

$$\langle \bar{\boldsymbol{k}}|T(\boldsymbol{r}_j)|\tilde{\boldsymbol{k}}\rangle = \frac{1}{(2\pi)^3} e^{i(\tilde{\boldsymbol{k}}-\bar{\boldsymbol{k}})\cdot\boldsymbol{r}_j} T_{\bar{\boldsymbol{k}},\tilde{\boldsymbol{k}}}(0). \tag{2.144}$$

We may then relate the matrix element of the T-matrix to the scattering amplitude

$$T_{\hat{\boldsymbol{k}},\tilde{\boldsymbol{k}}}(0) = \frac{-4\pi\hbar^2}{2m} f(\tilde{\boldsymbol{k}} \to \bar{\boldsymbol{k}}). \tag{2.145}$$

For a pseudopotential, which gives rise only to s-wave scattering, the scattering amplitude for low energy probes is approximately a constant, equal to the negative of the scattering length, a_s, so that

$$T_{\bar{\boldsymbol{k}},\tilde{\boldsymbol{k}}}(0) = \frac{4\pi\hbar^2}{2m} a_s \tag{2.146}$$

Substituting this result into the expression for $\langle \boldsymbol{r}' | \, T(\boldsymbol{r}_j) | \tilde{\boldsymbol{k}} \rangle$, we obtain our result,

$$\left\langle \boldsymbol{r}' \right| T(\boldsymbol{r}_j) | \tilde{\boldsymbol{k}} \rangle = \frac{e^{i\tilde{\boldsymbol{k}}\cdot\boldsymbol{r}_j}}{(2\pi)^{3/2}} \frac{2\pi\hbar^2}{m} a_s \, \delta^3(\boldsymbol{r}' - \boldsymbol{r}_j). \tag{2.147}$$

Using the outgoing Green's function,

$$\lim_{\epsilon \to 0} \langle \boldsymbol{r} | \, \frac{1}{E - H_0 + i\epsilon} \left| \boldsymbol{r}' \right\rangle = \frac{-m}{2\pi\hbar^2} \frac{e^{ik|\boldsymbol{r}-\boldsymbol{r}'|}}{|\boldsymbol{r} - \boldsymbol{r}'|}, \tag{2.148}$$

we are now in a position to write down the doubly scattered wave. This is

$$\langle \boldsymbol{r} | \, \frac{1}{E - H_0} T(\boldsymbol{r}_j) \, | \psi_s \rangle = \frac{a_s^2}{(2\pi)^{3/2}} \frac{e^{ik|\boldsymbol{r}-\boldsymbol{r}_j|}}{|\boldsymbol{r} - \boldsymbol{r}_j|} e^{i\boldsymbol{k}\cdot\boldsymbol{r}_s} \frac{1}{(2\pi)^3} \int d^3\tilde{k} \, e^{i\tilde{\boldsymbol{k}}\cdot(\boldsymbol{r}_j - \boldsymbol{r}_s)} \frac{4\pi}{\tilde{k}^2 - k^2}. \tag{2.149}$$

The integration gives us the inverse Fourier transform of a quantity that we obtained through the forward transform of a spherical wave. We may therefore immediately write the result of the integral, giving

$$\langle \boldsymbol{r} | \, \frac{1}{E - H_0} T(\boldsymbol{r}_j) \, | \psi_s \rangle = \frac{a_s^2}{(2\pi)^{3/2}} \frac{e^{ik|\boldsymbol{r}-\boldsymbol{r}_j|}}{|\boldsymbol{r} - \boldsymbol{r}_j|} \frac{e^{ik|\boldsymbol{r}_j-\boldsymbol{r}_s|}}{|\boldsymbol{r}_j - \boldsymbol{r}_s|} e^{i\boldsymbol{k}\cdot\boldsymbol{r}_s}. \tag{2.150}$$

This is a very satisfying and intuitive result, which lends itself readily to interpretation as a series of scattering events. From right to left, we have a plane wave incident on a scatterer at the position $\boldsymbol{r}_s$, which is scattered as a spherical wave. This wave expands until it encounters another scatterer at the position $\boldsymbol{r}_j$. The second scatterer generates another

spherical wave. The total scattered wave function including two bounces takes the form

$$\psi(\boldsymbol{r}) \approx \frac{1}{(2\pi)^{3/2}} \left(e^{i\boldsymbol{k}\cdot\boldsymbol{r}} - \sum_j a_s \frac{e^{ik|\boldsymbol{r}-\boldsymbol{r}_j|}}{|\boldsymbol{r}-\boldsymbol{r}_j|} e^{i\boldsymbol{k}\cdot\boldsymbol{r}_j} + \sum_j \sum_{s\neq j} a_s^2 \frac{e^{ik|\boldsymbol{r}-\boldsymbol{r}_j|}}{|\boldsymbol{r}-\boldsymbol{r}_j|} \frac{e^{ik|\boldsymbol{r}_j-\boldsymbol{r}_s|}}{|\boldsymbol{r}_j-\boldsymbol{r}_s|} e^{i\boldsymbol{k}\cdot\boldsymbol{r}_s} \right). \tag{2.151}$$

Let us return to the problem of a thin slab of width, w, filled with a uniform medium of density, n, of s-wave scatterers. We consider a plane wave incident perpendicular to the slab, such that $\boldsymbol{k}\cdot\boldsymbol{r}_j \approx 0$ for all the scatterers in the slab. We must evaluate the wave incident at the point $\boldsymbol{r}_j$ in the slab due to scattering from other points within the slab,

$$\sum_{s\neq j} \frac{e^{ik|\boldsymbol{r}_j-\boldsymbol{r}_s|}}{|\boldsymbol{r}_j-\boldsymbol{r}_s|}. \tag{2.152}$$

In the continuous limit, we treat the summation as $\sum_{s\neq j} \to \int d^3r_s\, n(\boldsymbol{r}_s)$, with the understanding that we must explicitly exclude the point $\boldsymbol{r}_s = \boldsymbol{r}_j$ from the integration. In the coordinate system, $\boldsymbol{u} = \boldsymbol{r}_s - \boldsymbol{r}_j$, the quantity $\rho = |\boldsymbol{r}_j - \boldsymbol{r}_s|$ is simply the distance from the origin within the plane, $z = 0$. It is constructive to evaluate the integral in cylindrical coordinates, therefore, as

$$\sum_{s\neq j} \frac{e^{ik|\boldsymbol{r}_j-\boldsymbol{r}_s|}}{|\boldsymbol{r}_j-\boldsymbol{r}_s|} \to \int_\epsilon^\infty d\rho\, \rho \int_0^{2\pi} d\theta \int_0^w dz\, n \frac{e^{ik\rho}}{\rho}. \tag{2.153}$$

We explicitly set the lower boundary on the ρ integral to be ϵ in order to exclude the point $\rho = 0$, which corresponds to $\boldsymbol{r}_s = \boldsymbol{r}_j$. We will consider the limit as $\epsilon \to 0$ after we have evaluated the integral. This is easily done using the usual trick,

$$\int_\epsilon^\infty d\rho\, e^{ik\rho} = \lim_{\alpha\to 0} \int_\epsilon^\infty d\rho\, e^{ik\rho} e^{-\alpha\rho} = \frac{i}{k} e^{ik\epsilon}. \tag{2.154}$$

Thus we find in the limit where $\epsilon \to 0$,

$$\sum_{s\neq j} \frac{e^{ik|\boldsymbol{r}_j-\boldsymbol{r}_s|}}{|\boldsymbol{r}_j-\boldsymbol{r}_s|} \to \frac{2\pi i n w}{k}. \tag{2.155}$$

We can use the result we obtained in Sec. 2.4.1 for the sum of spherical waves emanating

from the thin slab at a point, z, outside of the slab,

$$\sum_j \frac{e^{ik|\boldsymbol{r}-\boldsymbol{r}_j|}}{|\boldsymbol{r}-\boldsymbol{r}_j|} \to \frac{2\pi i n w}{k} e^{ikz}. \tag{2.156}$$

The total scattered wave function including single and double scattering events is then given by

$$\psi(z) \approx \frac{1}{(2\pi)^{3/2}} \left(1 + \frac{-2\pi a_s i n w}{k} + \left(\frac{-2\pi a_s i n w}{k}\right)^2\right) e^{ikz}. \tag{2.157}$$

The contribution to the scattered wave due to double scattering is reduced by a factor of the scattering length compared to single scattering. The same is true of the dependence on the density of the target. The implication is that multiple scattering of a probe weakly interacting with a dilute target can become negligible when a_s and n are sufficiently small.

Chapter 3

Matter Wave Interferometry

3.1 Mach-Zender Interferometer

3.1.1 Configuration of the Interferometer

Fig. 3-1 shows the configuration of a separated arm atom interferometer [1]. An atom beam is incident from the left on a diffraction grating with grating spacing, λ_g, which coherently splits the spatial wave function of each probe atom. The 0^{th} and 1^{st} diffraction orders form the two arms of the interferometer. A second diffraction grating is placed a distance, L, downstream, causing the arms of the interferometer to recombine an equal distance beyond the second diffraction grating. The atom wave function, $\psi(x)$, at the screen is given in [19] as

$$\psi(x) \propto u_1(x) + e^{i\phi_0} u_2(x) e^{ik_g x}, \tag{3.1}$$

where $u_1(x)$ and $u_2(x)$ are the real envelopes of the two arms, ϕ_0 is a relative phase, and $k_g = 2\pi/\lambda_g$. This wave function leads to the interference pattern,

$$I(x) \propto u_1(x)^2 + u_2(x)^2 + u_1(x)u_2(x)\cos(k_g x + \phi_0). \tag{3.2}$$

The phase, ϕ_0, depends on the arbitrary position of the coordinates at the screen, so that we can let $\phi_0 = 0$. If the two arms experience different interactions, an additional relative phase, $\Delta\phi$ will develop, leading to a shift in the interference fringes.

In [1], such an interferometer is used to measure the index of refraction of a gas of atoms for a matter wave. This is accomplished by placing a gas cell in the path of only one arm of

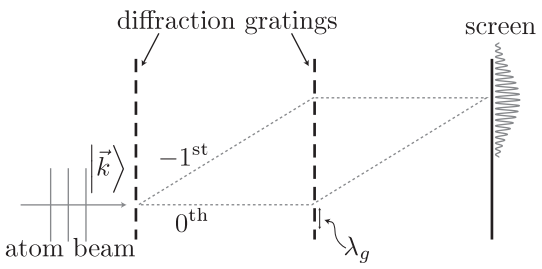

Figure 3-1: A Mach-Zender atom interferometer. Equally spaced diffraction gratings create two separated arms. The recombination of the arms at the position of the screen leads to an interference pattern. The frequency of the interference fringes is determined by the grating spacing. If the arms of the interferometer experience different interactions, the difference in the accumulated quantum mechanical phase shift in the two arms appears as a shift in the phase of the interference fringes.

the interferometer (Fig. 3-3). The relative phase acquired along the different paths of the interferometer is observed as a shift in the interference pattern that forms when the wave packets recombine [20, 21].

The appearance of interference fringes demonstrates that the free gas is able to act as a refracting medium for one arm of the interferometer, without a total loss of coherence. This is a remarkable feat, considering that any deflection of even a single atom in the gas would leave a disturbance that would eliminate the interference fringes entirely. Experimentally, however, interference fringes are observed, with a phase shift that can be on the order of π. In Sec. 3.2, we will examine how it is possible for the gas atoms to interact strongly enough with a coherent probe to cause the observed phase shift, without totally decohering the probe atom. First, we must introduce a formal description of decoherence in the Mach-Zender interferometer. This will direct us toward the aspects of the many-body scattering of the probe atom from the free gas that determine the decoherence in the atom interferometer.

3.1.2 Decoherence in an Interferometer

The separated arm atom interferometer exploits superposition by splitting the spatial wave function of an atom into two wave packets that can be made to travel along separate paths and experience different interactions. It takes advantage precisely of the ability of quantum systems to exist in superposition states. Such an apparatus is, consequently, a highly sensitive detector of decoherence. In the language of decoherence theory, the atom passing through the interferometer is the system, and the target it interacts with is the

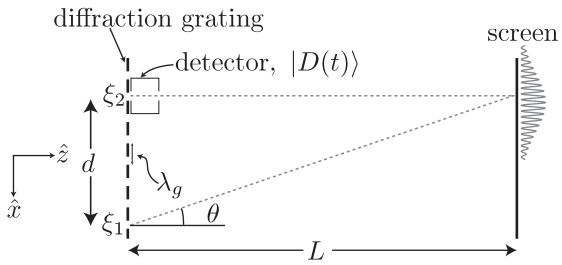

Figure 3-2: The second grating in the Mach-Zender interferometer. The separated paths of the probe wave function are depicted by dashed gray lines. The upper arm interacts with a detector, which evolves due to interactions with the probe. The lower arm is the first-order diffracted beam from the grating. An interference pattern forms at the position of the screen.

"environment". Entanglement with the state of the target is a which-way detection that causes decoherence and loss of fringe contrast when the arms of the interferometer are recombined [22].

Using the notation in [22], we will determine the decoherence due to interactions with a target placed in one arm of a Mach-Zender interferometer. This target serves as our which-way detector, and may be treated generically as a quantum mechanical system with some state, $|D(t)\rangle$. Fig. 3-2 shows the two arms of the interferometer at the position of the second grating. The upper arm interacts with the detector. The lower arm is the first-order diffracted beam from the grating. At time, t_1, a particle reaches the second grating. We will treat the particle wave function as emanating from the position of the center of the wave packets defining the arms of the interferometer. This point is $x = \xi_1$ for the lower arm, and $x = \xi_2$ for the upper arm. We will neglect changes to the z dependence of the particle, which we take to be traveling with constant momentum, $\hbar k$, between the grating and the screen. Then we need only consider x dependence of the probe particle. The initial state of the probe and detector is

$$|\psi(t_1)\rangle = \frac{1}{\sqrt{2}} \left(|\xi_1\rangle + |\xi_2\rangle\right) |D(t_1)\rangle \,. \tag{3.3}$$

The time at which the probe reaches the screen is t_2, with $\frac{mL}{\hbar k} = t_2 - t_1$. L is the distance between the second grating and the screen and m is the mass of the probe. We have treated the probe as moving with a constant speed in the z direction of $\frac{\hbar k}{m}$. The detector evolves in the absence of interactions with the probe into the state, $|D(t_2)\rangle = |D_1\rangle$. This is the

case in the event that the probe traverses the lower arm of the interferometer. In the event that the probe traverses the upper arm of the interferometer, there is some amplitude, S_{00}, associated with leaving the detector in an unchanged state. We must have the probability conservation relation,

$$|S_{00}|^2 + \left|\bar{S}_{00}\right|^2 = 1, \tag{3.4}$$

where $\left|\bar{S}_{00}\right|^2$ is the probability that the probe causes the detector to change state, aside from free evolution during its passage through the interferometer. We may express the state of the entire system at t_2 as

$$|\psi(t_2)\rangle = \frac{1}{\sqrt{2}}\left(U(t_2,t_1)\,|\xi_2\rangle\left(S_{00}\,|D_1\rangle + \bar{S}_{00}\,|D_2\rangle\right) + U(t_2,t_1)\,|\xi_1\rangle\,|D_1\rangle\right). \tag{3.5}$$

$U(t_2,t_1) = \exp(-iH(t_2-t_1)/\hbar)$ is the usual time propagator. $|D_2\rangle$ is the part of the final state of the detector which is orthogonal to $|D_1\rangle$. For the purposes of determining the decoherence, it is not necessary to explicitly write the entanglement of the probe state with the components of the detector state within $|D_2\rangle$. It is sufficient to recognize that the overlap $\langle D_2|D_1\rangle = 0$. The wave functions of the probe particle in the different arms of the interferometer are

$$\psi_1(x) = \langle x|\,U(t_2,t_1)\,|\xi_1\rangle \tag{3.6}$$

$$\psi_2(x) = \langle x|\,U(t_2,t_1)\,|\xi_2\rangle\,. \tag{3.7}$$

The interference pattern that appears on the screen is given by

$$I = \langle\psi(t_2)|x\rangle\,\langle x|\psi(t_2)\rangle \tag{3.8}$$

$$= \frac{1}{2}\left(|\psi_1(x)|^2 + |\psi_2(x)|^2\right) + \mathrm{Re}\left[S_{00}\,\psi_2(x)\psi_1^*(x)\right]. \tag{3.9}$$

The first two terms in parentheses give rise to an incoherent background, on top of which fringes due to the cross-term appear. The wave functions due to the upper and lower arms at time, t_2, are

$$\psi_j(x) = \sqrt{\frac{m}{2\pi i\hbar(t_2-t_1)}}\exp\left(\frac{im}{2\hbar}\frac{(x-\xi_j)^2}{t_2-t_1}\right). \tag{3.10}$$

Using these results the interference pattern gives

$$I(x) = |N|^2 \left(1 + \mathrm{Re}\left[S_{00} \exp\left(\frac{im}{2\hbar}\frac{1}{t_2 - t_1}\left(2x(\xi_1 - \xi_2) + \xi_2^2 - \xi_1^2\right)\right)\right]\right) \tag{3.11}$$

with $N = \sqrt{\frac{m}{2\pi i\hbar(t_2 - t_1)}}$. We may choose to set the origin of the x-axis midway between the two arms at the second diffraction grating. Then we have $\xi_1 = d/2$ and $\xi_2 = -d/2$. Using this choice of origin and $\frac{mL}{\hbar k} = t_2 - t_1$, allows us to simplify the expression for the interference pattern,

$$I(x) \propto 1 + \mathrm{Re}\left[S_{00} \exp(ik\frac{d}{L}x)\right]. \tag{3.12}$$

We have ignored the constant of proportionality, $|N|^2$, because we are primarily interested in the contrast of the interference fringes, which is unaffected by the overall scale of the interference pattern. The ratio $d/L = \tan(\theta)$ in the exponent is the tangent of the angle, θ, formed by the lower arm of the interferometer and the z-axis. For the first-order diffracted beam, the grating equation gives $k_g = k\sin(\theta)$, where $k_g = 2\pi/\lambda_g$, and λ_g is the grating spacing. The amplitude, S_{00}, associated with leaving the target untouched in its initial state is in general complex, so that $S_{00} = |S_{00}|\, e^{i\phi}$. Using this resolution of S_{00}, the interference pattern is

$$I(x) \propto 1 + |S_{00}| \cos(k_g x + \phi). \tag{3.13}$$

The phase shift, ϕ, of the fringes is due to interactions between the probe and target. We will revisit and determine this quantity from microscopic considerations of the scattering interaction of a probe atom from a thermal gas in Sec. 3.2. The decoherence of the probe particle in the interferometer causes the interference term in the interference pattern to be suppressed. We can define the contrast of the fringes as in [23] by

$$C = \frac{I_{\max} - I_{\min}}{I_{\max} + I_{\min}}. \tag{3.14}$$

Noting that $I_{\max} = 1 + |S_{00}|$ and $I_{\min} = 1 - |S_{00}|$, The contrast of the interference fringes is

$$C = |S_{00}|\,. \tag{3.15}$$

We will take advantage of this general relation in our treatment of the decoherence to due a free gas in an atom interferometer.

3.2 Decoherence due to a Free Gas

3.2.1 Introduction to the Free Gas as a Decohering Environment

We found in the previous section that the interaction between an atom in an interferometer with an environment leads to loss of fringe contrast due to the development of correlations between the state of the probe and the environment. In this section we consider the situation when a free gas is placed in one arm of the interferometer (Fig. 3-3). This configuration was used [1] to measure the index of refraction of a free gas for an atomic matter wave by causing a phase shift on the probe that is observable in the interference pattern. We seek to understand and calculate the decoherence, and corresponding loss of fringe contrast, due to the presence of the free gas.

Considering that the deflection of even a single gas atom due to scattering from the probe ought to cause a collapse of the interference fringes, we must ask, can a propagating atom run the gauntlet through a gas of free atoms, interacting with all of them at long range, and still remain coherent, leaving the quantum state of every gas atom unchanged? The answer is yes, much of the time, depending on gas density, propagation distance, atom-atom collision cross sections, etc. (the answer is no, however, if the force is Coulombic). If this were not the case, the measurement described in Sec. 3.1.1 [1] of the refractive index of a gas of atoms for an atomic matter wave would not have worked. Any collision that had disturbed the state of an atom in the gas cell would have been a which-way measurement that reduced the interference fringe contrast of the interferometer.

It is not correct to attribute, as in [1], the residual coherence in the interference signal to near-forward scattering. Here we describe the mechanism of the microscopic theory that determines the residual coherence of a matter wave undergoing scattering from a free gas. As collisions produce decoherence, we expect that the coherent part of the propagating wave should be determined using known atom-atom elastic quantum cross sections, computing the chance of avoiding a collision in the usual way. However, this leaves another question unanswered: if there is a large survival rate, avoiding any collisions, can the phase shift acquired by the coherent atom wave function be large compared to π?

It is well known that matter can act as a coherent, refracting medium for matter waves, as for example in the propagation of neutrons through condensed matter. In passing through a solid, neutrons may acquire large phase shifts relative to the vacuum and emerge coher-

ently; to wit, consider neutron diffraction from a crystal; the elastic diffractive spots are *prima facia* evidence of coherent scattering from the crystal. However solids are rather rigid compared to a low density gas, and it is therefore surprising perhaps that atoms passing through gaseous matter can also acquire large phase shifts without leaving a trace of their passing, since gas atoms are so easily perturbed. We will see that a low density gas is completely intolerant of any momentum transfer; momentum transfer will always lead to decoherence and reduction of interference fringe contrast.

Previous experiments, in which a free gas was placed in the path of one arm of such an interferometer [1], showed that, like light passing through glass, a matter wave passing through a dilute gas experiences a phase shift, with the dilute gas acting as a medium with an index of refraction for matter waves. When produced by propagation through a free gas, the phase shift of the interference fringes is a probe of the atom-atom interactions, and was the focus of much theoretical work [1, 24, 25]. These treatments build upon the multiple scattering theory derived in [3], and they neglect the possibility of recoil of the background atoms. Only the projectile is treated explicitly quantum mechanically. The background gas creates a background potential, and decoherence is obtained phenomenologically by averaging the resulting scattered projectile wave function over different realizations of the potential.

The fundamental source of decoherence in this system does not require an *ad hoc* averaging process. In order to properly understand the decoherence, however, we must take a substantial step beyond the case of a single particle scattering from a distribution of potential centers. It is imperative that we address the full many-body scattering problem, in which the background gas possesses a quantum mechanical state that is affected by scattering interactions with the projectile. This is critical because, in the absence of recoiling target particles, there would be no decoherence whatsoever that emerges naturally from the scattering theory. By eliminating the recoil of the targets, there remains no possibility of the gas recording the passage of the projectile and no which-way measurement.

Experiments have also been performed to measure the amount of decoherence experienced by an atom due to the scattering of photons from a laser [19, 26] and to the scattering of atoms in a free background gas [27, 23]. The decoherence is observed as a loss of contrast in the interference patterns formed.

The theoretical foundation of the analysis used to understand these experiments pos-

tulates that scattering events can be described as an instantaneous modification of the system-environment density matrix, $\rho_i \rightarrow \rho_f = T\rho_i T^\dagger$ [28]. The changes to the density matrix due to these scattering events may be explicitly added to the usual Heisenberg equation of motion. The additional term gives rise to decoherence of the system when the degrees of freedom of the environment are traced over. The effect on a quantum particle due to a gas environment, treated as a Markovian reservoir in which only two-body scattering is considered, has also been treated in a very general way by [29].

The physical mechanism by which decoherence occurs, however, remains hidden in the *ad hoc* addition to the purely coherent evolution of the density matrix. These explanations are incomplete because the decoherence phenomenon does not emerge directly as an outcome of the microscopic scattering process. In Sec. 3.1.2, we gave a general relationship between the decoherence and the S-matrix for scattering from a free gas. We will make this connection explicit here.

We wish to show the origin of the phase shift on an atom wave function due to scattering from other atoms. We also seek an explanation of the surprising lack of sensitivity of a free particle as a which-way detector based on microscopic multiple scattering theory. We will, therefore, calculate the reduction in interference fringe contrast due to the presence of a free gas interacting with only one arm of a separated arm atom interferometer. Our derivation shows how these processes emerge directly from microscopic quantum mechanical scattering and avoids the *ad hoc* modification of the Heisenberg equation of motion and the introduction of an average wave function. In fact, the coherent wave introduced in [3] *emerges* directly from our calculations, providing a justification for its use and bridging the gap in the literature between phenomenological results and the microscopic theory.

3.2.2 Paradox of Free Space Scattering without Decoherence

Standard scattering theory suggests a naïve argument that little or no coherence should remain after an atom passes through a column of gas. The usual expression for scattering in free space (in the center of mass frame) gives the wave function for the scattered atom as [6]

$$\psi(\vec{r}) = \frac{1}{(2\pi)^{3/2}} \left(e^{i\vec{k}\cdot\vec{r}} + f(\theta,\phi)\frac{e^{ikr}}{r} \right). \tag{3.16}$$

The first term on the right-hand side of this equation is the unscattered incident wave, which preserves coherence but has no phase shift. A phase shifted, coherent contribution cannot arise from this term. The second term on the right-hand side is the scattered wave, which corresponds to a momentum conserving recoil of the target gas atom, except when scattering into the exactly forward direction. Scattering into the infinitesimal solid angle around the forward direction occurs with zero probability. Any finite recoil changes the state of a free target gas atom and constitutes a which-way measurement that ought to eliminate the possibility of observing interference. Only an infinitesimal fraction of the incident beam would interact with the free gas atom and remain coherent. The rest is either not scattered at all or decoheres completely.

Nonetheless, the experimental results [1] clearly demonstrate that atoms in the beam do interact with the background gas coherently because the phase shift that results from the interaction is observable in the interference pattern. The beam atoms are able to "scatter" off of the free gas atoms and acquire a phase shift, without touching the free gas and changing its quantum state at all.

A better approach to understanding the phase shift and the decoherence is to enclose the target gas in a box, confining it in three dimensions. We may then treat the interactions between a projectile and a gas of confined particles. The projectile can be assumed to be unaffected by the walls of the box through which it passes, as we will eventually remove this artifice. The benefit of the box is immediate – there can be a finite amplitude associated with exactly "forward" scattering, in which the quantum state of the projectile and the target are unaffected by the interaction. A key point is that *this coherent amplitude automatically comes with a non-vanishing phase shift.* The argument of the complex amplitude gives rise to a phase shift, and its magnitude squared gives the probability of not disturbing the environment in any way, and thus leaving the system coherent. This result differs from free space scattering because there will in general be a finite flux of system atoms that acquire a phase shift and remain coherent. The coherent phase shift due to a single target atom will approach zero as the cross sectional area of the confining box is enlarged. This recalls the conundrum of (3.16); however, the phase shift does not vanish, even as the box is enlarged, if the column density of the gas remains constant. It is a crucial task here to consider this limit carefully.

We will solve the problem of scattering of a beam atom, the "system", or projectile, from

a gas of atoms, the "environment". The latter are confined to a three-dimensional box. The beam atom itself will be confined to a waveguide that overlaps the gas cell (Fig. 3-4). In this way, the transverse modes of the beam atom eigenstates are discrete, as are the modes in all three directions of the gas atoms. We will assume that the beam atom does not feel the confining wall that defines the length of the gas cell. We can then study the interactions that lead to phase shifts of the beam atom without changing the discrete state of the gas atoms. It is precisely this recoiless interaction that gives rise to the coherent wave.

The imposition of a cell and a waveguide are reasonable in the context of the experiments [1], where the gas was in fact confined to a cell. The cell was macroscopically large, however, so our results must not depend on the size of our cell. The relevant experimental parameter is the column density of the gas. When we consider the limit of large cell dimensions, we will choose the number of gas atoms correspondingly, so that the column density remains fixed. We will find that our results are independent of the dimensions of the waveguide and gas cell and only depend on the column density. In the limit where the cross section of the waveguide is very large, our results explain the coherent interactions in free space that cause a phase shift on the atom beam, while leaving the background atoms completely untouched.

3.2.3 Multiple Scattering Due to a Free Gas

In a dilute gas, any scattering event which leads to recoil of a target atom, placing it in an orthogonal state, leads also to complete decoherence of the two-arm projectile density matrix. The orthogonal target atom state constitutes which-way evidence and coherence cannot persist. To calculate the total decoherence, we need only calculate the amplitude of the many-particle state that remains unchanged by the interactions, other than the acquisition of a phase shift. This is equivalent to the result that we gave in Eq. (3.15). Over short enough distances traveled by the projectile, we may neglect multiple scattering altogether because the gas is dilute. If the projectile survives the interactions over a short distance by remaining in the initial state, then it is able to continue its journey toward the detector and scatter downstream. The projectile can have many sequential interactions with the gas atoms, so long as it remains in its initial state after each scattering event. In this way, it can accumulate a potentially large phase shift, even if the phase accumulated by a single scattering event is small. After passing through the entire cell, the amplitude of

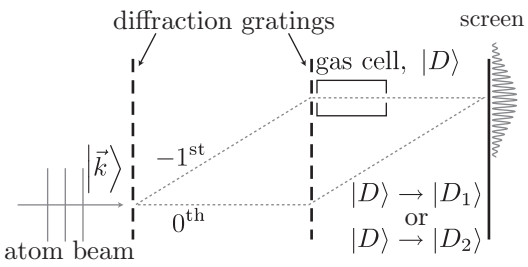

Figure 3-3: A Mach-Zender interferometer with the gas cell serving as a which-way detector. The atom beam is coherently split into the two arms of the interferometer by the leftmost diffraction grating. The initial state of the gas is $|D\rangle$, which evolves into $|D_1\rangle$ or $|D_2\rangle$ depending on whether an atom from the beam passes through the cell. An interference pattern forms on the screen at right where the arms overlap.

the initial state, which is coherent with the other arm of the interferometer, will also have been reduced due to scattering out of it.

Fig. 3-3 shows the experimental configuration we are considering. The projectile passes coherently through the upper and lower arms of the interferometer. A low pressure gas is present in the upper arm.

We model the upper arm as an overlapping waveguide and gas cell (Fig. 3-4). We discretize the transverse states of the projectile atom by requiring that its wave function satisfy periodic boundary conditions on the surface of the wave guide. Similarly the states of the N gas atoms are discretized by requiring that they satisfy periodic boundary conditions on all the surfaces of the gas cell. The projectile and target gas atoms are otherwise free. The Hamiltonian describing this $N+1$ particle system, in the absence of interactions, is H_o, with eigenstates $|k, \vec{n}\rangle$. The components of $\vec{n}$ are the $3N+2$ discrete quantum numbers describing the transverse state of the projectile and the states of the N target atoms. k is the initial longitudinal wave number of the projectile.

For a dilute gas we neglect interactions between target atoms. The interaction potential between the projectile and the targets is a sum of binary terms. The projectile is labeled as the 0^{th} particle, and the targets will be labeled 1 through N. The full interaction potential, V, is then

$$V = \sum_{i=1}^{N} V_{0i}. \tag{3.17}$$

V_{0i} gives the potential between the projectile and the i^{th} target, and the full Hamiltonian is $H = H_o + V$. We will take the projectile to be initially in an eigenstate of the waveguide.

Conservation of energy and momentum requires that if a target remains in its initial state, then so must the projectile.

The S-matrix connects the initial many body state, $|k, \vec{n}_0\rangle$, with the asymptotic output channel $|\psi\rangle$ [11],

$$|\psi\rangle = S\,|k, \vec{n}_0\rangle\,. \tag{3.18}$$

$|\psi\rangle$ is the many body state that emerges after interactions between the projectile and the gas are complete. We will refer to the diagonal element of the S-matrix that gives the $|k, \vec{n}_0\rangle$ component of $|\psi\rangle$ as $S_{0,0}$. This is the same quantity as that to which we referred in discussing decoherence in an interferometer in general in Sec. 3.1.2.

$$|\psi\rangle = S_{0,0}\,|k, \vec{n}_0\rangle + \text{orthogonal terms.} \tag{3.19}$$

The first term on the right hand side of (3.19) is the only part of $|\psi\rangle$ that interferes with the other arm of the interferometer. The probability of finding the system plus environment in this state is the probability that the system will remain coherent and interfere with itself. The contrast of the interference fringes will be reduced by the factor $|S_{0,0}|$ [22]. In order to calculate the amplitude of the coherent state after interactions with the gas, we need to calculate the $S_{0,0}$ matrix element. This task is facilitated by subdividing the gas cell into thin slabs, and computing the contributions to $S_{0,0}$ from each slab.

The volume of the gas cell can be thought of as the composition of many adjacent, thin slabs, which are the regions of space formed by the surface of the waveguide and two of its cross sections, placed a distance w apart, as in Fig. 3-4. Imagine subdividing the gas cell into N_s such regions, so that $l = N_s w$. If we number the slabs, $j = 1, 2, 3, \ldots$, beginning from the point of entry of the projectile into the gas cell, then slab j has the width and height of the waveguide, and runs from $z = (j-1)w$ to $z = jw$.

The total interaction potential can be rewritten in terms of the contribution from each slab,

$$V = \sum_{j=1}^{N_s} V^{(j)} = \sum_{j=1}^{N_s} \sum_{i=1}^{N} V_{0i}^{(j)}, \tag{3.20}$$

$$V_{0i}^{(j)} = V_{0i}\;\theta(\hat{z}_i - (j-1)w)\,\theta(jw - \hat{z}_i). \tag{3.21}$$

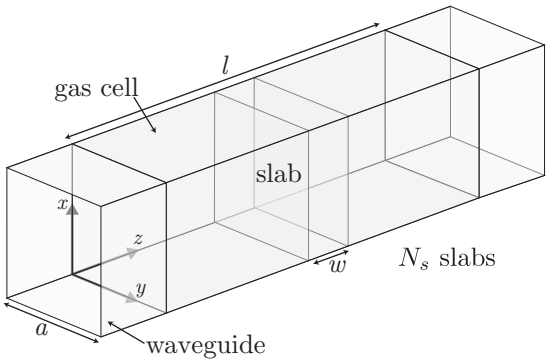

Figure 3-4: Details of the gas cell appearing in Fig. 3-3. The cell has length, l, and is embedded in a waveguide. The j^{th} slab, running from $z = (j-1)w$ to $z = jw$, is illustrated. The waveguide in which the projectile is confined is an infinite tube with a square cross section of dimensions, $a \times a$.

$\hat{z}_i$ is the z-position operator for the i^{th} target atom. $V^{(j)}$ picks out the contribution to the total interaction potential due to a particular region of space. Summing over these contributions, we obtain the original interaction potential.

For each $V^{(j)}$, we will define a corresponding $S^{(j)}$, which is the S-matrix due only to the interactions with the j^{th} slab. Beginning with the first slab, we can compute the scattered state due only to that slab. If we then use that result as the incident state to the subsequent slab (again removing all other slabs), the state we will obtain after N_s such iterations is

$$\left|\psi^{(N_s)}\right\rangle = S^{(N_s)} S^{(N_s-1)} \cdots S^{(1)} \left|k, \vec{n}_0\right\rangle . \tag{3.22}$$

$\left|\psi^{(N_s)}\right\rangle$ is different from $|\psi\rangle$ in general because the wave function at earlier slabs is unaffected by subsequent slabs. This excludes the possibility that the projectile could back scatter but be recovered into the incident state by scattering a second time from an earlier slab; however, for a dilute gas this process is negligible, so we may safely approximate $\left|\psi^{(N_s)}\right\rangle \approx |\psi\rangle$.

The decoherence, which causes the interference fringe contrast to be reduced, is due to the reduced amplitude of the initial many-body state. The phase shift that is measured as a spatial shift in the observed interference fringes is given by the argument of that amplitude. Equivalently, the magnitude of the overlap of the final states of the free gas associated with each arm gives the decoherence and the argument of the overlap gives the phase shift. We denote the state of the many body system by a single subscript, so that $|\phi_i\rangle = |k', \vec{n}\rangle$. The

initial state is $|\phi_0\rangle = |k, \vec{n}_0\rangle$. The $|\phi_0\rangle$ component of the scattered state after interactions with the gas is given by

$$S_{0,0}\,|\phi_0\rangle \approx S^{(N_s)}_{0,i_{n-1}} S^{(N_s-1)}_{i_{n-1},i_{n-2}} \ldots S^{(1)}_{i_1,0}\,|\phi_0\rangle \tag{3.23}$$

Repeated indices are implicitly summed over. The physical process that corresponds to each set of indices is scattering $|\phi_0\rangle \to |\phi_{i_1}\rangle \to |\phi_{i_2}\rangle \cdots \to \left|\phi_{i_{n-1}}\right\rangle \to |\phi_0\rangle$. When any of these intermediate states is not $|\phi_0\rangle$, we have argued that the projectile totally decoheres, so the contribution of these terms to the final coherent state amplitude can be neglected.

$$S_{0,0}\,|\phi_0\rangle \approx S^{(N_s)}_{0,0} S^{(N_s-1)}_{0,0} \ldots S^{(1)}_{0,0}\,|\phi_0\rangle\,. \tag{3.24}$$

The physical interpretation of this expression is that the probability amplitude for remaining in the initial state is reduced by each slab. Only this amplitude interferes with the other arm of the interferometer. $|S_{0,0}|^2$ is the probability that an atom in the beam will interfere with itself. The remaining fraction of the atomic beam contributes only to an incoherent background. The net result is that the interference fringe contrast is reduced by the factor $|S_{0,0}|$. The shift of the interference fringes compared to a vacuum is given by the argument of $S_{0,0}$.

We will now calculate these quantities by first calculating the $S^{(j)}_{0,0}$ matrix element due to scattering from a single slab. Then we may take the product in (3.24) to obtain $S_{0,0}$.

3.2.4 Calculation of the S-matrix

The S-matrix is the time evolution operator that takes a quantum state from the distant past, prior to a collision, into the distant future, after the collision; that is, $S = \lim_{t\to\infty} U(t, -t)$. In Sec. 2.2.6, we showed that it can be expressed in terms of the scattering matrix, T, as [30]

$$S = 1 - 2\pi i \delta(E - H_o)T, \tag{3.25}$$

where T is defined [31] by

$$T = V + \lim_{\epsilon\to 0} V \frac{1}{E - H_o + i\epsilon} T. \tag{3.26}$$

The limit will not appear in what follows; it is understood that we must take the small ϵ limit. V and H_o are the $N+1$ particle operators defined above. $S^{(j)}$ is the S-matrix due to the potential $V^{(j)}$. Replacing V with $V^{(j)}$ in the definition of T gives $T^{(j)}$. We calculate $S^{(j)}_{0,0}$ by expanding $S^{(j)}\left|k,\vec{n}_0\right\rangle$ to find the coefficient on its $\left|k,\vec{n}_0\right\rangle$ component,

$$S^{(j)}\left|k,\vec{n}_0\right\rangle = \left|k,\vec{n}_0\right\rangle - 2\pi i\delta(E-H_o)T^{(j)}\left|k,\vec{n}_0\right\rangle . \tag{3.27}$$

In order to extract the $\left|k,\vec{n}_0\right\rangle$ component of the second term in (3.27), we insert a complete set of eigenstates of H_o between the delta function and $T^{(j)}$,

$$\delta(E-H_o)T^{(j)}\left|k,\vec{n}_0\right\rangle = \int dk' \sum_{\vec{n}} \delta\left(E-E_{k',\vec{n}}\right)\left|k',\vec{n}\right\rangle\left\langle k',\vec{n}\right|T^{(j)}\left|k,\vec{n}_0\right\rangle . \tag{3.28}$$

The terms of the sum with $\vec{n}\neq\vec{n}_0$ are orthogonal to $\left|k,\vec{n}_0\right\rangle$. They do not contribute to $S^{(j)}_{0,0}$. It is only necessary to consider the term $\vec{n}=\vec{n}_0$. There, the argument of the delta function is considerably simplified due to the cancellation of the energy contribution of the discrete quantum numbers. In that case, $E-E_{k',\vec{n}_0}=\frac{\hbar^2k^2}{2m}-\frac{\hbar^2k'^2}{2m}$, where m is the mass of the projectile. The integral over k' can then be performed easily to find that the coefficient on the $\left|k,\vec{n}_0\right\rangle$ component of $S^{(j)}\left|k,\vec{n}_0\right\rangle$ is

$$S^{(j)}_{0,0} = 1 - i\frac{2\pi m}{\hbar^2 k}\left\langle k,\vec{n}_0\right|T^{(j)}\left|k,\vec{n}_0\right\rangle . \tag{3.29}$$

The net effect of the gas on the amplitude of the initial state is obtained according to (3.24) as the product of the individual slab results,

$$S_{0,0} \approx \prod_{j=1}^{N_s}\left(1 - i\frac{2\pi m}{\hbar^2 k}\left\langle k,\vec{n}_0\right|T^{(j)}\left|k,\vec{n}_0\right\rangle\right). \tag{3.30}$$

$T^{(j)}$ is the full scattering matrix due to a single slab, including multiple scattering within the slab. In a dilute gas, sequential scattering from different targets is unlikely within a slab that is much thinner than the length of the gas cell. Neglecting multiple scattering *within* single slabs, the $N+1$ particle matrix element of $T^{(j)}$ reduces to a sum of 2-particle matrix elements.

3.2.5 Approximation of the Many-body T-Matrix

In order to simplify the expression for $S_{0,0}$ in (3.30), we must extract single scattering events from the many-body T-matrix. In particular, we are interested in the diagonal matrix element in which the probe and all N targets are in their initial states, given by $|\chi\rangle$ and $|\phi_i\rangle$, respectively.

$$\langle T \rangle = \langle \chi, \phi_1, \ldots, \phi_N | \, T \, | \chi, \phi_1, \ldots, \phi_N \rangle \, . \tag{3.31}$$

The Hamiltonian is a sum of operators acting only on the Hilbert spaces of the indicated particles,

$$H = H_o + V = (H_0 + \cdots + H_N) + (V_{0i} + \cdots + V_{0N}). \tag{3.32}$$

Recall the definition [31] of the corresponding T-matrix is

$$T = V + V G_o T \tag{3.33}$$

$$G_o = \lim_{\epsilon \to 0} \frac{1}{E - H_o + i\epsilon} \tag{3.34}$$

We will introduce the operators $T_{01}, \ldots, T_{0N}$ that satisfy

$$T = \sum_{i=1}^{N} T_{0i} \tag{3.35}$$

$$T_{0i} = V_{0i} + V_{0i} G_o T_{0i} + \sum_{j \neq i} V_{0i} G_o T_{0j}. \tag{3.36}$$

It is only the third term on the right-hand side of (3.36) that contributes to multiple scattering. The expression for T_{0i} that excludes multiple scattering is

$$T_{0i} \approx V_{0i} + V_{0i} G_o T_{0i}. \tag{3.37}$$

This approximation of T_{0i} differs from the definition of the 2-particle scattering matrix, t_{0i}, by the replacement of the $N+1$-particle operator, G_o, with a 2-particle operator, g_{0i}.

$$t_{0i} = V_{0i} + V_{0i} \, g_{0i} \, t_{0i}, \tag{3.38}$$

$$g_{0i} = \lim_{\epsilon \to 0} \frac{1}{(E_0 + E_i) - (H_0 + H_i) + i\epsilon}. \tag{3.39}$$

Consider $i = 1$, and note that

$$\langle \phi_2, \ldots, \phi_N | \, T_{01} \, | \phi_2, \ldots, \phi_N \rangle \approx V_{01} + V_{01} \, g_{01} \, \langle \phi_2, \ldots, \phi_N | \, T_{01} \, | \phi_2, \ldots, \phi_N \rangle \, . \tag{3.40}$$

We have used

$$\langle \phi_2, \ldots, \phi_N | \, G_o = \langle \phi_2, \ldots, \phi_N | \, g_{01}. \tag{3.41}$$

(3.40) is identical to (3.38), so when multiple scattering is ignored, we can identify

$$t_{01} \approx \langle \phi_2, \ldots, \phi_N | \, T_{01} \, | \phi_2, \ldots, \phi_N \rangle \, . \tag{3.42}$$

This result is the same for any i. Summing the contributions due to each $\langle T_{0i} \rangle$ gives the approximation we desired

$$\langle T \rangle \approx \sum_{i=1}^{N} \langle \chi, \phi_i | \, t_{0i} \, | \chi, \phi_i \rangle \, . \tag{3.43}$$

$$\langle k, \vec{n}_0 | \, T^{(j)} \, | k, \vec{n}_0 \rangle \approx \sum_{i=1}^{N} \langle \chi, \varphi_i | \, t_{0i}^{(j)} \, | \chi, \varphi_i \rangle \, , \tag{3.44}$$

where χ designates the initial state of the projectile, φ_i designates the initial state of the i^{th} particle, and $t_{0i}^{(j)}$ is the scattering matrix for the 0^{th} and i^{th} particles without any other atoms present,

$$t_{0i}^{(j)} = V_{0i}^{(j)} + V_{0i}^{(j)} \frac{1}{E_0 + E_i - H_0 - H_i + i\epsilon} t_{0i}^{(j)}. \tag{3.45}$$

The expression for $S_{0,0}$, excluding multiple scattering within individual slabs, is

$$S_{0,0} \approx \prod_{j=1}^{N_s} \left(1 - i \frac{2\pi m}{\hbar^2 k} \sum_{i=1}^{N} \langle \chi, \varphi_i | \, t_{0i}^{(j)} \, | \chi, \varphi_i \rangle \right) . \tag{3.46}$$

This result gives the complex probability amplitude for the component of the projectile that remains coherent after interactions with the gas. We have explicitly taken into account multiple scattering. It remains to examine the limit in which the dimensions of the gas cell and waveguide become arbitrarily large. This will allow us to remove the artificial confinement depicted in Fig. 3-4. We find that the result is independent of the confinement and that a solution of the coherent wave equation emerges directly from these considerations, without invoking the concept of an average wave function [3]. Even for an arbitrarily large

cell, the projectile may remain partially coherent after scattering from a completely free gas. This resolves the conflict between the experimental results and our expectations based on the usual expression for scattering in free space.

The initial state of each target and the transverse states of the projectile appropriate to the waveguide and gas cell are box-normalized plane waves. Along the z direction, the projectile remains a free particle. $|\chi, \phi_i\rangle$ in (3.46) will be denoted using the wave vectors of the projectile and target as $\left|\vec{k}_0, \vec{k}_i\right\rangle$. The normalization of $\left|\vec{k}_0, \vec{k}_i\right\rangle$ reflects the free nature of the projectile along the longitudinal axis of the waveguide,

$$\left\langle \vec{r}_0, \vec{r}_i | \vec{k}_0, \vec{k}_i \right\rangle = \frac{e^{i\vec{k}_0 \cdot \vec{r}_0}}{a\sqrt{2\pi}} \frac{e^{i\vec{k}_i \cdot \vec{r}_i}}{a\sqrt{l}}. \tag{3.47}$$

When we convert this expression to center-of-mass coordinates, we must allocate the normalization constants,

$$\left\langle \vec{r}_{0i}, \vec{R}_{0i} | \vec{k}_{0i}, \vec{K}_{0i} \right\rangle = \frac{e^{i\vec{K}_{0i} \cdot \vec{R}_{0i}}}{a\sqrt{2\pi}} \frac{e^{i\vec{k}_{0i} \cdot \vec{r}_{0i}}}{a\sqrt{l}}, \tag{3.48}$$

$\vec{R}_{0i}$ is the center-of-mass coordinate and $\vec{r}_{0i} = \vec{r}_0 - \vec{r}_i$ is the relative coordinate of the 0^{th} and i^{th} particles. The center-of-mass momentum, $\vec{K}_{0i} = \vec{k}_0 + \vec{k}_i$, is normalized to the waveguide and the relative momentum, $\vec{k}_{0i} = \frac{m_i}{m+m_i}\vec{k}_0 - \frac{m}{m+m_i}\vec{k}_i$, is normalized to the dimensions of the gas cell. m is the mass of the projectile and m_i is the mass of the i^{th} target.

The potential $V_{0i}^{(j)}$ depends only on the relative coordinates of the projectile and i^{th} target, with the exception that it vanishes if the target coordinates lie outside of the j^{th} slab. When the range of the potential is much smaller than the width of the slab, this has the effect of limiting the domain of the matrix element $\left\langle \vec{k}_0, \vec{k}_i \right| V_{0i}^{(j)} \left| \vec{k}_0, \vec{k}_i \right\rangle$ to the j^{th} slab. As such, only when both particles are in the slab is there a contribution to the matrix element. This requires that the center-of-mass coordinate must also be in the slab. In principle, the domain of the relative coordinate that contributes to the matrix element depends on the position of the center-of-mass coordinate relative to the slab boundaries, but for local potentials we may take the domain of the relative coordinate $\vec{r}_{0i}$ to be all space, and replace $t_{0i}^{(j)}$ with t_{0i}. t_{0i} is obtained by replacing $V_{0i}^{(j)}$ with V_{0i} in (3.45). Using these assumptions, we can rewrite

$$\langle \chi, \varphi_i | \, t_{0i}^{(j)} \, | \chi, \varphi_i \rangle \approx \left\langle \vec{k}_{0i} \right| t_{0i} \left| \vec{k}_{0i} \right\rangle \left\langle \vec{K}_{0i} | \vec{K}_{0i} \right\rangle. \tag{3.49}$$

Taken over a slab, $\left\langle \vec{K}_{0i} | \vec{K}_{0i} \right\rangle = w/2\pi = l/(2\pi N_s)$. Substituting this result into (3.46)

gives,

$$S_{0,0} \approx \prod_{j=1}^{N_s} \left(1 - i \frac{2\pi m}{\hbar^2 k} \sum_{i=1}^{N} \left\langle \vec{k}_{0i} \right| t_{0i} \left| \vec{k}_{0i} \right\rangle \frac{l}{2\pi N_s} \right). \tag{3.50}$$

The expression under the product sign in (3.50) does not depend on the slab index j. We can express the matrix element of t_{0i} in terms of the forward scattering amplitude in the center of mass frame, $f(k_{0i}, 0)$, of the 0^{th} and i^{th} particles [9] and rewrite the sum over the particles as N times the average,

$$S_{0,0} \approx \left(1 + i\, 2\pi \frac{N}{a^2} \frac{1}{N_s} \left\langle \frac{f(k_{0i}, 0)}{\mu_{0i} k/m} \right\rangle \right)^{N_s}. \tag{3.51}$$

$N/a^2 = \rho\, l$ is the column density of the gas. We have explicitly written μ_{0i} to indicate the reduced mass for each combination of the projectile and a target. In the case of a target gas comprised of a single species of atom, we will write μ for the reduced mass. The situation in which the projectile velocity dominates the target velocities permits us to simplify, $k_{0i} \approx (\mu/m)\, k$ [25, 32]. As the number of slabs becomes large, and the width of each slab becomes small compared to the length of the gas cell, $S_{0,0}$ approaches

$$S_{0,0} \approx \exp \left(i 2\pi \rho l \left\langle \frac{f(k_{0i}, 0)}{k_{0i}} \right\rangle \right). \tag{3.52}$$

We may take the dimensions of the waveguide and gas cell to be arbitrarily large under the condition that we also choose the number of target atoms so that the column density remains fixed. Eq. (3.52) is valid in this free space limit, and gives precisely a solution of the coherent wave equation when we take the incident projectile wave function to be a plane wave.

This central result accounts completely for the phase shift and persistence of coherence after multiple scattering with a dilute, many-body quantum mechanical target of free particles. The probability of remaining in the coherent state decays as $|S_{0,0}|^2 = e^{-\rho\sigma l}$, where σ is the average quantum mechanical scattering cross section,

$$\sigma = \left\langle \frac{4\pi}{k_{0i}} \text{Im}\left[f(k_{0i}, 0) \right] \right\rangle. \tag{3.53}$$

The cross section is proportional to the imaginary part of the forward scattering amplitude,

whereas the phase shift of the interference fringes is proportional to the real part,

$$\Delta\phi = \left\langle \frac{2\pi}{k_{0i}} \rho l \,\mathrm{Re}\left[f(k_{0i}, 0)\right] \right\rangle. \tag{3.54}$$

The ratio of the real and imaginary parts of the forward scattering amplitude, which is directly measured in interferometric measurements such as [1], characterizes the extent that the interference pattern can be shifted before it is washed out due to decoherence. For weak interactions – the typical situation in interferometry – the real part of the forward scattering amplitude is proportional to the interaction potential, V, whereas the imaginary part is second order in V, as we show in Sec. 3.2.6.

3.2.6 Dependence of the Phase Shift and Decoherence on the Interaction Potential Strength

We seek the dependence of the real and imaginary parts of the forward scattering amplitude, $f(k_{0i}, 0)$, on the interaction potential, V_{0i}, between the projectile and the i^{th} target. This may be accomplished by relating the scattering amplitude to the two-body scattering matrix, t_{0i}, defined in (3.38), [9]

$$\left\langle \vec{k}_{0i} \right| t_{0i} \left| \vec{k}_{0i} \right\rangle = \frac{-2\pi\hbar^2}{\mu a^2 l} f(k_{0i}, 0) \tag{3.55}$$

$f(k_{0i}, 0)$ is the forward scattering amplitude in the center of mass frame of the projectile and target. μ is the reduced mass, a and l are the previously defined dimensions of the gas cell, and k_{0i} is the relative wave vector. Expanding t_{0i} in a Dyson series to second order gives

$$t_{0i} \approx V_{0i} + V_{0i} g_{0i} V_{0i}. \tag{3.56}$$

Separating the real and imaginary parts of the two-body Green's function, g_{0i}, gives [33]

$$g_{0i} = \mathrm{P} \frac{1}{(E_0 + E_i) - (H_0 + H_i)} - i\pi\delta((E_0 + E_i) - (H_0 + H_i)). \tag{3.57}$$

Substituting this result into (3.56), we find that the real part of the two-body scattering matrix is first order in V_{0i}, whereas the imaginary part is second order,

$$\mathrm{Re}\,[t_{0i}] \approx V_{0i} \tag{3.58}$$

$$\mathrm{Im}\,[t_{0i}] \approx -\pi V_{0i}\delta((E_0+E_i)-(H_0+H_i))V_{0i}. \tag{3.59}$$

Therefore, $\mathrm{Im}\,[f(k_{0i},0)]$ is a factor of the interaction potential smaller than $\mathrm{Re}\,[f(k_{0i},0)]$.

Consequently, the phase shift acquired by the projectile can be made large by increasing the column density of the gas, while the loss of contrast,

$$1-|S_{0,0}| \approx 2\pi\rho l\,\mathrm{Im}\left\langle \frac{f(k_{0i},0)}{k_{0i}} \right\rangle \propto V^2, \tag{3.60}$$

remains smaller by a factor of the interaction strength. The difference in the dependence on the interaction strength clarifies the ability of a seemingly sensitive, free gas to generate a large phase shift on a projectile wave function due to scattering. This occurs essentially without loss of contrast if the target gas is sufficiently dilute and weakly interacting with the projectile.

3.2.7 Low Energy Projectile: Pseudopotential

It is well known that a collection of potential centers, which are assumed to form a uniform medium in a thin slab, can give rise to an index of refraction for matter waves [2]. Furthermore, [3] has shown that a finite collection of scattering centers can, when the scattered waves are appropriately averaged, act as a medium. The scattered wave is the so-called coherent wave, which suffers attenuation due to the averaging process. We have shown here that even a finite collection of recoiling quantum mechanical particles in free space can act as a refractive medium. In addition, decoherence is a natural consequence of entanglement with the target particles.

In order to illustrate the broader context of our results, it is instructive to compare the phase shift we obtain for a special case of the interaction potential with the well-known results of pure potential scattering. When the projectile is moving slowly relative to the target atoms, only s-wave scattering needs to be considered, and we can model the

interaction as a contact potential,

$$V_{0i} = V_o\,\delta(\vec{r}_0 - \vec{r}_i). \tag{3.61}$$

Recall that the coefficient on the coherent state after interactions is given by

$$S_{0,0} \approx \prod_{j=1}^{N_s}\left(1 - 2\pi i\frac{m}{\hbar^2 k}\sum_{i=1}^{N}\langle\chi,\phi_i|\,T_{0i}^{(j)}\,|\chi,\phi_i\rangle\right). \tag{3.62}$$

For weak potentials, we may approximate $T_{0i}^{(j)}$ to first order in a Dyson series expansion as

$$T_{0i}^{(j)} \approx V_{0i}^{(j)}. \tag{3.63}$$

The matrix element $\langle\chi,\phi_i|\,V_{0i}^{(j)}\,|\chi,\phi_i\rangle$ is readily computed using box normalized plane waves as before,

$$\langle\chi,\phi_i|\,V_{0i}^{(j)}\,|\chi,\phi_i\rangle = \frac{V_o}{2\pi a^2}\frac{1}{N_s}. \tag{3.64}$$

Substituting (3.64) into (3.62) gives

$$S_{0,0} \approx \exp\left(i\frac{2\pi}{k}\left(\frac{-mV_o}{2\pi\hbar^2}\right)\rho l\right). \tag{3.65}$$

$S_{0,0}$ is a pure phase factor in this approximation. The gas acts as a medium with an index of refraction for the projectile matter wave, producing a phase shift $\phi = \frac{2\pi}{k}\left(\frac{-mV_o}{2\pi\hbar^2}\right)\rho l$.

This may be compared directly with the the calculation shown in Sec. 2.4.1 [2] that ignores the quantum state of the gas atoms and treats them as potential centers. There we found the index of refraction, n_r. Designating the density of the scatterers as ρ, and noting that the scattering length, $a_0 = -C_0$, we find that the corresponding phase shift is

$$\phi = (n_r - 1)kl = -\frac{2\pi}{k}a_o\rho l, \tag{3.66}$$

where the scattering length a_o can be determined from the solution to the delta potential scattering problem [17],

$$a_o = \frac{mV_o/(2\pi\hbar^2)}{1 + ikmV_o/(2\pi\hbar^2)} \approx mV_o/(2\pi\hbar^2). \tag{3.67}$$

The approximation of a_o is valid under the same conditions as our expansion of the T-matrix. The first order term in (3.62) gives precisely the result for the phase shift that is obtained due to potential scattering. If we were to keep terms up to second order in the expansion of $T_{0i}^{(j)}$, $S_{0,0}$ would also reduce the amplitude of the coherent state, giving rise to decoherence.

Chapter 4

Ultracold atoms in an Optical Lattice

4.1 Physics of the Optical Lattice

4.1.1 AC Stark Shift and the Lattice Potential

In this section, we will show the origin of the lattice potential that arises from the interaction of a standing wave laser field with a two-level atom, which is shown schematically in Fig. 4-1 [34, 35]. A pair of counter-propagating traveling wave lasers gives rise to a standing wave electric field,

$$\boldsymbol{E} = \boldsymbol{\varepsilon}(\boldsymbol{r})e^{-i\omega_L t} + \boldsymbol{\varepsilon}^*(\boldsymbol{r})e^{i\omega_L t}. \tag{4.1}$$

ω_L is the radial frequency of the light. Let us consider a two-level atom with ground state, $|1\rangle$, and excited state, $|2\rangle$, whose energy exceeds the ground state by the amount, $\hbar\omega_0$. The interaction of the laser light with the atom is given by the dipole interaction, $V = -\boldsymbol{d}\cdot\boldsymbol{E}$, where $\boldsymbol{d} = q_e\boldsymbol{r}$ is the dipole moment operator and q_e is the charge of the electron. The Hamiltonian for the two level atom interacting with the laser light is

$$H = H_0 + V = |2\rangle\langle 2|\,\hbar\omega_0 - \boldsymbol{d}\cdot\boldsymbol{E}. \tag{4.2}$$

The diagonal matrix elements of the dipole moment vanish. Along the direction of the electric field at the position of the atom, we define the off-diagonal dipole moment to be

$$\mu = \langle 2| \hat{d}_{\boldsymbol{E}} |1\rangle \tag{4.3}$$

$$\mu^* = \langle 1| \hat{d}_{\boldsymbol{E}} |2\rangle . \tag{4.4}$$

In terms of this quantity, the Hamiltonian for the two-level atom is

$$H = \hbar\omega_0 |2\rangle \langle 2| - (|1\rangle \langle 2| \mu^* + |2\rangle \langle 1| \mu)(\varepsilon(\boldsymbol{r})e^{-i\omega_L t}\varepsilon^*(\boldsymbol{r})e^{i\omega_L t}). \tag{4.5}$$

We can eliminate the time dependence in this Hamiltonian by switching to a rotating frame. A wave vector, $|\psi\rangle$, in the stationary frame is related to a wave vector in the rotating frame, $|\tilde{\psi}\rangle$, by

$$|\psi\rangle = U|\tilde{\psi}\rangle; \tag{4.6}$$

$$U = e^{-i\omega_L t|2\rangle\langle 2|}. \tag{4.7}$$

Likewise, the Hamiltonian in the rotating frame is given by

$$\tilde{H} = U^{-1}HU - i\hbar U^{-1}\frac{\partial}{\partial t}U. \tag{4.8}$$

Expanding this expression for the Hamiltonian in the rotating frame gives

$$\tilde{H} = -\hbar\Delta |2\rangle \langle 2| - (\hbar\Omega |2\rangle \langle 1| + \hbar\Omega^* |1\rangle \langle 2| + \mu^*\varepsilon |1\rangle \langle 2| e^{-2i\omega_L t} + \mu\varepsilon^* |2\rangle \langle 1| e^{2i\omega_L t}), \tag{4.9}$$

where we have introduced the Rabi frequency, $\Omega = \mu\varepsilon/\hbar$, and the detuning, $\Delta = \omega_L - \omega_0$. Here, we make the usual rotating wave approximation and discard the the rapidly oscillating terms, leaving

$$\tilde{H} = -\hbar\Delta |2\rangle \langle 2| - \hbar\Omega |2\rangle \langle 1| - \hbar\Omega^* |1\rangle \langle 2| ; \tag{4.10}$$

$$\tilde{H} = -\hbar \begin{pmatrix} 0 & \Omega^* \\ \Omega & \Delta \end{pmatrix}. \tag{4.11}$$

The off-diagonal terms in this Hamiltonian, due to the interaction of the two-level atom with the radiation field, induce mixing of the two free levels of the atom. The eigenvalues of this Hamiltonian are

$$\tilde{E} = -\hbar\frac{\Delta}{2} \pm \frac{\hbar}{2}\sqrt{\Delta^2 + 4\left|\Omega\right|^2}. \tag{4.12}$$

Consider that when the Rabi frequency is small compared to the detuning, $|\Omega| \ll \Delta$, the energies of the new eigenstates of the atom, including interactions with the light, are

$$\tilde{E} \approx \begin{cases} \frac{\hbar|\Omega|^2}{\Delta} & (+) \\ -\hbar\Delta - \frac{\hbar|\Omega|^2}{\Delta} & (-) \end{cases} \tag{4.13}$$

Let us disregard for the moment the normalization and write a set of eigenvectors of $\tilde{H}$,

$$|-\rangle = \left(-\frac{\Delta}{2\Omega} + \frac{1}{2\Omega}\sqrt{\Delta^2 + 4|\Omega|^2}\right)|1\rangle + |2\rangle \tag{4.14}$$

$$|+\rangle = \left(-\frac{\Delta}{2\Omega} - \frac{1}{2\Omega}\sqrt{\Delta^2 + 4|\Omega|^2}\right)|1\rangle + |2\rangle\,. \tag{4.15}$$

Examining these expressions under the same condition as above, a Rabi frequency that is small compared to the detuning, we see that $|-\rangle$ corresponds to the original excited state, $|2\rangle$, and $|+\rangle$ to the ground state, $|1\rangle$. In the $|\pm\rangle$ basis, the Hamiltonian is approximately

$$\tilde{H} = \begin{pmatrix} \frac{\hbar|\Omega|^2}{\Delta} & 0 \\ 0 & -\hbar\Delta - \frac{\hbar|\Omega|^2}{\Delta} \end{pmatrix}. \tag{4.16}$$

Treating the eigenvectors of the light-atom Hamiltonian approximately as the original basis, we may undo the rotating frame transformation

$$H = U\left(\tilde{H} + i\hbar U^{-1}\frac{\partial}{\partial t}U\right)U^{-1} \tag{4.17}$$

$$H = \hbar\omega_0\left|2\right\rangle\left\langle 2\right| - \hbar\frac{\left|\Omega\right|^2}{\Delta}\left|2\right\rangle\left\langle 2\right| + \hbar\frac{\left|\Omega\right|^2}{\Delta}\left|1\right\rangle\left\langle 1\right|. \tag{4.18}$$

In the large detuning regime that we have specified, in which we may neglect excitations out of the ground state, we find that the effect of the light field is to cause a shift in the energy of the atom, $\hbar\left|\Omega\right|^2/\Delta$, as depicted in Fig. 4-1. The light, therefore, creates a conservative potential for the atom. Recall that the Rabi frequency is proportional to the amplitude of the electric field, so the shift in the energy is proportional to the intensity of the electric field.

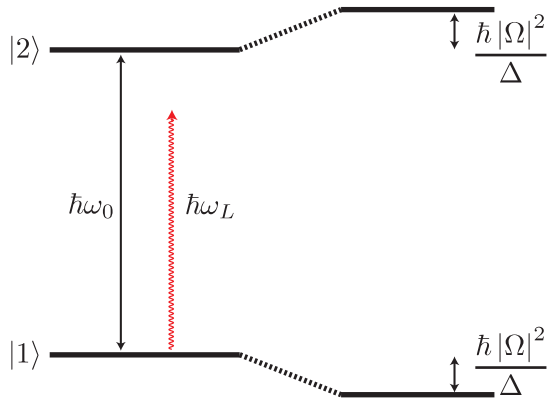

Figure 4-1: Model of a two level atom with resonance frequency, ω_0, interacting with a light field of frequency, ω_L. The Rabi frequency, proportional to the intensity of the light, is Ω, and the detuning is Δ. Here we have shown the case in which the light is red detuned from the resonance ($\Delta < 0$), which causes the atom to be attracted to the anti-nodes of the laser.

Typically, the laser field is a Gaussian beam with a standing wave along one dimension, x. When the laser is red detuned from the transition, $\Delta < 0$, the energy of the atom is shifted downward in locations where the intensity of the light is peaked. Thus the atoms will be drawn to the longitudinal axis of the beam, and will see potential minima at the anti-nodes of the standing wave. Along the axis of the laser, the potential is given by

$$V(x) = V_0 \sin^2(k_L x), \tag{4.19}$$

where $k_L = 2\pi/\omega_L$ is the wave number of the laser. The wells of this potential form a one-dimensional lattice, with a spacing between sites, $d = \pi/k_L$. Higher dimensional lattices can be constructed by including additional counter-propagating pairs of lasers along the other axes.

4.2 Solutions of the Schrödinger Equation in the Optical Lattice

4.2.1 Bloch Waves: Single Particle Eigenstates of the Lattice

The Hamiltonian for an atom interacting with the optical lattice potential in one-dimension is

$$H = -\frac{\hbar^2}{2m}\frac{\partial^2}{\partial x^2} + V_0 \sin^2(\pi x/d). \tag{4.20}$$

This Hamiltonian is periodic, and it will have Bloch wave solutions [36, 37]. In order to review the general properties of the solutions of the lattice Hamiltonian, we introduce the displacement operator, $\hat{D}_\xi$ [38], defined by

$$\hat{D}_\xi \psi(x) = \psi(x - \xi); \tag{4.21}$$

$$\hat{D}_\xi = e^{-i\hat{k}\xi}. \tag{4.22}$$

The periodicity of the Hamiltonian requires that its eigenfunctions also be eigenfunctions of $\hat{D}_\xi$, with $\xi = d$. The eigenfunctions of the displacement operator are also momentum eigenfunctions,

$$\hat{D}_\xi \left|k\right\rangle = e^{ikx} \left|k\right\rangle. \tag{4.23}$$

Evidently, any state, $|k + 2\pi j/\xi\rangle$, separated from the momentum, k, by an integer multiple, j, of $2\pi/\xi$ is also an eigenstate of the displacement operator, with the same eigenvalue as $|k\rangle$. Any range of momenta of width, $2\pi/\xi$, generates all the unique eigenvalues of the displacement operator. In particular, the range around $k = 0$ given by $-\pi/\xi < k \leq \pi/\xi$, the first Brillouin zone, generates all of the eigenvalues of $\hat{D}_\xi$. For our one-dimensional optical lattice, we have $-\pi/d < k \leq \pi/d$, or equivalently, $-k_L < k \leq k_L$, for the first Brillouin zone.

The degenerate eigenfunctions of the displacement operator with eigenvalue, $\exp(-ik\xi)$, have the form

$$f_k(x) = e^{i\left(k + \frac{2\pi j}{\xi}\right)x}. \tag{4.24}$$

We may create arbitrary superpositions of these to produce a general eigenfunction

$$g_k(x) = \sum_{j=-\infty}^{\infty} c_j e^{i\left(k+\frac{2\pi j}{\xi}\right)x} \tag{4.25}$$

$$= e^{ikx}u(x), \tag{4.26}$$

where $u(x)$ can be any function that has period, ξ, and c_j is a complex coefficient. Any such function, $g_k(x)$, is a Bloch wave solution of the optical lattice potential. The periodicity of $u(x)$ will impose a discrete index, n, on the choices of this function. In general, we designate the Bloch wave by

$$\psi_{n,k}(x) = e^{ikx}u_n(x). \tag{4.27}$$

Here k is a continuous value giving the quasimomentum of the Bloch wave, and the index, n, is the band number.

So far, we have considered an optical potential that extends over an infinite region. Any realistic experimental implementation of this potential, however, is necessarily finite. This raises the issue of how to treat the boundary conditions at the edges of a finite lattice. Fortunately, as the size of the lattice grows, we expect the importance of the particular boundary conditions on the lattice to become less important. A common choice, which we will employ, are the Born-von Karman boundary conditions, in which we insist on periodic boundary conditions at the edges of the lattice. Suppose we have a lattice with N_L sites. Our boundary conditions then are

$$\psi_{n,k}(x) = \psi_{n,k}(x + N_L d); \tag{4.28}$$

$$e^{ikN_L d} = 1. \tag{4.29}$$

The second line is obtained by substituting the form of the Bloch wave given in (4.27) into the first line. There are N_L unique solutions of $\exp(iN_L kd) = 1$ for k, given by

$$k = \frac{2\pi}{N_L d} j, \tag{4.30}$$

where j is any integer between 0 and $N_L - 1$. The fundamental reciprocal lattice vector of this one-dimensional lattice is $G = 2\pi/d$. In terms of G, the discrete, acceptable quasimomenta

that satisfy the Born-von Karman boundary conditions are

$$k = G\frac{j}{N_L}. \tag{4.31}$$

The range of values of the quasimomentum, k, that satisfy the boundary conditions covers the width of a Brillouin zone. The discrete values of k represent N_L equally spaced points subdividing this zone. We may just as well choose these points such that they lie within the first Brillouin zone.

It is straightforward to extend these solutions to multiple dimensions, in which case the Bloch wave is

$$\psi_{n,\boldsymbol{k}}(\boldsymbol{r}) = e^{i\boldsymbol{k}\cdot\boldsymbol{r}}u_n(\boldsymbol{r}). \tag{4.32}$$

We normalize the Bloch wave, $\psi_{n,\boldsymbol{k}}(\boldsymbol{r})$ to unity over a unit cell of the lattice, so that over the entire lattice,

$$\int_{\text{lattice}} d^3r\, \psi^*_{n',\boldsymbol{k}'}(\boldsymbol{r})\psi_{n,\boldsymbol{k}}(\boldsymbol{r}) = N_L\, \delta_{n,n'}\, \delta_{\boldsymbol{k},\boldsymbol{k}'}. \tag{4.33}$$

4.2.2 Wannier Functions: States at a Particular Lattice Site

Eventually, we would like to be able to discuss a model of the lattice in which we specify how many atoms are at a particular site. A single atom wave function representing an atom at a particular site is given by the Wannier function, $w_n(\boldsymbol{r})$, [39]

$$w_n(\boldsymbol{r}-\boldsymbol{R}) = \frac{1}{N_L}\sum_{\boldsymbol{k}} e^{-i\boldsymbol{k}\cdot\boldsymbol{R}}\psi_{n,\boldsymbol{k}}(\boldsymbol{r}), \tag{4.34}$$

where $\boldsymbol{R}$ is the lattice site around which the Wannier function is localized [40, 41], and the sum is over the quasimomenta in the first Brillouin zone. Notice that each band of the lattice has a specific Wannier function. Treating the physics of ultracold atoms in the optical lattice, in which we discard the possibility of excitations out of the lowest band of the lattice, we will only require $w_0(\boldsymbol{r})$. This function serves our purpose of an on-site atom wave function because of the orthogonality of the Wannier functions that are centered on different lattice sites,

$$\int_{\text{lattice}} d^3r\, w^*_n(\boldsymbol{r}-\boldsymbol{R})w_{n'}(\boldsymbol{r}-\boldsymbol{S}) = \delta_{n,n'}\, \delta_{\boldsymbol{R},\boldsymbol{S}}. \tag{4.35}$$

Moreover, the Wannier functions are complete,

$$\sum_{n,\boldsymbol{R}} w_n^*(\boldsymbol{r}' - \boldsymbol{R}) w_n(\boldsymbol{r} - \boldsymbol{R}) = \delta(\boldsymbol{r} - \boldsymbol{r}'), \tag{4.36}$$

so we can construct arbitrary states in the lattice by sums of Wannier functions at each of the lattice sites.

4.2.3 Exact Eigenfunctions of the Optical Lattice Hamiltonian

The exact eigenfunctions of the Hamiltonian (4.20) for an atom interacting with the light field of the optical lattice are the known Mathieu functions [42, 43]. Mathieu's equation is given generically by

$$\frac{\partial^2}{\partial w^2}\psi(w) + \pi^2 \left(a - 2q\cos(2\pi w)\right)\psi(w) = 0. \tag{4.37}$$

The even and odd solutions for $\psi(w)$ in this equation are denoted, $\mathrm{ce}(a, q, \pi w)$ and $\mathrm{se}(a, q, \pi w)$, respectively. The optical lattice eigenvalue equation is

$$\frac{\hbar^2}{2m}\frac{\partial^2}{\partial x^2}\psi(x) + (E - V_0 \sin^2(\pi x/d))\psi(x) = 0. \tag{4.38}$$

This eigenvalue equation is equivalent to Eq. (4.37) under the identifications, $w = x/d$, $a = E - s/2$, $q = -s/4$, $s = V_0/E_r$, and $E_r = \hbar^2 k_L^2/(2m)$. The coordinate w is the position in units of the lattice spacing, d. s is the depth of the lattice in units of the photon recoil energy, E_r, of an atom of mass, m. Using these relations, the eigenfunctions of the lattice Hamiltonian are

$$\begin{array}{ll} \mathrm{ce}\left(a, \frac{-V_0}{4E_r}, k_L x\right) & \text{(even)} \\ \mathrm{se}\left(a, \frac{-V_0}{4E_r}, k_L x\right) & \text{(odd).} \end{array} \tag{4.39}$$

In terms of the generic parameters a and q, the solutions to the Mathieu equation are periodic only for characteristic values of $a = a(r, q)$ (for the even solution) and $a = b(r, q)$ (for the odd solution) [43]. $a(r, q)$ is a multivalued function that implicitly depends on the band number, n. r is a rational number that allows us to construct the relation

$$e^{\mp ir\pi w} f(\pi w) = \mathrm{ce}(a(r, q), q, \pi w) \pm i\,\mathrm{se}(b(r, q), q, \pi w), \tag{4.40}$$

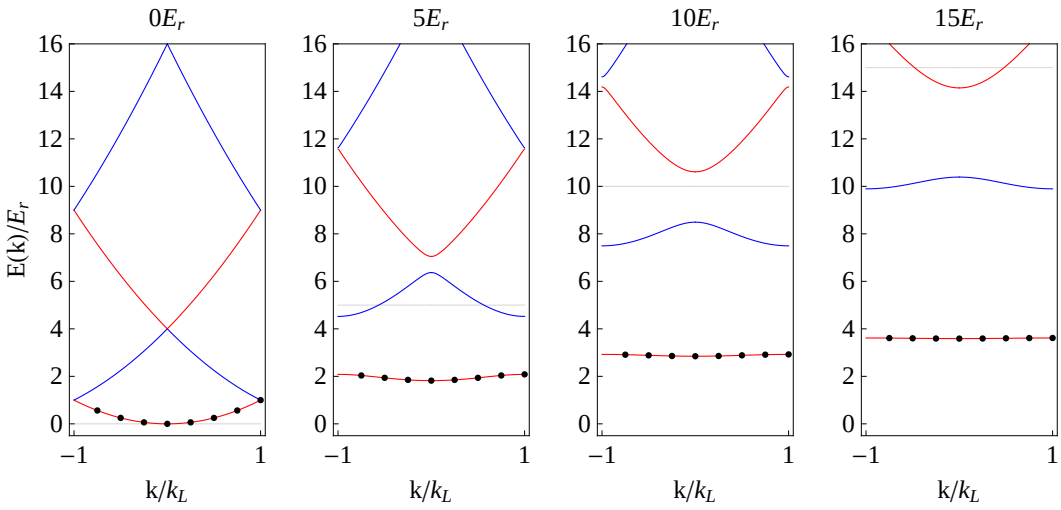

Figure 4-2: Band diagrams for the optical lattice. The energy of the Bloch waves in the first Brillouin zone are shown for the first few bands of the lattice as a function of the quasimomentum for lattice depths, $V_0 = 0, 5, 10,$ and, 15. The black dots in the lowest band indicate the discrete quasimomenta permitted by the Born von-Karman boundary conditions for a lattice with $N_L = 8$ sites. The light gray line shows the lattice depth.

where $f(\pi w)$ is a function that has a periodicity of one. If we note that $r\pi w = (rk_L)x$, we see that r is simply the quasimomentum of the Bloch wave solution in units of the laser wave number, k_L. The relationship between a and the energy, E,

$$a = a\left(\frac{k}{k_L}, -\frac{V_0}{4E_r}\right) = E - \frac{V_0}{2E_r}, \tag{4.41}$$

gives the relationship between the energy of an eigenfunction and its quasimomentum, in each band. We show this energy band diagram for several choices of the lattice depth, V_0, in Fig. 4-2.

In studying the dynamics of ultracold atoms in the optical lattice, we will constrain ourselves to the lowest band of the lattice. The Bloch wave solutions in this band are

$$\psi_{0,r} = \begin{cases} \mathrm{ce}(a(r,q),q,w) + i\,\mathrm{se}(b(r,q),q,w); & r < 0 \\ \mathrm{ce}(a(r,q),q,w) - i\,\mathrm{se}(b(r,q),q,w); & r > 0 \\ \mathrm{ce}(a(r,q),q,w); & r = 0 \end{cases} . \tag{4.42}$$

We plot these Bloch waves for three of the points in the lowest band in Fig. 4-3.

Using the definition given in Eq. (4.34), we can construct the Wannier function for the

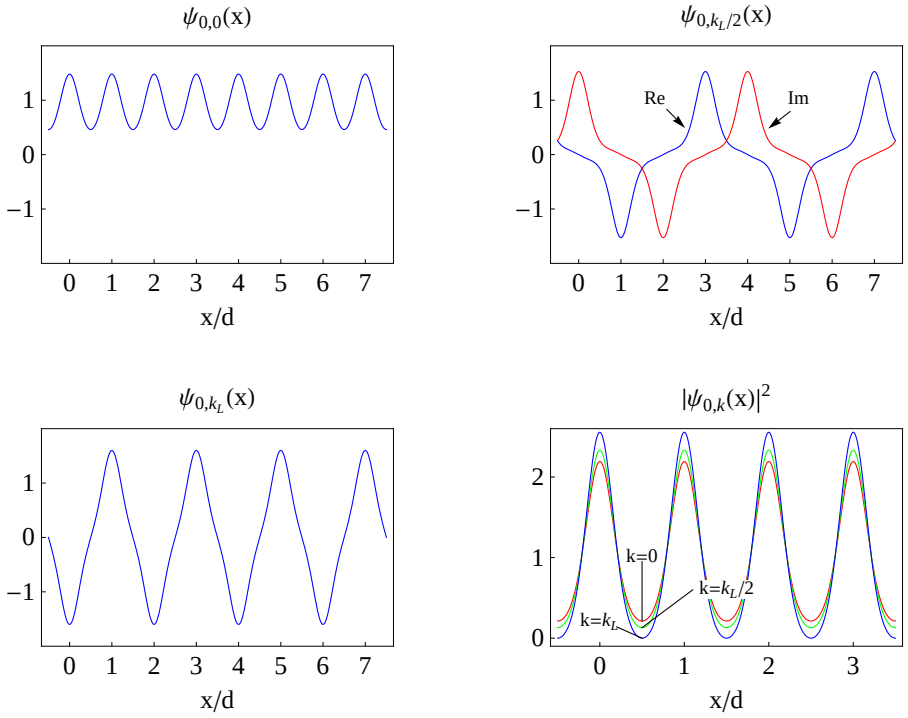

Figure 4-3: (a)-(c) Bloch waves at quasimomenta, $k = 0, k_L/2,$ and k_L in a lattice of depth, $V_0 = 5E_r$. (d) Profiles of the Bloch wave amplitude squared for the corresponding choices of the quasimomentum.

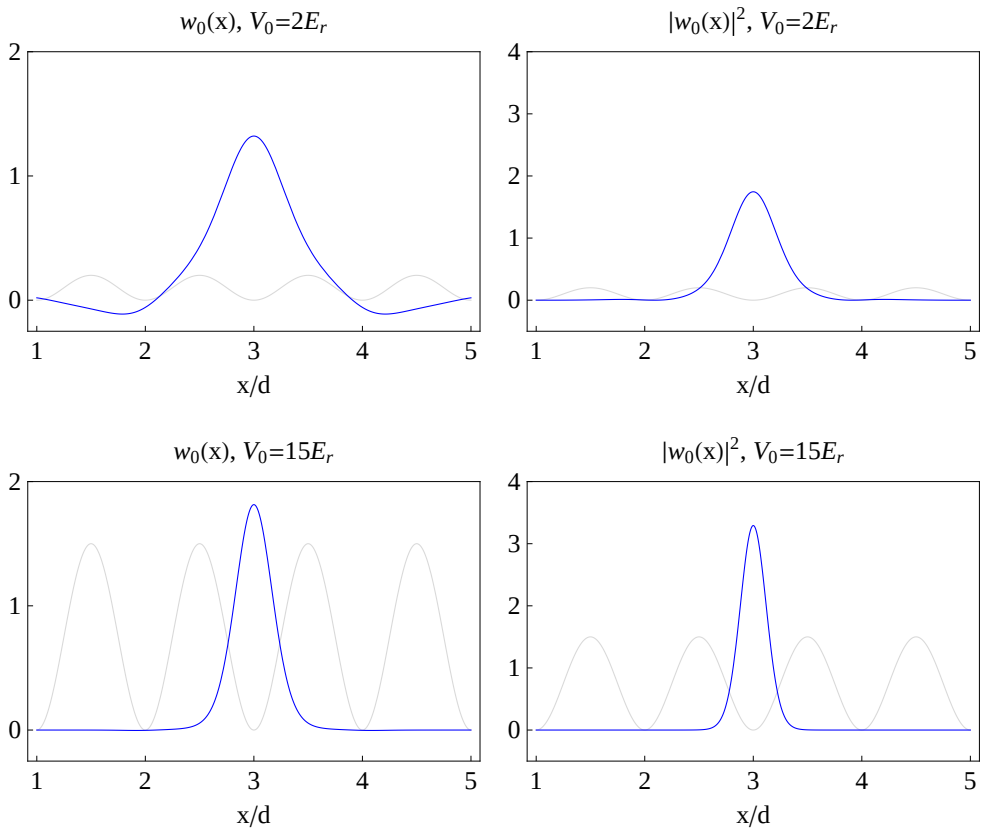

Figure 4-4: The Wannier function of the lowest band for lattice depths, $V_0 = 2E_r, 5E_r, 10E_r,$ and $15E_r$. A scaled plot of the optical lattice is shown in light gray. For shallow lattices, the Wannier function has pronounced lobes. At a depth, $V_0 = 15E_r$, the Wannier function closely resembles the Gaussian ground state of a harmonic well.

lowest band of an $N_L = 8$ site lattice as a sum of the Bloch waves at each of the discrete quasimomenta indicated by the points in Fig. 4-2. We show the Wannier function for the lowest band at several lattice depths in Fig. 4-4. In shallow lattices, the lobes of the Wannier function on either side of the central peak are pronounced. As the depth of the lattice is increased, these lobes disappear, and the Wannier function increasingly resembles the Gaussian ground state of a harmonic well.

4.2.4 Approximations of the Exact Optical Lattice Eigenfunctions

Near to the center of a lattice site, the optical lattice potential can be treated approximately as a harmonic potential,

$$V = V_0 \sin^2(k_L x) \approx V_0 k_L^2 x^2. \tag{4.43}$$

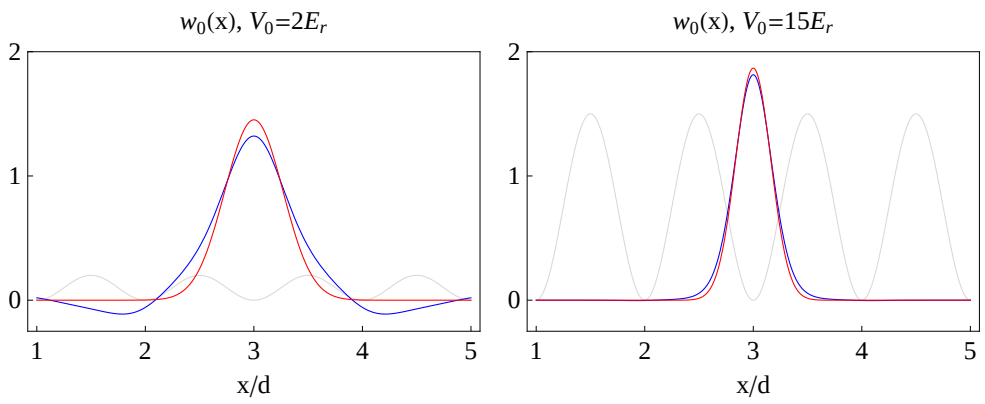

Figure 4-5: The Wannier function for the lowest band of the lattice (blue) and the ground state of the Harmonic approximation (red) are shown for a lattice with 8 sites and depths of $2E_r$ and $15E_r$.

The oscillation frequency of this harmonic oscillator is, ω_0, given by,

$$\hbar\omega_0/E_r = 2\sqrt{V_0/Er}. \tag{4.44}$$

A lattice with depth, $V_0 = 15E_r$, has an actual ground state energy of $3.59E_r$. This compares with the harmonic oscillator ground state energy of $\hbar\omega_0/2 = \sqrt{V_o/E_r}E_r = 3.87E_r$.

The spacing between the ground state and first excited state of the harmonic oscillator gives an approximation of the spacing between the lowest two bands of the lattice. For ^{87}Rb atoms with a temperature on the order of $10^{-9}K$, the thermal energy in units of the photon recoil energy is $k_BT/E_r \sim 0.007$. The spacing between the harmonic oscillator levels, for $V_0 = 5E_r$, is $\hbar\omega_0/E_r = 4.5$. This suggests that we may safely assume that the ultracold atoms in the lattice are restricted to the lowest band.

The ground state wave function of the harmonic oscillator gives us an approximation of the Wannier function for the lowest band of the lattice,

$$w(x) \approx (\pi\sqrt{s})^{1/4} \exp\left(\frac{-\pi^2}{2}\sqrt{s}x^2\right). \tag{4.45}$$

Distance in this expression is measured in units of the lattice spacing. Fig. 4-5 shows the actual Wannier function plotted alongside the harmonic approximation for a shallow lattice of depth $2E_r$ and a deeper lattice of depth $15E_r$. In the shallower lattice, the negative side lobes that ensure orthogonality between Wannier functions centered on different lattice sites

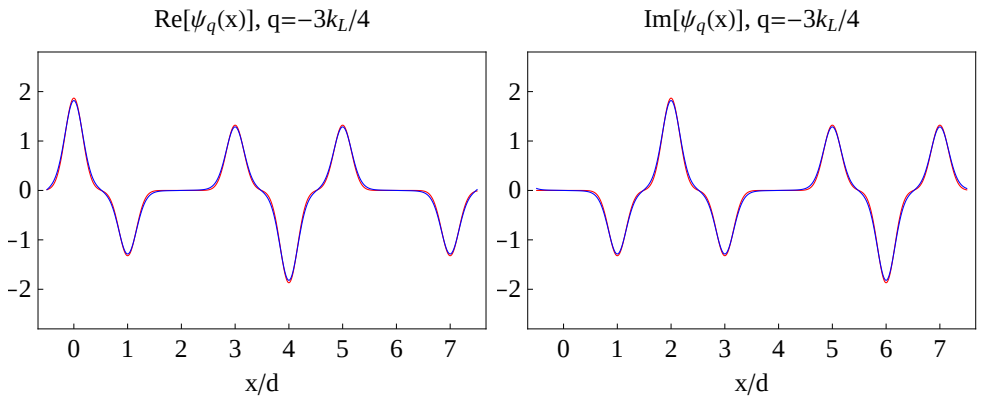

Figure 4-6: The Bloch wave for the $q = -3k_L/4$ mode of the lowest band of the lattice (blue) plotted alongside the reconstruction using the Gaussian approximation of the Wannier function. The wave functions are determined for a lattice with 8 sites and a depth, $V_0/E_r = 15$.

are pronounced, clearly distinguishing it from the Gaussian approximation. As the depth increases, however, the approximation becomes increasingly good, and we can see that the overlap of the Wannier function and the Gaussian approximation is quite high at a depth of $15E_r$.

We can use the Gaussian approximation to construct approximations to the Bloch waves. Inverting the definition of the Wannier function given in Eq. (4.34) in the one-dimensional case leads to

$$\psi_q(x) = \sum_{j=0}^{N_L-1} w(x-j)e^{i\nu\pi j}. \tag{4.46}$$

Here q and ν designate modes of the lattice and are related by,

$$qx = \nu\left(\frac{\pi}{d}\right)x = \nu\pi j \tag{4.47}$$

$$\nu = \frac{2}{N_L}n. \tag{4.48}$$

n is an integer, taking values in the range $\left[\frac{-(N_L-1)}{2}, \frac{(N_L-1)}{2}\right]$ if N_L is odd and $\left[\frac{-N_L}{2}+1, \frac{N_L}{2}\right]$ if N_L is even. Fig. 4-6 shows the real and imaginary parts of the approximation of the $\nu = -3/4$ mode, along with the actual Bloch wave, for a lattice of depth, $V_o = 15E_r$. At the depth of $V_0 = 15E_r$, the Bloch waves strongly overlap with the harmonic approximation. The harmonic approximation is unsatisfactory for shallow lattices, and the actual Bloch and Wannier functions are necessary to obtain reliable results. In sufficiently deep lattices,

however, it becomes reasonable to take advantage of these approximations in cases where we wish to reduce our computational burden or produce analytic expressions for quantities involving the states of the lattice.

4.3 Bose Hubbard Model

We have dealt so far with single particle solutions to the optical lattice potential. Placing a large number of interacting, Bose condensed atoms in the optical lattice leads to dramatically different physics from the single particle case. Due to the slow relative motion of the ultracold atoms, interactions between them may be treated as a pseudopotential, with scattering length, a, as we discussed in Sec. 2.3

$$U(\boldsymbol{x}, \boldsymbol{x}') = \frac{2\pi a\hbar^2}{\mu}\,\delta(\boldsymbol{x} - \boldsymbol{x}'). \tag{4.49}$$

μ is the reduced mass of the two colliding atoms in the BEC. For a homogeneous sample of atoms with mass, m, the reduced mass is $\mu = m/2$. When we restrict the dynamics of the atoms to the lowest band of the lattice and use the tight-binding approximation, neglecting interactions between atoms at different lattice sites and only including tunneling between adjacent lattice sites, the many body Hamiltonian for the BEC in an optical lattice has the form of the Bose Hubbard Hamiltonian [4]. This can be seen by rewriting the many body Hamiltonian in terms of on-site creation and annihilation operators. The regular many body Hamiltonian is given by,

$$H = \sum_{j=1}^{N}\left(\frac{-\hbar^2}{2m}\nabla_j^2 + V_T(\boldsymbol{x}_j) + V_{\text{lat}}(\boldsymbol{x_j})\right) + \frac{1}{2}\sum_{j\neq k} U(\boldsymbol{x}_j, \boldsymbol{x}_k). \tag{4.50}$$

The single summation gives all of the single particle contributions to the energy. $V_T(\boldsymbol{x})$ allows for the possibility of a trapping potential other than the optical lattice potential, $V_{\text{lat}}(\boldsymbol{x})$. The double summation gives the added effect of interactions between atoms in the lattice. We may re-express this Hamiltonian in second quantized notation in the standard way using the usual Bosonic field operators, $\hat{\psi}(\boldsymbol{x})$ and $\hat{\psi}^\dagger(\boldsymbol{x})$. In order to facilitate interpretation of the Hamiltonian in terms of the motion of atoms from site to site in the lattice, we expand $\hat{\psi}(\boldsymbol{x})$ and $\hat{\psi}^\dagger(\boldsymbol{x})$ in terms of the Wannier function, $w(\boldsymbol{x})$, for the lowest band of

the lattice,

$$\hat{\psi}(\boldsymbol{x}) = \sum_{\boldsymbol{R}} \hat{a}_{\boldsymbol{R}} w(\boldsymbol{x} - \boldsymbol{R}). \tag{4.51}$$

The sum is over locations of the lattice sites. The resulting Hamiltonian is

$$\begin{aligned} H = &\int d^3x \sum_{\boldsymbol{R}} \hat{a}^\dagger_{\boldsymbol{R}} w^*(\boldsymbol{x} - \boldsymbol{R}) \left(\frac{-\hbar^2}{2m}\nabla^2 + V_{\text{lat}}(\boldsymbol{x}) + V_T(\boldsymbol{x}) \right) \sum_{\boldsymbol{R}'} \hat{a}_{\boldsymbol{R}'} w(\boldsymbol{x} - \boldsymbol{R}') \\ &+ \frac{2\pi a}{m}\hbar^2 \int d^3x \sum_{\boldsymbol{R}_1, \boldsymbol{R}_2, \boldsymbol{R}_3, \boldsymbol{R}_4} \hat{a}^\dagger_{\boldsymbol{R}_1} \hat{a}^\dagger_{\boldsymbol{R}_2} \hat{a}_{\boldsymbol{R}_3} \hat{a}_{\boldsymbol{R}_4} w^*(\boldsymbol{x} - \boldsymbol{R}_1) w^*(\boldsymbol{x} - \boldsymbol{R}_2) w(\boldsymbol{x} - \boldsymbol{R}_3) w(\boldsymbol{x} - \boldsymbol{R}_4). \end{aligned} \tag{4.52}$$

We can simplify this expression in the tight binding approximation. First let us define the parameters governing site-to-site tunneling and the on-site interactions. The hopping matrix element, J, is defined by

$$J = -\int d^3x\, w^*(\boldsymbol{x} - \boldsymbol{R}_j) \left(\frac{\hbar^2}{2m}\nabla^2 + V_{\text{lat}}(\boldsymbol{x}) \right) w(\boldsymbol{x} - \boldsymbol{R}_k), \tag{4.53}$$

for adjacent lattice sites. We consider in particular a slowly varying trap, so that the trapping potential is approximately constant over a lattice site, and we can approximate,

$$\int d^3x\, w^*(\boldsymbol{x} - \boldsymbol{R}_j) V_T(\boldsymbol{x}) w(\boldsymbol{x} - \boldsymbol{R}_k) \approx \epsilon_j \delta_{j,k}. \tag{4.54}$$

ϵ_j is the energy at the site $\boldsymbol{R}_j$. The magnitude of the on-site repulsion is U,

$$U = \frac{4\pi a}{m}\hbar^2 \int d^3x \left| w(\boldsymbol{x} - \boldsymbol{R}_j) \right|^4. \tag{4.55}$$

As we described above, we will make the tight binding approximation and discard interactions between atoms at different sites and only include tunneling between adjacent sites. The Hamiltonian reduces under these conditions to the Bose Hubbard Hamiltonian,

$$H = -J \sum_{\langle \boldsymbol{R}, \boldsymbol{R}' \rangle} \hat{a}^\dagger_{\boldsymbol{R}} \hat{a}_{\boldsymbol{R}'} + \frac{1}{2} U \sum_{\boldsymbol{R}} \hat{n}_{\boldsymbol{R}} (\hat{n}_{\boldsymbol{R}} - 1) + \sum_{\boldsymbol{R}} \epsilon_{\boldsymbol{R}} \hat{n}_{\boldsymbol{R}}, \tag{4.56}$$

where $\hat{n}_{\boldsymbol{R}} = \hat{a}^\dagger_{\boldsymbol{R}} \hat{a}_{\boldsymbol{R}}$ is the on-site particle number operator. This Hamiltonian allows different many body ground states depending on the relative sizes of the hopping matrix element, J, and the interaction strength, U. When the interaction strength is small compared to

the hopping matrix element, the atoms in the lattice are able to delocalize and occupy Bloch states. In the reverse situation, when interactions between the atoms dominate the kinetic term, the atoms can minimize their energy by localizing within individual wells of the lattice. The transition between these states is an example of a quantum many body phase transition that we examine in the next section.

4.4 Quantum Many-body Phases in the Optical Lattice

4.4.1 Superfluid Phase

In the limiting cases, where J is much larger than U or vice versa, the solutions of the Bose Hubbard Hamiltonian can be readily determined. Consider a uniform lattice ($\epsilon_{\boldsymbol{R}} = 0$) in which the atoms are non-interacting ($U = 0$). The Hamiltonian reduces to

$$H = -J \sum_{\langle \boldsymbol{R}, \boldsymbol{R}' \rangle} \hat{a}^\dagger_{\boldsymbol{R}} \hat{a}_{\boldsymbol{R}'}. \tag{4.57}$$

Eigenstates of the kinetic part of the Bose Hubbard Hamiltonian are Fock states of the single particle Bloch modes. Let us introduce the field operator, $\hat{\psi}_{\boldsymbol{q}}(\boldsymbol{x}) = \int d^3x \, \psi^*_{\boldsymbol{q}}(\boldsymbol{x}) \hat{\psi}(\boldsymbol{x})$, which annihilates particles in the Bloch mode with quasimomentum $\boldsymbol{q}$. If the atoms in the lattice are Bose condensed, then all N atoms will sit in the ground state of the lattice, and the many body ground state is

$$|\psi_0\rangle = \frac{1}{N!} \left(\frac{\hat{\psi}^\dagger_0}{\sqrt{N_L}} \right)^N |0\rangle \,. \tag{4.58}$$

The many body ground state may be replaced by a coherent state when the number of atoms and lattice sites is large. In general, a coherent state of the single particle state, A, is given by, [44]

$$|\psi_{\text{coh}}\rangle = \sum_{N_A} \frac{\bar{n}^{N_A/2}}{\sqrt{N_A!}} e^{i\phi_A N_A} e^{-\bar{n}/2} \, |N_A\rangle \,. \tag{4.59}$$

$\bar{n}$ is the average number of particles occupying A and ϕ_a is a real number. By constructing the density matrix corresponding to the coherent state, we can determine the distribution

in the occupancy of A. The density matrix is

$$\rho = \sum_{N_A,N_B} \frac{\bar{n}^{(N_A+N_B)/2}}{\sqrt{N_A!N_B!}} e^{i(\phi_A N_A - \phi_B N_B)} e^{-\bar{n}} \left|N_A\right\rangle \left\langle N_B\right| . \tag{4.60}$$

The diagonal density matrix element giving the probability of measuring the particle number to be N_A is

$$P(N_A) = \frac{\bar{n}^{N_A}}{N_A!} e^{-\bar{n}}. \tag{4.61}$$

This is a Poisson distribution with a mean of $\bar{n}$. When the average occupancy is large, the distribution becomes narrowly centered on $\bar{n}$. Thus it is reasonable for large $\bar{n}$ to treat a state with exactly $\bar{n}$ particles in A approximately as a coherent state.

Rewriting the general expression for the coherent state in Eq. (4.59), the approximation of the ground state of the lattice is

$$\left|\psi\right\rangle \approx e^{-N/2} e^{\sqrt{N}\hat{\psi}_0^\dagger} \left|0\right\rangle . \tag{4.62}$$

The advantage of the coherent state representation of the many body state is the fact that it is an eigenstate of the field operator, $\hat{\psi}_0$,

$$\hat{\psi}_0 \, e^{-N/2} e^{\sqrt{N}\hat{\psi}_0^\dagger} \left|0\right\rangle = \sqrt{N} \left(e^{-N/2} e^{\sqrt{N}\hat{\psi}_0^\dagger} \left|0\right\rangle \right). \tag{4.63}$$

We wish to investigate correlations in the positions of atoms at different lattice sites, so it is more convenient to express the non-interacting ground state in terms of the on-site creation operator. Inserting an expansion of $\hat{\psi}(\boldsymbol{x})$ in terms of the Wannier function into the general expression for $\hat{\psi}_0$ gives

$$\hat{\psi}_0 = \sum_{\boldsymbol{R}} \hat{a}_{\boldsymbol{R}}. \tag{4.64}$$

This expression leads to a normalization of the Bloch state equal to the number of lattice sites. We may insert a factor of $1/\sqrt{N_L}$ to obtain unity normalization. The properly normalized coherent state representation of the ground state can then be written

$$\left|\psi_0\right\rangle \approx e^{-N/2} e^{\sqrt{\bar{n}} \sum_{\boldsymbol{R}} \hat{a}_{\boldsymbol{R}}^\dagger} \left|0\right\rangle = \prod_{\boldsymbol{R}} e^{-\bar{n}/2} e^{\sqrt{\bar{n}}\hat{a}_{\boldsymbol{R}}^\dagger} \left|0\right\rangle , \tag{4.65}$$

where $\bar{n} = N/N_L$. We see that a coherent state with N atoms in the lowest Bloch wave is

equivalent to the product of a coherent state at each lattice site with an average number of atoms per site equal to N/N_L. Evidently, the ground state of the non-interacting BEC in the lattice is also an eigenstate of $\hat{a}_{\boldsymbol{R}}$ for any $\boldsymbol{R}$, with an eigenvalue equal to the square root of the average number of atoms per site in the lattice,

$$\hat{a}_{\boldsymbol{R}} |\psi_0\rangle = \sqrt{\bar{n}} |\psi_0\rangle . \tag{4.66}$$

Using this property of the coherent state, we may immediately calculate the first-order correlator, $\langle\psi_0| \hat{a}^\dagger_{\boldsymbol{R}} \hat{a}_{\boldsymbol{R}'} |\psi_0\rangle = \bar{n}$. The correlation between any two points in the lattice, no matter how distantly separated, is constant. This long-range off-diagonal order is a hallmark of the superfluid phase of the lattice.

4.4.2 Mott insulator Phase

The opposite limit to that which we have been considering above is the strongly-interacting case. In the limit, $U \gg J$, the Bose Hubbard Hamiltonian reduces to

$$H = \frac{1}{2} U \sum_{\boldsymbol{R}} \hat{n}_{\boldsymbol{R}} (\hat{n}_{\boldsymbol{R}} - 1). \tag{4.67}$$

It is apparent that the eigenstates of this Hamiltonian are products of Fock states at each lattice site. For an integer density of atoms, $\bar{n}$, in a uniform lattice, the ground state is

$$|\psi_0\rangle = \prod_{\boldsymbol{R}} \frac{1}{\sqrt{\bar{n}!}} \left(\hat{a}^\dagger_{\boldsymbol{R}}\right)^{\bar{n}} |0\rangle . \tag{4.68}$$

In order for an atom in this many body ground state to shift to another site, the total energy of the system must increase by the discrete quantity, U, giving rise to a gap in the excitation spectrum. This ground state is a so-called Mott insulating state. We can readily determine the first-order correlator as we did for the superfluid. We obtain $\langle\psi_0| \hat{a}^\dagger_{\boldsymbol{R}} \hat{a}_{\boldsymbol{R}'} |\psi_0\rangle = \delta_{\boldsymbol{R},\boldsymbol{R}'}$. That is, this ground state shows no correlation between lattice sites separated by any distance. Higher-order correlators also show distinct differences between the superfluid and Mott insulating ground states [5, 45, 34].

4.4.3 Superfluid Fraction

In Sec. 4.4.1, we referred to the ground state of the Bose Hubbard Hamiltonian in the non-interacting limit as the superfluid phase. Now we will make this terminology more concrete in terms of the superfluid fraction of atoms in the lattice, and we will see that the superfluid disappears as the interactions are increased and the Mott insulator phase is reached.

Superfluidity can be illustrated macroscopically by the response of a fluid to the motion of the boundary containing the fluid. When the boundary begins to move sufficiently slowly, some fraction behaves ordinarily and is dragged along with it. The fraction of the fluid which does not respond to the motion of the boundary, and which remains at rest, is referred to as the superfluid fraction. In the frame of reference of the boundary, the normal component remains at rest, and the superfluid fraction begins to move [46, 47, 48]. This two-fluid description motivates a microscopic definition in which the shift in energy of a many body system due to a velocity boost of its Hamiltonian is attributed to the motion of a superfluid mass. In one dimension, if we call the boosted Hamiltonian, H_v, and the stationary Hamiltonian, H_0, the energy of the system after the boost is $\langle H_v \rangle = E_v$, and the energy of the stationary system is $\langle H_0 \rangle = E_0$. The superfluid mass is $M_s = f_s N m$, where the fluid is comprised of N particles of mass, m, and f_s is the superfluid fraction. If we attribute the gain in energy entirely to the motion of the superfluid mass, then we have [46]

$$E_v - E_0 = \frac{1}{2} M_s v^2 = \frac{1}{2} f_s N m v^2. \tag{4.69}$$

This expression is valid in the limit that $v \to 0$. Noting that the momentum operator of the boosted system is related to the Hamiltonian by $\boldsymbol{P_v} = \frac{\partial H_{\boldsymbol{v}}}{\partial \boldsymbol{v}}$, the relation in Eq. (4.69) is equivalent to the general definition in three dimensions of the superfluid fraction [49]

$$f_s = \frac{1}{3mN} \lim_{v \to 0} \frac{\partial}{\partial \boldsymbol{v}} \cdot \langle \boldsymbol{P_v} \rangle_{\boldsymbol{v}} \,. \tag{4.70}$$

We will examine the superfluid fraction in one dimension and show that the solution we gave to the Bose Hubbard Hamiltonian in the non-interacting case in Sec. 4.4.1 has a superfluid fraction of one. It is therefore correctly described as the superfluid phase. The

defining relation for the superfluid fraction (4.69) gives a definition in one dimension,

$$f_s = \lim_{v\to 0} \frac{E_v - E_0}{v^2} \frac{2}{mN}. \tag{4.71}$$

Henceforth we will not write the limit, but it is understood that the expression must eventually be evaluated for a vanishing velocity boost. The optical lattice is governed by the Bose Hubbard Hamiltonian [49],

$$H_0 = -J \sum_{\langle i,j \rangle} \hat{a}_i^\dagger \hat{a}_j + \frac{U}{2} \sum_i \hat{n}_i(\hat{n}_i - 1) + \sum_i \epsilon_i \hat{n}_i. \tag{4.72}$$

We denote the on-site creation and annihilation operators here for the i^{th} site with the shorthand, $\hat{a}_i^\dagger$ and $\hat{a}_i$. Following [49], we use the Galilean transformation for the field operator, $\hat{\psi}_v(x,t) = \hat{\psi}(x-vt,t)e^{imvx}e^{-imv^2t/2}$. The boosted on-site field operator, $\hat{a}_i(v,t) = \int dx\, w^*(x-x_i)\hat{\psi}_v(x,t)$, is then given by expanding $\hat{\psi}(x-vt,t) = \sum_i \hat{a}_i(0,t)w(x-vt-x_i)$. x_i is the position of the i^{th} lattice site. For a system in equilibrium, it is reasonable to choose $t = 0$. Furthermore, assuming a tight binding situation, we may approximate the integral, $\int dx\, w^*(x-x_i)w(x-x_j)e^{imvx} \approx \delta_{ij}e^{imvx_i}$. The resulting expression for the boosted on-site creation operator in terms of the stationary operator is

$$\hat{a}_i(v) = \hat{a}_i e^{imvx_i}. \tag{4.73}$$

Substituting this into the Bose Hubbard Hamiltonian gives the boosted Hamiltonian,

$$H_v = -J \sum_{\langle i,j \rangle} \hat{a}_i^\dagger \hat{a}_j e^{-imvx_{ij}} + \frac{U}{2} \sum_i \hat{n}_i(\hat{n}_i - 1) + \sum_i \epsilon_i \hat{n}_i, \tag{4.74}$$

where $x_{ij} = x_i - x_j$. The magnitude of x_{ij} is the lattice spacing, d. The net effect of the velocity boost is to add a phase, $\theta/N_L = mvd$, to the kinetic part of the Hamiltonian. In terms of this phase, the boosted Hamiltonian is,

$$H_\theta = -J \sum_{i=1}^{N_L} \left(\hat{a}_{i+1}^\dagger \hat{a}_i e^{-i\theta/N_L} + \hat{a}_i^\dagger \hat{a}_{i+1} e^{i\theta/N_L} \right) + \frac{U}{2} \sum_{i=1}^{N_L} \hat{n}_i(\hat{n}_i - 1) + \sum_{i=1}^{N_L} \epsilon_i \hat{n}_i. \tag{4.75}$$

Likewise, in terms of θ and the Bose Hubbard parameters, the superfluid fraction is [46]

$$f_s = \frac{N_L^2}{JN} \frac{E_\theta - E_0}{\theta^2}. \tag{4.76}$$

Following [46], we can expand Eq. (4.75) to second order in θ. Higher order terms do not contribute to the superfluid fraction in the limit $\theta \to 0$. The Hamiltonian then takes the form,

$$H_\theta - H_0 = \frac{\theta}{N_L} \hat{J} - \frac{1}{2} \frac{\theta^2}{N_L^2} \hat{T}, \tag{4.77}$$

where

$$\hat{J} = iJ \sum_{i=1}^{N_L} \left(\hat{a}_{i+1}^\dagger \hat{a}_i - \hat{a}_i^\dagger \hat{a}_{i+1} \right), \tag{4.78}$$

$$\hat{T} = -J \sum_{i=1}^{N_L} \left(\hat{a}_{i+1}^\dagger \hat{a}_i + \hat{a}_i^\dagger \hat{a}_{i+1} \right). \tag{4.79}$$

The expression for the shifted energy due to the velocity boost can be treated perturbatively in θ, without introducing an approximation to the superfluid fraction, because we will ultimately take the limit as θ goes to zero. The perturbative expression for the energy shift to lowest order is

$$E_\theta - E_0 = -\frac{1}{2} \frac{\theta^2}{N_L^2} \langle \psi_0 | \hat{T} | \psi_0 \rangle + \frac{\theta^2}{N_L^2} \sum_k \frac{\left| \langle \psi_k | \hat{J} | \psi_0 \rangle \right|^2}{E^0 - E^k}. \tag{4.80}$$

The states $|\psi_k\rangle$ are the eigenstates of the Bose Hubbard Hamiltonian, with corresponding energy, E^k. $|\psi_0\rangle$ is the ground state. The superfluid fraction is given by Eq. (4.76) as, [46]

$$f_s = f_s^{(1)} - f_s^{(2)}, \tag{4.81}$$

where the two contributions are $f_s^{(1)} = -\frac{1}{2JN} \langle \psi_0 | \hat{T} | \psi_0 \rangle$ and $f_s^{(2)} = \frac{1}{JN} \sum_k \frac{\left| \langle \psi_k | \hat{J} | \psi_0 \rangle \right|^2}{E^k - E^0}$. We can compute the superfluid fraction of the ground state of the superfluid phase given in Eq. (4.65). Recall that $|\psi_0\rangle$ is an eigenstate of the on-site annihilation operator with an eigenvalue of $\sqrt{\bar{n}}$, where $\bar{n} = N/N_L$ is the average density. It is then immediately apparent that $f_s^{(1)} = 1$ and $f_s^{(2)} = 0$, giving a total superfluid fraction of one.

We may readily evaluate $f_s^{(1)} = 0$ for the Mott insulator state by noticing that the

effect of the operator $\hat{T}$ is to shift an atom from one site to another. The net result of that operation on the ground state of the Mott insulator, which has a fixed number of atoms at each site, is to produce an orthogonal state in which one site has one extra atom and an adjacent site has one fewer atom. Without evaluating $f_s^{(2)}$ in detail, we notice that $f_s^{(2)} \geq 0$, so the superfluid fraction in this case is at most zero because $f_s^{(1)} = 0$. Since a negative superfluid fraction is non-physical, we must have zero superfluid fraction in the Mott insulator case.

In transitioning from the weakly interacting ($J \gg U$) to the strongly interacting ($U \gg J$) limit, the superfluid fraction of the Bose Hubbard ground state changes from one to zero. The weakly interacting case is, therefore, appropriately called the superfluid phase.

4.4.4 Condensate Fraction

The optical lattice is initially loaded with an atomic Bose Einstein condensate. The condensate fraction, that part of the population of atoms in the lattice in the condensate, decays to zero as the interaction strength between the atoms is increased. As [46] illustrates, the condensate fraction in the lattice depends only on the properties of the ground state, in contrast with the superfluid fraction, which depends on the entire spectrum of the Bose Hubbard Hamiltonian. Although the condensate fraction shows similar behavior to the superfluid, varying from one to zero as the parameter, U/J, is increased, the superfluid fraction decays much more rapidly. For interaction strengths at which the superfluid fraction is nearly gone, a significant fraction of the sample may still be in the condensate.

The condensate fraction is defined in terms of the single particle density matrix, $\sigma_{ij}^{(1)} = \langle\psi_0|\, \hat{a}_j^\dagger \hat{a}_i \,|\psi_0\rangle$, of the ground state. $\sigma = |\psi_0\rangle \langle\psi_0|$ is the von Neumann statistical operator for the N particle ground state. The single particle operator is obtained by tracing over $N-1$ particles, $\sigma^{(1)} = \mathrm{Tr}_{2,\ldots,N}(\sigma)$. The condition for BEC is that the eigenvalue, N_c, corresponding to one of the eigenvectors of $\sigma^{(1)}$, designated $|\chi_c\rangle$, is a finite fraction of the total number of particles, in the limit that $N \to \infty$. This fraction, $f_c = N_c/N$, is the condensate fraction. In the case of a lattice, we also insist that the average density, N/N_L, remain constant. The normalization of $\sigma^{(1)}$ is given by $\mathrm{Tr}(\sigma(1)) = N$, so that we must have at least one state occupied by at least N/N_L atoms. This state would have a condensate fraction, $f_c = N_c/N = (N/N_L)/N = 1/N_L$. For an infinite lattice, the condensate fraction associated with this state would vanish. For a finite lattice, however, the condensate fraction

takes a minimum, finite value, $1/N_L$.

The superfluid ground state density matrix is readily evaluated using the fact that it is an eigenstate of the lattice field operator,

$$\sigma_{ij}^{(1)} = \langle \psi_0 | \, \hat{a}_j^\dagger \hat{a}_i \, | \psi_0 \rangle = \bar{n}. \tag{4.82}$$

All of the eigenvalues of this matrix are zero except one, which equals N, corresponding to the eigenvector, $|\chi_c\rangle = \sum_{i=1}^{N_L} |1_i\rangle$. $|1_i\rangle$ designates a Fock state with one atom at site i. This is the Bloch mode with zero quasimomentum. This is not surprising because $|\psi_0\rangle$ was chosen to be the state with N particles in the lowest mode of the lattice. The condensate fraction of the superfluid ground state is one.

The Mott insulator ground state density matrix is given by

$$\sigma_{ij}^{(1)} = \langle \psi_0 | \, \hat{a}_j^\dagger \hat{a}_i \, | \psi_0 \rangle = \bar{n} \delta_{ij}. \tag{4.83}$$

The Mott insulator single particle density matrix is diagonal in the basis of Fock states at each lattice site. Each site is uniformly occupied with N/N_L atoms. The condensate fraction of each of those sites is $1/N_L$, the minimum possible in a finite lattice.

Both the condensate fraction and the superfluid fraction decay in the transition from the superfluid phase to the Mott insulating phase. Nonetheless, these quantities have key differences. Most importantly, the condensate fraction depends only on properties of the ground state of the lattice. The superfluid fraction can be separated into two terms. One of these, $f_s^{(1)}$, also depends only on correlation properties of the ground state. The other contribution, $f_s^{(2)}$, however, depends on the entire excitation spectrum of the Bose Hubbard Hamiltonian. We must keep this point in mind while examining the utility of measurements of properties of the lattice that are intended to be indicators of the many body phase.

Chapter 5

Probing an Optical Lattice with Matter Wave Scattering and Interferometry

5.1 Scattering from a Single Target

A many-body system in an optical lattice permits physical phenomena due to the interactions between particles that would not exist for a single particle in a lattice. The behavior of a single particle, however, is replicated by the behavior of many non-interacting particles, and provides intuition to guide expectations. It is of interest to us, therefore, to investigate the scattering first of a free probe particle from a single target particle occupying one of the Bloch modes of an optical lattice. As we are primarily interested in the physics of ultracold atoms in the optical lattice, we will consider a single particle state which is confined to the lowest band of the lattice, and which rests prior to interaction with the probe in the ground state.

The Hamiltonian for the probe and target is

$$H = H_P + H_T + V, \tag{5.1}$$

where $H_P = \frac{\hat{p}^2}{2m}$, H_T is the lattice Hamiltonian and V gives the interaction between the probe and target. We are considering the situation in which the probe atom is not affected by the lattice light. As both the probe and target are initially in eigenstates of the Hamiltonian

without interactions, we may formally apply a two-body Lippmann-Schwinger equation to obtain the scattered state, $|\psi\rangle$.

$$|\psi\rangle = |\varphi\rangle + \frac{1}{E - (H_P + H_T) + i\varepsilon} V |\psi\rangle \,. \tag{5.2}$$

The initial state of the system is $|\phi\rangle = |\boldsymbol{k}_0, \boldsymbol{q}_0\rangle$, where $\boldsymbol{k}_0$ is the wave vector of the probe particle plane wave state and $\boldsymbol{q}_0$ is the quasimomentum of the target particle in the lowest band of the lattice. $E = \frac{\hbar^2 k_0^2}{2m} + \epsilon_{\boldsymbol{q}_0}$ is the total initial energy and m is the mass of the probe. $\epsilon_{\boldsymbol{q}_0}$ is the energy of the lattice mode $\boldsymbol{q}_0$.

The quantity, $\langle \boldsymbol{r}, \boldsymbol{q}|\psi\rangle$, can be interpreted as the scattered probe wave function, conditional upon the final target state being the mode of the lattice with quasimomentum, $\boldsymbol{q}$. This conditionally scattered wave has a probability current $\boldsymbol{j}_{\boldsymbol{q}}(\hat{\boldsymbol{r}})$, associated with it. The total probability current of the scattered probe will be given by a sum of the conditional probability currents over final target states that conserve energy. We begin our pursuit of the cross section for the single target, therefore, by computing the conditionally scattered wave function of the probe, given by

$$\begin{aligned} \psi_{\boldsymbol{q}}(\boldsymbol{r}) &= \langle \boldsymbol{r}, \boldsymbol{q}|\psi\rangle \\ &= \varphi_{\boldsymbol{q}}(\boldsymbol{r}) + \int d^3 r' \, \langle \boldsymbol{r}| \frac{1}{\frac{\hbar^2 k_0^2}{2m} + (\epsilon_{\boldsymbol{q}_0} - \epsilon_{\boldsymbol{q}}) - H_P + i\varepsilon} \left|\boldsymbol{r}'\right\rangle \left\langle \boldsymbol{r}', \boldsymbol{q}\right| V |\psi\rangle \,. \end{aligned} \tag{5.3}$$

We recognize in the kernel of this integral a factor which is the free particle time independent Green's function, $G(\boldsymbol{r}, \boldsymbol{r}'; k)$, at the shifted energy, $\frac{\hbar^2 k^2}{2m} = \frac{\hbar^2 k_0^2}{2m} + (\epsilon_{\boldsymbol{q}_0} - \epsilon_{\boldsymbol{q}})$.

$$\begin{aligned} G(\boldsymbol{r}, \boldsymbol{r}'; k) = \langle \boldsymbol{r}| \frac{1}{\frac{\hbar^2 k_0^2}{2m} + (\epsilon_{\boldsymbol{q}_0} - \epsilon_{\boldsymbol{q}}) - H_P + i\varepsilon} \left|\boldsymbol{r}'\right\rangle &= -\frac{m}{2\pi\hbar^2} \frac{e^{ik|\boldsymbol{r} - \boldsymbol{r}'|}}{|\boldsymbol{r} - \boldsymbol{r}'|} \\ &\approx -\frac{m}{2\pi\hbar^2} \frac{e^{ikr}}{r} e^{-i\boldsymbol{k}\cdot\boldsymbol{r}'} . \end{aligned} \tag{5.4}$$

$\boldsymbol{k} = k\hat{r}$ is the outgoing wave vector of the probe. The approximation is valid in the far field, in which $|\boldsymbol{r}| \gg |\boldsymbol{r}'|$. Inserting this into our expression for the conditionally scattered probe wave function, we obtain

$$\psi_{\boldsymbol{q}}(\boldsymbol{r}) = \varphi_{\boldsymbol{q}}(\boldsymbol{r}) - \frac{m}{2\pi\hbar^2} \frac{e^{ikr}}{r} \int d^3 r' \, e^{-i\boldsymbol{k}\cdot\boldsymbol{r}'} \langle \boldsymbol{r}', \boldsymbol{q}| V |\psi\rangle \,. \tag{5.5}$$

This expression for the scattered wave function of the probe presents a difficulty due to the appearance of the scattered wave function on the right-hand side. We may proceed in the first Born approximation by replacing $|\psi\rangle$ with $|\varphi\rangle$. Furthermore, as we are requiring that the probe be of sufficiently low energy that it not excite interband transitions in the lattice, we will treat the interaction potential as a pseudopotential, [17]

$$V = \frac{2\pi\hbar^2}{m} a_s \, \delta\left(\hat{\boldsymbol{r}}_P - \hat{\boldsymbol{r}}_T\right). \tag{5.6}$$

a_s is the scattering length of the interaction and $\hat{\boldsymbol{r}}_P$ and $\hat{\boldsymbol{r}}_T$ are the position operators of the probe and target, respectively. Inserting the pseudopotential into Eq. 5.5 allows us to simplify the conditionally scattered probe wave function,

$$\begin{aligned}
\psi_{\boldsymbol{q}}(\boldsymbol{r}) &= \varphi_{\boldsymbol{q}}(\boldsymbol{r}) - \frac{a_s}{(2\pi)^{3/2}} \frac{e^{ikr}}{r} \int d^3r' \, e^{i(\boldsymbol{k}_0 - \boldsymbol{k})\cdot\boldsymbol{r}'} \, \langle \boldsymbol{q}| \, \delta(\boldsymbol{r}' - \hat{\boldsymbol{r}}_T) \, |\boldsymbol{q}_0\rangle \, . \\
&= \varphi_{\boldsymbol{q}}(\boldsymbol{r}) - \frac{a_s}{(2\pi)^{3/2}} \frac{e^{ikr}}{r} \, \langle \boldsymbol{q}| \, e^{i\boldsymbol{\kappa}\cdot\hat{\boldsymbol{r}}_T} \, |\boldsymbol{q}_0\rangle \, ,
\end{aligned} \tag{5.7}$$

where $\boldsymbol{\kappa} = \boldsymbol{k}_0 - \boldsymbol{k}$ is the momentum transferred from the probe to the lattice. The conditionally scattered wave function in (5.7) consists of an unscattered part, plus an outgoing spherical wave modulated by the matrix element giving the amplitude for a transition from the Bloch mode $\boldsymbol{q}_0$ to $\boldsymbol{q}$ due to a momentum boost, $\boldsymbol{\kappa}$.

5.2 Single Target Cross Section: Limiting Cases of Low and High Probe Energy

In this section, we will use Eq. (5.7) to construct a general expression for the scattering cross section of a single target. We will examine the cross section in the case of low probe energy, when the scattering is elastic, and in the case of high probe energy, when the target will be excited with uniform weight into all of the modes of the lowest band of the lattice. Recall that, due to the imposition of periodic boundary conditions on the lattice, the so-called Born-von Karman boundary conditions [50], the modes of the lattice are discrete. In the following section, we will calculate the cross sections for a one-dimensional lattice at arbitrary probe energy.

The conditionally scattered probe wave function from a target initially in the ground

state of the lattice, with $\boldsymbol{q}_0 = 0$, was given in Eq. (5.7) as,

$$\psi_{\boldsymbol{q}}(\boldsymbol{r}) = \frac{1}{(2\pi)^{3/2}} \left(e^{i\boldsymbol{k}_o \cdot \boldsymbol{r}} \delta_{\boldsymbol{q},0} - a_s \frac{e^{ikr}}{r} \langle \boldsymbol{q} | \, e^{i\boldsymbol{\kappa} \cdot \hat{\boldsymbol{r}}_T} \, | \boldsymbol{q}_o = 0 \rangle \right). \tag{5.8}$$

In order to determine the cross section, we need to calculate the probability current of the scattered part of the wave function in Eq. (5.8). The current in the direction $\hat{\boldsymbol{r}}$ due to scattering the target into the mode, $\boldsymbol{q}$, is $\boldsymbol{j}_{\boldsymbol{q}}(\hat{\boldsymbol{r}})$. It is calculated in the usual way, $\boldsymbol{j}_{\boldsymbol{q}}(\hat{\boldsymbol{r}}) = \frac{\hbar}{2mi} \left(\psi^*_{\boldsymbol{q}}(\boldsymbol{r}) \nabla \psi_{\boldsymbol{q}}(\boldsymbol{r}) - \psi_{\boldsymbol{q}}(\boldsymbol{r}) \nabla \psi^*_{\boldsymbol{q}}(\boldsymbol{r}) \right)$. Inserting our result for $\psi_{\boldsymbol{q}}(\boldsymbol{r})$ into this expression gives,

$$\boldsymbol{j}_{\boldsymbol{q}}(\hat{\boldsymbol{r}}) = \frac{a_s^2}{(2\pi)^3} \frac{\hbar k}{m} \frac{\hat{\boldsymbol{r}}}{r^2} \left| \langle \boldsymbol{q} | \, e^{i\boldsymbol{\kappa} \cdot \hat{\boldsymbol{r}}_T} \, | \boldsymbol{q}_0 \rangle \right|^2. \tag{5.9}$$

The incident probe probability current is $\boldsymbol{j}_{\rm inc} = \frac{1}{(2\pi)^3} \frac{\hbar k_o}{m} \hat{\boldsymbol{z}}$. The elastic part of the scattered current, given by $\boldsymbol{q} = \boldsymbol{q}_0$, will be peaked around $\boldsymbol{\kappa} = 0$ and reciprocal lattice vectors. The total cross section for scattering into the solid angle $d\Omega$ in the $\hat{\boldsymbol{r}}$ direction is given by summing over final states of the lattice that conserve energy. For a probe with energy greater than the band width of the lowest band and less than the gap to the next excited band, the sum will be over modes in the lowest band of the lattice. The resulting expression for the cross section is

$$\frac{d\sigma}{d\Omega d\epsilon} = \frac{\sum_{\boldsymbol{q}} \boldsymbol{j}_{\boldsymbol{q}} \cdot \hat{\boldsymbol{r}} \, r^2}{|\boldsymbol{j}_{\rm inc}|} = a_s^2 \frac{k}{k_o} \sum_{\boldsymbol{q}} \left| \langle \boldsymbol{q} | \, e^{i\boldsymbol{\kappa} \cdot \hat{\boldsymbol{r}}_T} \, | \boldsymbol{q}_o \rangle \right|^2 \delta(\hbar\omega + \varepsilon(0) - \varepsilon(\boldsymbol{q})). \tag{5.10}$$

$\varepsilon(\boldsymbol{q})$ is the energy of the Bloch wave in the lowest band with quasimomentum $\boldsymbol{q}$. $\hbar\omega = \hbar^2/2m(k_0^2 - k^2)$ is the energy transferred from the probe to the atom in the lattice. The total cross section, independent of the energy of the scattered probe, is given by

$$\begin{aligned} \frac{1}{a_s^2} \frac{d\sigma}{d\Omega} &= \frac{\hbar}{a_s^2} \int d\omega \frac{d\sigma}{d\Omega d\epsilon} \\ &= \sum_{\boldsymbol{q}} \sqrt{1 - \frac{\varepsilon(\boldsymbol{q}) - \varepsilon(0)}{\hbar^2 k_o^2/(2m)}} \left| \langle \boldsymbol{q} | \, e^{i\boldsymbol{\kappa} \cdot \hat{\boldsymbol{r}}_T} \, | \boldsymbol{q}_o \rangle \right|^2. \end{aligned} \tag{5.11}$$

We expanded k/k_0, giving the factor under the square root that weights the contribution of each mode in the sum. The sum is restricted to energy conserving modes, for which

$$\varepsilon(\boldsymbol{q}) - \varepsilon(0) \leq \hbar^2 k_0^2/(2m).$$

Note that the momentum transfer also depends on the final mode of the target atom,

$$\boldsymbol{\kappa} = \boldsymbol{k}_o - k_o \hat{\boldsymbol{r}} \sqrt{1 - \frac{\varepsilon(\boldsymbol{q}) - \varepsilon(0)}{\hbar^2 k_o^2/(2m)}}. \tag{5.12}$$

In the extreme case that the energy of the probe were too little to excite any other modes in the lowest band of the lattice, the probe would be perfectly elastically scattered and no excitations would be created. In that case, the cross section would be peaked at values of $\boldsymbol{\kappa}$ that are reciprocal lattice vectors. Although these peaks exist in principle, there is a competing factor, which is that, in making the initial probe energy small, we are also limiting the size of the momentum transfer to the lattice. As a consequence, the peaked behavior may not be observable because the total momentum transferred to the lattice is insufficient to observe any peaks other than at $\boldsymbol{\kappa} = 0$. We will see this in more detail in the next section, where we show exact inelastic scattering cross sections due to a one-dimensional lattice.

In the opposite extreme, when the probe energy significantly exceeds the width of the lowest band of the lattice, the inelastic scattering channels will contribute equally, and we can not expect peaked behavior. This situation is equivalent to the so-called static approximation [51]. Mathematically, this is represented by,

$$\sqrt{1 - \frac{\varepsilon(\boldsymbol{q}) - \varepsilon(0)}{\hbar^2 k_o^2/2m}} \approx 1. \tag{5.13}$$

Then we have the considerably simpler expression for the cross section,

$$\begin{aligned} \frac{1}{a_s^2}\frac{d\sigma}{d\Omega} &\approx \sum_{\boldsymbol{q}} \left| \langle \boldsymbol{q}| \exp\left(i\left(\boldsymbol{k}_o - k_o\hat{\boldsymbol{r}}\right)\cdot\hat{\boldsymbol{r}}_T\right)|\boldsymbol{q}_o\rangle \right|^2 \\ &= \langle \boldsymbol{q}_o|\, e^{-i\boldsymbol{\kappa}\cdot\hat{\boldsymbol{r}}_T} \sum_{\boldsymbol{q}} |\boldsymbol{q}\rangle \langle \boldsymbol{q}|\, e^{i\boldsymbol{\kappa}\cdot\hat{\boldsymbol{r}}_T} |\boldsymbol{q}_o\rangle . \end{aligned} \tag{5.14}$$

Recall that we are constrained to the lowest band of the lattice. In this subspace of the Hilbert space, the sum over modes of the lowest band of the lattice is an identity,

$$\sum_{\boldsymbol{q}} |\boldsymbol{q}\rangle \langle \boldsymbol{q}| = 1. \tag{5.15}$$

Making this simplification, we find that the cross section reduces to a constant,

$$\frac{1}{a_s^2}\frac{d\sigma}{d\Omega} = 1. \tag{5.16}$$

This result is equivalent to scattering from a pseudopotential at the origin with scattering length a_s in the limit $k_0 a_s \ll 1$. What we have shown is that when the probe energy is large compared to the band width of the lowest band of the lattice, the Bragg peaks are completely washed out. This would not be true for a large number of non-interacting particles in the lattice. In Sec. 5.6, we will find that even under the above assumptions, there would be peaks in the cross section due to many particles.

5.3 Single Target Cross Section: Arbitrary Probe Energy

The general result for the cross section for a matter wave due to a single particle in the $\boldsymbol{q}_0 = 0$ mode of a lattice was shown in (5.11). This result is valid in the far-field and the first Born approximation, and it includes the contribution due to all of the inelastic processes in the lowest band of the lattice. In this section, we will examine the impact of each of the terms in that expression separately for arbitrarily energetic probes and compute the full inelastic scattering cross section for the single target. The full cross section was given by,

$$\frac{1}{a_s^2}\frac{d\sigma}{d\Omega} = \sum_{\boldsymbol{q}} \sqrt{1 - \frac{\varepsilon(\boldsymbol{q}) - \varepsilon(0)}{\hbar^2 k_o^2/2m}} \left| \langle \boldsymbol{q}| \, e^{i\boldsymbol{\kappa}\cdot\hat{\boldsymbol{r}}_T} \, |\boldsymbol{q}_o\rangle \right|^2. \tag{5.17}$$

$\boldsymbol{\kappa}$ is the momentum transferred to the lattice, given in Eq. (5.12). The sum is over modes of the lowest band that conserve energy. The matrix element between the initial and final states of the particle in the lattice gives the probability of finding the target in the excited state, $|\boldsymbol{q}\rangle$, due to a momentum boost, $\boldsymbol{\kappa}$, of the ground state of the lattice, $|\boldsymbol{q}_0\rangle$. The factor, $\sqrt{1 - \frac{\varepsilon(\boldsymbol{q})-\varepsilon(0)}{\hbar^2 k_o^2/(2m)}}$, is a weight on the contribution of each inelastic channel to the total cross section.

Let us consider the impact of the weighting factor first. In Sec. 5.2, we discussed the effect on the cross section of an incident probe energy much larger than the transfers of energy to the lattice. That allowed us to make the approximation of a uniform weighting

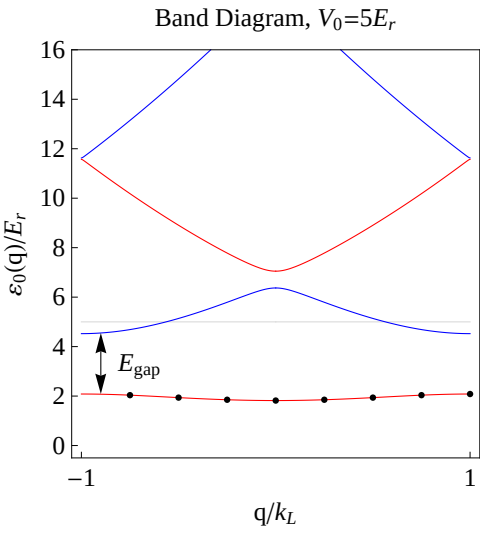

Figure 5-1: The lowest four energy bands of the optical lattice. The flat line is the depth of the lattice. The dots on the lowest band are the acceptable modes for a lattice with 8 sites and periodic boundary conditions. All quantities on the y-axis are in units of the recoil energy. The band structure is for a lattice of depth $5E_r$.

factor for every mode,

$$\sqrt{1 - \frac{\varepsilon(\boldsymbol{q}) - \varepsilon(0)}{\hbar^2 k_o^2/2m}} \approx 1. \tag{5.18}$$

We also assumed that the probe energy was insufficient to induce interband transitions of the particle in the lattice. The range of possible probe energies that satisfy these criteria can be understood graphically by examining the band structure of the optical lattice. Fig. 5-1 shows the band structure for the lowest few bands of a lattice with depth $V_0 = 5E_r$. The relevant comparison is between the width of the lowest band and the band gap. It is clear that at this depth, the gap significantly exceeds the lowest band's width. The determining quantity in the weighting factor is the ratio of the energy transfer to the incident probe energy. If the probe energy is much larger than the maximum transfer to the lowest band, $\varepsilon(1) - \varepsilon(0)$, then our previous approximation is valid. The maximum energy that the probe can have without risking interband transitions is the first energy gap. Fig. 5-2 shows the ratio of the width of the lowest band to the band gap between the first and second bands as a function of the lattice depth. The gap exceeds the band width of the lowest band even for very shallow lattices ($V_0 \gtrsim E_r$). For the typical depths, $V_0 \sim 15E_r$, that we will consider, the band width is much smaller than the band gap.

In the opposite regime, as we lower the energy of the probe, so that it becomes compa-

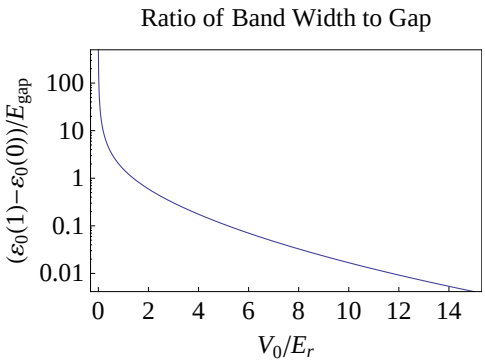

Figure 5-2: The band width of the lowest band divided by the gap to the first band. As the lattice becomes deeper, the lowest band flattens, and the band width becomes smaller. At the same time, the gap to the first excited band widens.

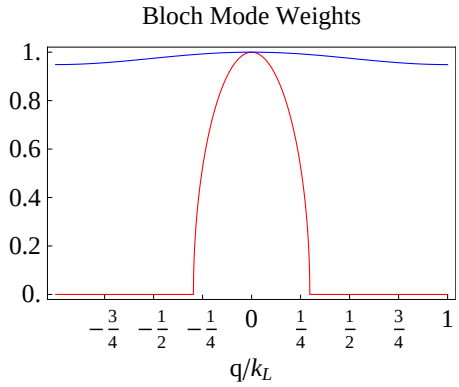

Figure 5-3: This plot shows the weight of the contribution to the cross section of each quasimomentum in the lowest band of a lattice of depth $V_0 = 15E_r$. Two different incident probe energies are shown. An incident probe with one-fifth the energy of the lowest band width (red) can only excite the lowest three modes. A probe with ten times the energy of the lowest band width (blue) excites all of the modes with nearly equal weights.

rable to the width of the lowest band of the lattice, the contribution of the higher energy modes is reduced. Fig. 5-3 shows the value of the weighting factor for probe energies a factor of 1/5 and 10 times the band width. At the higher energy, we already have near uniform contributions from all of the modes. At the lower energy, all except three of the lowest modes are totally excluded from contributing to the scattering. If we were to lower the incident energy further, eventually, only the ground state of the lattice would contribute, and the scattering would be purely elastic.

In order to calculate the cross section at arbitrary probe energies, we must determine

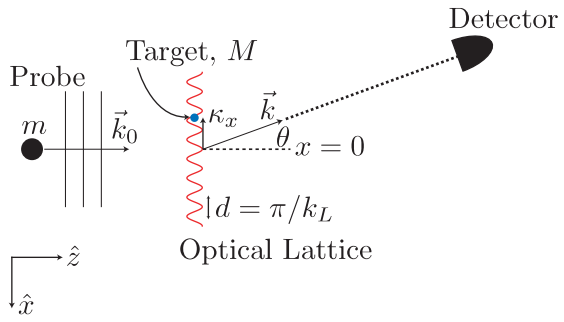

Figure 5-4: Diagram of the scattering configuration. The one-dimensional optical lattice, with a single target atom, is arranged perpendicular to the incident probe wave vector. A detector is placed in the far-field to measure the scattering cross section at the angle, θ.

the probability of scattering into a particular final mode, $|\boldsymbol{q}\rangle$,

$$P(\boldsymbol{q}, \boldsymbol{\kappa}, s = Vo/Er) = \left|\langle \boldsymbol{q}| \exp\left(i\boldsymbol{\kappa} \cdot \hat{\boldsymbol{r}}_T\right) |\boldsymbol{q}_o\rangle\right|^2 . \tag{5.19}$$

The dependence of the probability on the lattice depth, V_0/E_r, is implicit in the expression on the right-hand side. The scattering configuration that we are imagining is shown in Fig. 5-4. The probe atom is incident on a one-dimensional lattice, whose axis is arranged perpendicular to the wave vector of the probe. We will use the approximate form of the Bloch waves that we derived in Sec. 4.2.4 to calculate the probabilities for the one-dimensional lattice. We denote the wave function of the Bloch wave in the mode, q, by $\psi_q(x)$. The analytic result for $P(q, \boldsymbol{\kappa}, s)$ in this approximation is,

$$P(q, \boldsymbol{\kappa}, s) = \left| \int dx \; e^{i\kappa_x x} \psi_q^*(x) \, \psi_0(x) \right|^2 , \tag{5.20}$$

$$\int dx \; e^{i\kappa_x x} \psi_q^*(x) \, \psi_0(x) = \sum_{j,l=0}^{N_L - 1} e^{-i\nu\pi j} \int dx \; w^*(x - j) w(x - l). \tag{5.21}$$

The domain of the integrals is the lattice. The Wannier functions are strongly localized,

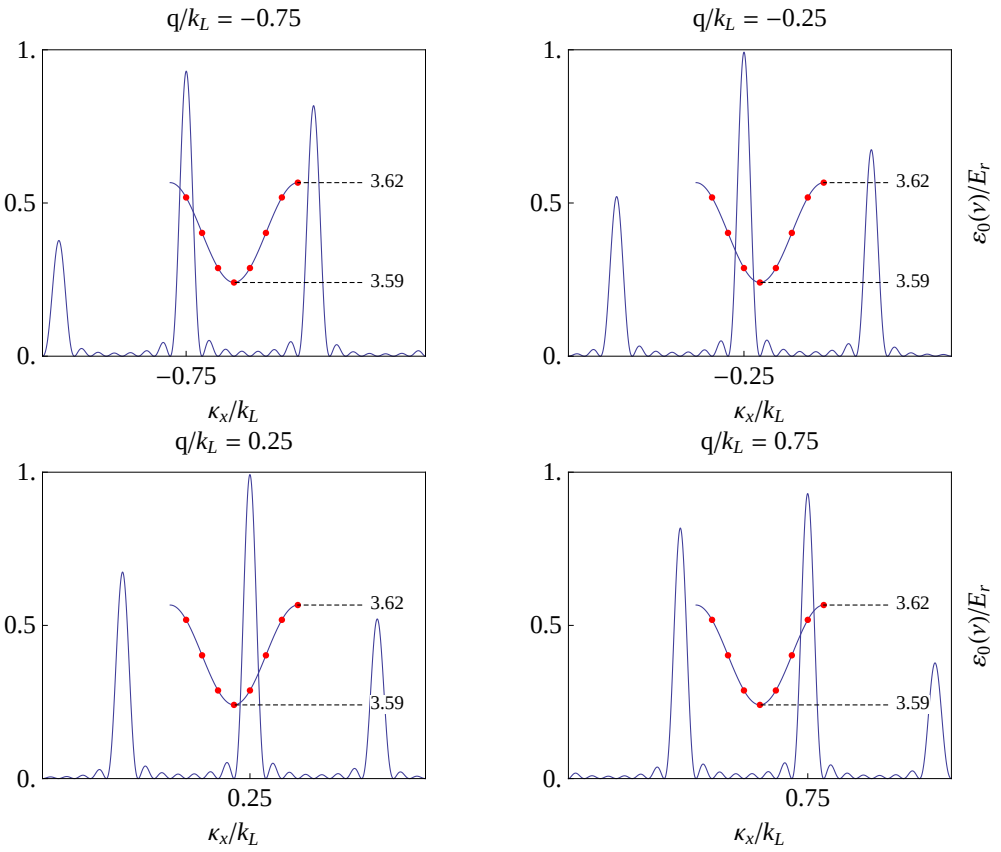

Figure 5-5: The probabilities of scattering into several modes (q/k_L) of the lattice ($V_0 = 15E_r$) are shown as a function of the momentum transferred to the lattice, κ_x. The probability is peaked when the momentum transferred to the lattice equals the quasimomentum of the specified mode, or is separated from it by a reciprocal lattice vector. The energy diagram of the lowest band of the lattice is superimposed on the probability to indicate the location of the modes.

however, so we will calculate that integral over all space. This gives

$$\int_{-\infty}^{+\infty} dx\; e^{i\kappa_x x}\psi_q^*(x)\,\psi_0(x) = \sum_{j,l=0}^{N_L-1} e^{-i\nu\pi j}\int dx\; e^{i\kappa_x x}w^*(x-j)w(x-l)$$
$$= \sum_{j,l=0}^{N_L-1} e^{-i\nu\pi j}e^{i\kappa_x l}\exp\left(-\frac{\kappa_x^2}{4\pi^2\sqrt{s}}\right)\exp\left(i\frac{\kappa_x}{2}(j-l)\right)\exp\left(\frac{-\pi^2\sqrt{s}}{4}(j-l)^2\right). \quad (5.22)$$

Fig. 5-5 shows the probability for scattering into each mode of the lattice separately, as a function of the momentum, κ_x, transferred to the lattice. The probability for scattering into a particular mode is peaked when the momentum transferred to the lattice matches that mode's quasimomentum or is separated by a reciprocal lattice vector. Fig. 5-6 shows the different conditional scattering probabilities side by side, so that the envelope is apparent.

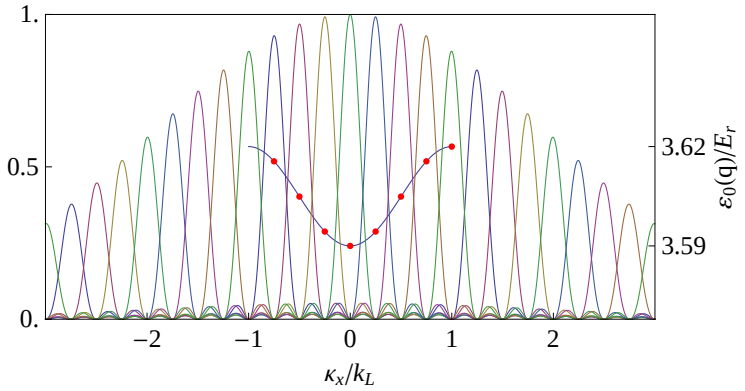

Figure 5-6: All of the conditional scattering probabilities for a lattice of depth $V_0 = 15E_r$ are plotted together. Summing these would give the cross section due to uniform weighting of the possible inelastic scattering channels. The envelope apparent in this plot indicates the overall shape of the cross section in that case.

Adding these functions directly, as in the case of uniform weighting, illustrates how the peaked behavior is washed out.

Each of the modes contributes to the overall scattering with a weight that depends on the energy of the mode. Combining these probabilities according to their weight, as specified in Eq. (5.17), gives the total inelastic cross section. Recall that $\boldsymbol{\kappa} = \boldsymbol{k}_o - k\hat{\boldsymbol{r}}$, so $\kappa_x = -k\sin(\theta)$, where θ is measured from the forward direction, for a lattice oriented perpendicular to the incident probe wave vector. We are working in units of distance of lattice spacings, so $\kappa_x x = \pi\frac{\kappa_x}{k_L}w$, where w is the unitless measure of distance. κ_x measured in units of the laser wave number is

$$\frac{\kappa_x}{k_L} = -\frac{k_o}{k_L}\sin(\theta)\sqrt{1 - \frac{\varepsilon(q) - \varepsilon(0)}{E_0 W}}; \tag{5.23}$$

$$\frac{k_o^2}{k_L^2} = \frac{m}{M}E_0\frac{W}{E_r}. \tag{5.24}$$

W is the band width, and E_0 is the energy of the probe measured in units of W. m is the mass of the probe, and M is the mass of the target. E_r is the photon recoil energy of the target. We plot the cross section as a function of the angle from forward scattering for a variety of values of the incident probe energy in Fig. 5-7.

At first glance, some of these results might seem surprising. Notice for instance that at very low probe energies, $E_0 = 0.01W$, in which only elastic scattering contributes, there is

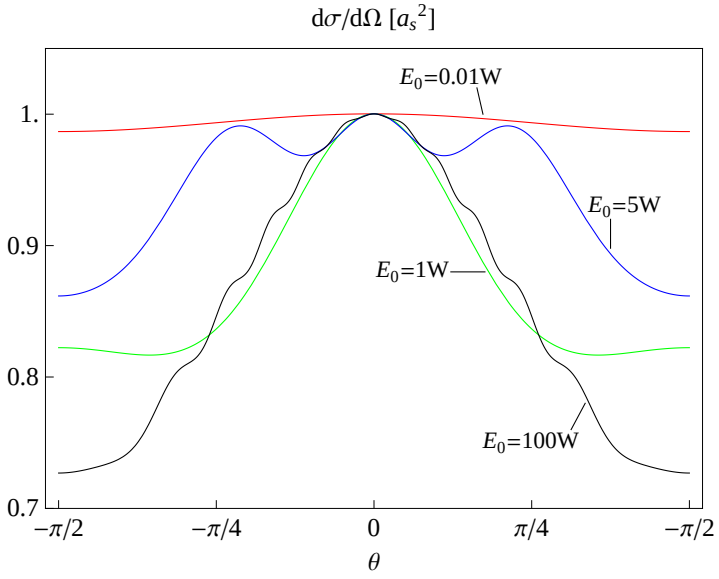

Figure 5-7: The total inelastic scattering cross section, $\frac{1}{a_s^2}\frac{d\sigma}{d\Omega}(\theta)$, for a single particle in a lattice of depth $V_0 = 15E_r$. The cross section is shown for several incident probe energies, specified in units of the band width of the lattice.

no structure in the cross section. This is due to the fact that at energies that are sufficiently low not to excite any modes of the lattice, κ_x never deviates far from 0. The cross section that we probe as we vary θ from 0 to π is then just the tip of the peak at $\kappa_x = 0$. In Fig. 5-5, we showed such peaks for several values of q.

We also examined the regime in which E_0 is large. We found that to the extent that we could ignore the energy transferred to the lattice compared to the incident probe energy, there would be no structure in the cross section. We compare this with the cross section at $E_0 = 100W$. The peaked behavior is clearly washed out, and all that remains is the overall envelope that we anticipated in Fig. 5-6.

In the intermediate regime, at $E_0 = 1W$ and $5W$, we have a balance between the range of values that κ_x can take and the residual peaked behavior. In this regime, κ_x is large enough to be able to see oscillations, and yet still small enough that the peaked behavior is not completely washed out by inelastic scattering.

5.4 The Van Hove Formalism and Multiple Scattering

We wish to treat the scattering of a matter wave from a BEC in an optical lattice. This is a complex problem involving many interacting bodies. In order to get an analytical handle on

that problem, we will first review the formal scattering theory and typical approximations that give rise to the van Hove cross section for a generic many body target [51]. We will do this with an eye toward treating the target with the Bose Hubbard model. We choose a probe particle which does not interact with the light field that creates the optical lattice, but only with atoms in the lattice. As we described in Sec. 4.3, the BEC is well-described by the Bose Hubbard Hamiltonian, H_{BH}. The many-body eigenstates of the lattice are labelled $|n\rangle$, such that $H_{BH}|n\rangle = E_n|n\rangle$, and the ground state is $|n_0\rangle$. The probe is a free particle of mass, m, with Hamiltonian $H_p = \hat{p}^2/2m$. The interaction between the probe and the N particles in the BEC is determined by the operator, $V = \sum_{j=1}^{N} V(\hat{\boldsymbol{r}} - \hat{\boldsymbol{r}}_j)$, where $\hat{r}$ is the position operator of the probe and $\hat{r}_j$ is the position operator of the j^{th} target particle.

Our starting point is the Lippmann-Schwinger equation. Initially, the probe is in the plane wave state, $|\boldsymbol{k}_0\rangle$, and the target is in the ground state, $|n_0\rangle$, of the Bose Hubbard Hamiltonian. Denoting the scattered many body state, including the degrees of freedom of both the probe and target, as $|\psi\rangle$, we can write down the formal expression,

$$|\psi\rangle = |\boldsymbol{k}_0, n_0\rangle + \lim_{\varepsilon\to 0} \frac{1}{E_{n_0} + \frac{\hbar^2 k_0^2}{2m} - H_{BH} - H_p + i\varepsilon} V|\psi\rangle\,. \tag{5.25}$$

We will follow the same approach we took in dealing with a single target, and consider the conditionally scattered probe wave function for each possible final state of the target, $|n\rangle$. The projection of the scattered state onto the position space of the probe is given by $\langle \boldsymbol{r}\,|\,\psi\rangle = \sum_n \psi_n(\boldsymbol{r})\,|n\rangle$, where $\psi_n(\boldsymbol{r}) = \langle \boldsymbol{r}, n\,|\,\psi\rangle$. An excitation of the target, from the ground state energy, E_0, to the excited state energy, E_n, is accompanied by a commensurate loss of energy from the probe. The lowered energy of the probe in that case would be $\hbar^2k^2/(2m) = \hbar^2k_0^2/(2m) + (E_{n_0} - E_n)$. Using the Lippmann-Schwinger equation, the conditionally scattered probe wave function is,

$$\psi_n(\boldsymbol{r}) = \frac{1}{(2\pi)^{3/2}} e^{i\boldsymbol{k}_0\cdot\boldsymbol{r}}\delta_{n_0,n} + \int d^3r'\ \langle \boldsymbol{r}|\ \frac{1}{\frac{\hbar^2k^2}{2m} - H_p + i\varepsilon}\ |\boldsymbol{r}'\rangle\,\langle \boldsymbol{r}', n|\,V|\psi\rangle\,. \tag{5.26}$$

It is evident in comparing (5.26) and (5.25) that a significant simplification has occurred. Whereas we originally faced the challenge of computing a many body Green function for a free particle plus lattice, the conditionally scattered probe wave function depends only on the usual one-body, energy-dependent Green's function. We will use the far-field approximation

of the Green's function.

$$G(\boldsymbol{r},\boldsymbol{r}';k) = \langle \boldsymbol{r}| \frac{1}{\frac{\hbar^2 k^2}{2m} - H_p + i\varepsilon} \left|\boldsymbol{r}'\right\rangle \approx \frac{-m}{2\pi\hbar^2}\frac{e^{ikr}}{r} e^{-i\boldsymbol{k}\cdot\boldsymbol{r}'}, \tag{5.27}$$

where $\boldsymbol{k} = k_0\hat{r}$. This is valid when $r \gg r'$. Inserting this expression for the Green function into (5.26) gives

$$\psi_n(\boldsymbol{r}) = \frac{1}{(2\pi)^{3/2}}\left(e^{i\boldsymbol{k}_0\cdot\boldsymbol{r}}\delta_{n_0,n} + \left(\frac{-m}{2\pi\hbar^2}(2\pi)^3 \langle \boldsymbol{k}, n| V |\psi\rangle\right)\frac{e^{ikr}}{r}\right). \tag{5.28}$$

In this expression, we can read off the scattering amplitude of the probe as,

$$f(\boldsymbol{k}_0 \to \boldsymbol{k}) = \frac{-m}{2\pi\hbar^2}(2\pi)^3 \langle \boldsymbol{k}, n| V |\psi\rangle . \tag{5.29}$$

We face a difficulty in that the full scattered state of the probe and lattice appears on the right-hand side of our expression for the conditionally scattered probe wave function. As in the single target case, we may proceed in the first Born approximation, treating the scattered state on the right-hand side of (5.28) as approximately equal to the initial state, so that $\langle \boldsymbol{k}, n| V |\psi\rangle \approx \langle \boldsymbol{k}, n| V |\boldsymbol{k}_0, n_0\rangle$. We can expand this matrix element of V into a sum of terms due to the interaction between the probe and each target atom.

$$\langle \boldsymbol{k}, n| V |\boldsymbol{k}_0, n_0\rangle = \langle \boldsymbol{k}, n| \sum_{j=1}^{N} V(\hat{\boldsymbol{r}} - \hat{\boldsymbol{r}}_j) |\boldsymbol{k}_0, n_0\rangle \tag{5.30}$$

$$= \int d^3r' \left\langle \boldsymbol{k}|\boldsymbol{r}'\right\rangle \left\langle \boldsymbol{r}'|\boldsymbol{k}_0\right\rangle \langle n| \sum_{j=1}^{N} V(\boldsymbol{r}' - \hat{\boldsymbol{r}}_j) |n_0\rangle \tag{5.31}$$

We inserted a complete set of probe position operators and expanded the plane wave states of the probe. It is useful to do likewise for each $\boldsymbol{r}_j$. Introducing $\boldsymbol{\kappa} = \boldsymbol{k}_0 - \boldsymbol{k}$, the momentum transferred from the probe to the lattice, simplifies the expression.

$$\langle \boldsymbol{k}, n| V |\boldsymbol{k}_0, n_0\rangle = \sum_{j=1}^{N} \int d^3r_j \int d^3r' \frac{e^{i\boldsymbol{\kappa}\cdot\boldsymbol{r}'}}{(2\pi)^3} \langle n| |\boldsymbol{r}_j\rangle \langle \boldsymbol{r}_j| V(\boldsymbol{r}' - \boldsymbol{r}_j) |n_0\rangle , \tag{5.32}$$

We may change variables in the integration over $\boldsymbol{r}'$ to $\boldsymbol{u} = \boldsymbol{r}' - \boldsymbol{r}_j$. In terms of $\boldsymbol{u}$, the matrix

element of V is

$$\langle \boldsymbol{k}, n| \, V \, |\boldsymbol{k}_0, n_0\rangle = \left(\int d^3u \, \frac{e^{i\boldsymbol{\kappa}\cdot\boldsymbol{u}}}{(2\pi)^3} V(\boldsymbol{u}) \right) \times \left(\langle n| \sum_{j=1}^{N} \int d^3r_j \; |\boldsymbol{r}_j\rangle \langle \boldsymbol{r}_j| \, e^{i\boldsymbol{\kappa}\cdot\boldsymbol{r}_j} \, |n_0\rangle \right). \quad (5.33)$$

At this point, The complete sets of target position operators that we introduced earlier are no longer necessary, and we may remove them. This leads to the final expression for the many body matrix element of V.

$$\langle \boldsymbol{k}, n| \, V \, |\boldsymbol{k}_0, n_0\rangle = \left(\int d^3u \, \frac{e^{i\boldsymbol{\kappa}\cdot\boldsymbol{u}}}{(2\pi)^3} V(\boldsymbol{u}) \right) \left(\langle n| \sum_{j=1}^{N} e^{i\boldsymbol{\kappa}\cdot\hat{\boldsymbol{r}}_j} \, |n_0\rangle \right). \quad (5.34)$$

Working in the Born approximation has the remarkable consequence that the matrix element of the interaction operator separates into two terms. The first depends only on the nature of the interaction potential between the probe and each target atom, and the second depends only on the details of the structure of the target. This is the basis of the separation of terms in the van Hove cross section [51]. Using this expression for the matrix element, the conditionally scattered probe wave function is,

$$\psi_n(\boldsymbol{r}) = \frac{1}{(2\pi)^{3/2}} \left(e^{i\boldsymbol{k}_0\cdot\boldsymbol{r}} \delta_{n_0,n} + \frac{-m}{2\pi\hbar^2} \left(\int d^3u \, e^{i\boldsymbol{\kappa}\cdot\boldsymbol{u}} V(\boldsymbol{u}) \right) \left(\langle n| \sum_{j=1}^{N} e^{i\boldsymbol{\kappa}\cdot\hat{\boldsymbol{r}}_j} \, |n_0\rangle \right) \frac{e^{ikr}}{r} \right). \quad (5.35)$$

We can compute the probability current associated with the scattered part of this probe wave function using the usual expression,

$$\boldsymbol{j}(\boldsymbol{r}) = \frac{\hbar}{2mi} \left(\psi(\boldsymbol{r})^* \nabla\psi(\boldsymbol{r}) - \psi(\boldsymbol{r}) \nabla\psi(\boldsymbol{r})^* \right). \quad (5.36)$$

The differential scattering cross section, depending on both the solid angle and the energy of the outgoing probe, is then given by

$$\frac{d^2\sigma}{d\Omega d\epsilon} = \frac{\boldsymbol{j}_{sc} \cdot \hat{r} \, r^2 d\Omega}{|\boldsymbol{j}_{inc}|}, \quad (5.37)$$

where $\boldsymbol{j}_{sc}$ and $\boldsymbol{j}_{inc}$ are the scattered and incident probability currents. The cross section thus calculated can be summed over all final target states that are energetically accessible

to obtain the total cross section. The total cross section is given by

$$\frac{d^2\sigma}{d\Omega d\epsilon} = \frac{m^2}{4\pi^2\hbar^5}\frac{k}{k_0}\left|\int d^3u\, e^{i\boldsymbol{\kappa}\cdot\boldsymbol{u}}V(\boldsymbol{u})\right|^2 \times \sum_n \left|\langle n|\sum_{j=1}^{N} e^{i\boldsymbol{\kappa}\cdot\hat{\boldsymbol{r}}_i}\,|n_0\rangle\right|^2 \delta\left(\omega + \frac{E_{n_0}-E_n}{\hbar}\right). \quad (5.38)$$

$\hbar\omega = \hbar^2/(2m)\left(k_0^2 - k^2\right)$ is the energy lost by the projectile to the lattice. The cross section is a product of terms, which depend exclusively on the nature of the interaction between the target and the probe and on the structure of the target. Using the van Hove notation, we can express this as,

$$\frac{d^2\sigma}{d\Omega d\epsilon} = AS(\boldsymbol{\kappa},\omega). \quad (5.39)$$

$S(\boldsymbol{\kappa},\omega)$ is the so-called structure factor,

$$S(\boldsymbol{\kappa},\omega) = \sum_n \left|\langle n|\sum_{j=1}^{N} e^{i\boldsymbol{\kappa}\cdot\hat{\boldsymbol{r}}_i}\,|n_0\rangle\right|^2 \delta\left(\omega + \frac{E_{n_0}-E_n}{\hbar}\right). \quad (5.40)$$

The term due to the interaction potential is,

$$A = \frac{m^2}{4\pi^2\hbar^5}\frac{k}{k_0}\left|\int d^3u\, e^{i\boldsymbol{\kappa}\cdot\boldsymbol{u}}V(\boldsymbol{u})\right|^2. \quad (5.41)$$

5.5 Scattering Cross Section of a BEC in an Optical Lattice

The states of the lattice before and after scattering of a probe atom are many body states of the N atoms in the lattice. The particular ground state in the lattice depends on the relative sizes of the the interaction strength, U, and the tunneling matrix element, J, appearing in the Bose Hubbard model. For weak repulsion between the atoms in the lattice, the atoms will delocalize and the superfluid fraction will increase to one as the interaction strength goes to zero [46]. As the repulsion between the atoms in the lattice becomes large compared to the tunneling matrix element, the atoms will localize, the superfluid fraction will go to zero, and a gap will open in the excitation spectrum, giving rise to the Mott insulator state. It is possible to alter the interaction strength between the atoms in the lattice by adjusting the depth of the lattice, or by manipulating the scattering length of lattice atom collisions through a Feshbach resonance. It is best for the purpose of probing the many body phase of the lattice to retain a constant lattice depth so that the scattering patterns are not trivially

affected by the changing density profile associated with a changing lattice potential.

The context of our scattering analysis is in probing an ultracold sample of atoms in an optical lattice. We showed in Sec. 4.3 that the Bose Hubbard Model applies when we neglect interband transitions and restrict the dynamics of the atoms to the lowest band of the lattice. In dealing with a BEC, in which all of the atoms are resting in the ground state of the lattice, this is the relevant regime. Our intention is that the matter wave probe should disturb the target as little as possible. In particular, we will choose probe particles which are sufficiently low in energy that excitations to excited bands of the lattice are energetically excluded. The scattering of these low-energy probes with individual targets atoms in the lattice will then consist primarily of s-wave scattering, so that it is valid to treat the interaction between the probe atom and each target atom as a pseudopotential [17]. The interaction potential is then given by

$$V(\boldsymbol{u}) = \frac{2\pi\hbar^2}{m} a_s \, \delta(\boldsymbol{u}), \tag{5.42}$$

where a_s is the scattering length of the interaction. Inserting this into (5.41), we find

$$A = \frac{a_s^2}{\hbar} \frac{k}{k_0}. \tag{5.43}$$

In order to facilitate handling the Bose statistics of the target atoms, it will be most convenient for us to re-express the momentum boost operators acting on the ground state of the lattice. Using second quantized notation and the usual field operators, $\hat{\psi}(\boldsymbol{r})$ and $\hat{\psi}^\dagger(\boldsymbol{r})$, we have

$$\begin{aligned} \sum_{j=1}^{N} e^{i\boldsymbol{\kappa}\cdot\hat{\boldsymbol{r}}_j} &= \int d^3r \, e^{i\boldsymbol{\kappa}\cdot\boldsymbol{r}} \, \hat{\psi}^\dagger(\boldsymbol{r})\hat{\psi}(\boldsymbol{r}) \\ &= \int d^3r \, e^{i\boldsymbol{\kappa}\cdot\boldsymbol{r}} \, \hat{n}(\boldsymbol{r}). \end{aligned} \tag{5.44}$$

This is the Fourier transform of the density operator, $\hat{n}(\boldsymbol{r}) = \hat{\psi}^\dagger(\boldsymbol{r})\hat{\psi}(\boldsymbol{r})$. The cross section in second-quantized notation takes the form

$$\frac{d^2\sigma}{d\Omega d\epsilon} = \frac{a_s^2}{\hbar} \sqrt{1 - \frac{\hbar\omega}{\hbar^2 k_0^2/(2m)}} \sum_n \left| \int d^3r \, e^{i\boldsymbol{\kappa}\cdot\boldsymbol{r}} \, \langle n| \, \hat{n}(\boldsymbol{r}) \, |n_0\rangle \right|^2 \delta\left(\omega + \frac{E_{n_0} - E_n}{\hbar}\right). \tag{5.45}$$

We substituted in this expression for k/k_0 in terms of ω. This enables us to compute the differential cross section per solid angle, independent of the energy transfer, by integration over $\epsilon = \hbar\omega$. That integration is trivial due to the presence of the energy conserving delta function. We obtain

$$\frac{d\sigma}{d\Omega} = \hbar \int d\omega \, \frac{d\sigma}{d\Omega d\epsilon} = a_s^2 \sum_n \sqrt{1 - \frac{E_n - E_{n_0}}{\hbar^2 k_0^2/2m}} \left| \int d^3r \; e^{i\boldsymbol{\kappa}\cdot\boldsymbol{r}} \langle n| \, \hat{n}(\boldsymbol{r}) \, |n_0\rangle \right|^2 . \tag{5.46}$$

The cross section in (5.46) is valid in the far field and the first Born approximation. The sum over n includes only energy conserving channels, for which $E_n - E_0 \leq \hbar^2 k_0^2/(2m)$. Recall that the momentum transfer, $\boldsymbol{\kappa} = \boldsymbol{k}_0 - k\hat{r}$, also depends on the final target state, n, through the outgoing probe wave number, k. A convenient choice of units for the cross section is the square of the scattering length, a_s, which appears on the right-hand side in (5.46). In units of the scattering length squared, the general expression for the cross section is

$$\frac{1}{a_s^2}\frac{d\sigma}{d\Omega} = \sum_n \sqrt{1 - \frac{E_n - E_{n_0}}{\hbar^2 k_0^2/2m}} \left| \int d^3r \; e^{i\boldsymbol{\kappa}\cdot\boldsymbol{r}} \langle n| \, \hat{n}(\boldsymbol{r}) \, |n_0\rangle \right|^2 . \tag{5.47}$$

Let us begin our investigation of the cross section of the atoms in the optical lattice for a matter wave by considering what happens in the limiting cases of the incoming probe energy. We will determine the cross section for arbitrary probe energies subsequently in Sec. 5.7.

When the probe energy is insufficient to excite the many body target in the lattice out of the ground state, the only contribution to the sum is due to the elastic term, $n = n_0$. The elastic cross section is given by

$$\frac{1}{a_s^2}\frac{d\sigma}{d\Omega} = \left| \int d^3r \; e^{i\boldsymbol{\kappa}\cdot\boldsymbol{r}} \langle n_0| \, \hat{n}(\boldsymbol{r}) \, |n_0\rangle \right|^2 . \tag{5.48}$$

The elastic cross section is simply the amplitude squared of the Fourier transform of the density profile of the atoms in the ground state of the lattice.

The opposite case is an initial probe energy that is large compared to the largest excitation energy available to the lattice atoms, but smaller than the excitation energy to the next higher band of the lattice,

$$E_n - E_{n_0} \ll \hbar^2 k_0^2/(2m). \tag{5.49}$$

In this case, we may treat the weighting factor as approximately equal to 1,

$$\sqrt{1 - \frac{E_n - E_{n_0}}{\hbar^2 k_0^2/2m}} \approx 1. \tag{5.50}$$

$\boldsymbol{\kappa}$ is independent of the final target state in this approximation, and the cross section becomes

$$\begin{aligned} \frac{1}{a_s^2}\frac{d\sigma}{d\Omega} &= \int d^3r d^3r' e^{i\boldsymbol{\kappa}\cdot(\boldsymbol{r}-\boldsymbol{r}')} \langle n_0| \hat{n}(\boldsymbol{r}') \sum_n |n\rangle \langle n| \hat{n}(\boldsymbol{r}) |n_0\rangle \\ &= \int d^3r d^3r' e^{i\boldsymbol{\kappa}\cdot(\boldsymbol{r}-\boldsymbol{r}')} \langle n_0| \hat{n}(\boldsymbol{r}')\hat{n}(\boldsymbol{r}) |n_0\rangle . \end{aligned} \tag{5.51}$$

We used the fact that in the subspace of the Hilbert space that is restricted to the lowest band of the lattice, the sum over states above is an identity,

$$\sum_n |n\rangle \langle n| = 1. \tag{5.52}$$

In the high energy case, the scattering cross section takes the form of the Fourier transform of a density-density correlator.

5.6 Scattering from the Superfluid: High Probe Energy

The cross section in the high probe energy regime given in (5.51) depends on the ground state of the target. We will evaluate this cross section for the superfluid phase. The ground state of the superfluid may be treated both exactly, as N atoms in the lowest Bloch mode of the lattice, and approximately, as a coherent state with an average density of $\bar{n} = N/N_L$. We find that the expressions for the cross section due to these different states are equivalent in the large N limit. For $N = 1$, when there is only a single target, the elastic Bragg peaks vanish only for the exact ground state. Most importantly, we find that the superfluid cross section exhibits an inelastic background that scales as the number of atoms in the lattice.

5.6.1 Exact Ground State

The ground state of the non-interacting BEC has N particles in the lowest energy Bloch wave of the lattice. The operator which creates a particle in the lowest energy Bloch wave

is $\hat{\psi}_{0,0} = \int d^3r\ \psi^*_{0,0}(\boldsymbol{r})\,\hat{\psi}(\boldsymbol{r})$. Using this, we can construct the superfluid ground state as

$$|\mathrm{SF}\rangle = \frac{1}{\sqrt{N!}}\left(\frac{\hat{\psi}^\dagger_{0,0}}{\sqrt{N_L}}\right)^N |0\rangle\,. \tag{5.53}$$

N_L is the number of lattice sites. We must calculate the correlator that appears in the expression for the cross section in (5.51),

$$\begin{aligned}\left\langle \hat{n}(\boldsymbol{r})\hat{n}(\boldsymbol{r}')\right\rangle &= \frac{1}{N!N_L^N}\,\langle 0|\,\hat{\psi}^N_{0,0}\,\hat{\psi}^\dagger(\boldsymbol{r})\hat{\psi}(\boldsymbol{r})\,\hat{\psi}^\dagger(\boldsymbol{r}')\hat{\psi}(\boldsymbol{r}')\,\hat{\psi}^{\dagger\,N}_{0,0}\,|0\rangle \\ &= \frac{1}{N!N_L^N}\,\langle 0|\,\hat{\psi}^N_{0,0}\,\hat{\psi}^\dagger(\boldsymbol{r})\hat{\psi}^\dagger(\boldsymbol{r}')\hat{\psi}(\boldsymbol{r})\hat{\psi}(\boldsymbol{r}')\,\hat{\psi}^{\dagger\,N}_{0,0}\,|0\rangle \\ &\quad + \frac{1}{N!N_L^N}\,\delta(\boldsymbol{r}-\boldsymbol{r}')\,\langle 0|\,\hat{\psi}^N_{0,0}\,\hat{\psi}^\dagger(\boldsymbol{r})\hat{\psi}(\boldsymbol{r}')\,\hat{\psi}^{\dagger\,N}_{0,0}\,|0\rangle \end{aligned}\tag{5.54}$$

In order to do this, it is useful to first calculate $\hat{\psi}(\boldsymbol{r}')\hat{\psi}^{\dagger\,N}_{0,0}\,|0\rangle$. Notice that the commutator of $\hat{\psi}(\boldsymbol{r}')$ and $\hat{\psi}^\dagger_{0,0}$ is

$$\left[\hat{\psi}(\boldsymbol{r}'),\hat{\psi}^\dagger_{0,0}\right] = \psi_{0,0}(\boldsymbol{r}'). \tag{5.55}$$

So it is straightforward to successively commute $\hat{\psi}(\boldsymbol{r}')$ rightward. Each time we generate an additional term $\psi_{0,0}(\boldsymbol{r}')\hat{\psi}^{\dagger\,(N-1)}_{0,0}\,|0\rangle$. After N such commutations, we find

$$\hat{\psi}(\boldsymbol{r}')\hat{\psi}^{\dagger\,N}_{0,0}\,|0\rangle = \psi_{0,0}(\boldsymbol{r}')N\hat{\psi}^{\dagger\,(N-1)}_{0,0}\,|0\rangle\,. \tag{5.56}$$

This gives us also

$$\hat{\psi}(\boldsymbol{r})\hat{\psi}(\boldsymbol{r}')\hat{\psi}^{\dagger\,N}_{0,0}\,|0\rangle = \psi_{0,0}(\boldsymbol{r})\psi_{0,0}(\boldsymbol{r}')N(N-1)\hat{\psi}^{\dagger\,(N-2)}_{0,0}\,|0\rangle\,. \tag{5.57}$$

Notice that this expression is also valid for $N = 1$, in which case it equals 0. Using these results, we can simplify the expression for the correlator,

$$\begin{aligned}\left\langle \hat{n}(\boldsymbol{r})\hat{n}(\boldsymbol{r}')\right\rangle &= \frac{1}{N!N_L^N}N^2(N-1)^2\,|\psi_{0,0}(\boldsymbol{r})|^2\,\left|\psi_{0,0}(\boldsymbol{r}')\right|^2\,\langle 0|\,\hat{\psi}^{(N-2)}_{0,0}\hat{\psi}^{\dagger\,(N-2)}_{0,0}\,|0\rangle \\ &\quad + \frac{1}{N!N_L^N}\,\delta(\boldsymbol{r}-\boldsymbol{r}')\,|\psi_{0,0}(\boldsymbol{r})|^2\,N^2\,\langle 0|\,\hat{\psi}^{(N-1)}_{0,0}\hat{\psi}^{\dagger\,(N-1)}_{0,0}\,|0\rangle\,. \end{aligned}\tag{5.58}$$

We can deal with terms like $\langle 0|\,\hat{\psi}^{(N-2)}_{0,0}\hat{\psi}^{\dagger\,(N-2)}_{0,0}\,|0\rangle$ using the commutation relation $\left[\hat{\psi}_{0,0},\hat{\psi}^\dagger_{0,0}\right] = N_L$. Each time we commute $\hat{\psi}_{0,0}$ rightward, we generate an additional term $N_L\,\langle 0|\,\hat{\psi}^{(N-3)}_{0,0}\hat{\psi}^{\dagger\,(N-3)}_{0,0}\,|0\rangle$.

Thus we find

$$\langle 0|\, \hat{\psi}_{0,0}^{(N-2)} \hat{\psi}_{0,0}^{\dagger\,(N-2)}\, |0\rangle = (N-2) N_L \,\langle 0|\, \hat{\psi}_{0,0}^{(N-3)} \hat{\psi}_{0,0}^{\dagger\,(N-3)}\, |0\rangle = (N-2)!\, N_L^{(N-2)}. \tag{5.59}$$

Substituting these results into (5.58), we may write down the final form of the correlator,

$$\left\langle \hat{n}(\boldsymbol{r}) \hat{n}(\boldsymbol{r}') \right\rangle = \frac{N(N-1)}{N_L^2} \left|\psi_{0,0}(\boldsymbol{r})\right|^2 \left|\psi_{0,0}(\boldsymbol{r}')\right|^2 + \frac{N}{N_L} \left|\psi_{0,0}(\boldsymbol{r})\right|^2 \delta(\boldsymbol{r}-\boldsymbol{r}'). \tag{5.60}$$

Recall that the Bloch waves are normalized to unity over a single lattice spacing, so that, integrated over the length of the lattice, we have

$$\int d^3r \;\; \left|\psi_{0,0}(\boldsymbol{r})\right|^2 = N_L. \tag{5.61}$$

Substituting the expression for the correlator in (5.60) into the expression for the cross section, (5.51), and using the normalization condition on the Bloch wave to simplify, we obtain a final form for the cross section,

$$\frac{1}{a_s^2}\frac{d\sigma}{d\Omega} = \frac{N(N-1)}{N_L^2} \left| \int d^3r \; e^{i\boldsymbol{\kappa}\cdot\boldsymbol{r}} \left|\psi_{0,0}(\boldsymbol{r})\right|^2 \right|^2 + N. \tag{5.62}$$

We can compare this to the elastic scattering cross section, (5.48). First, we must expand the ground state matrix element of the density as above,

$$\langle n_0|\, \hat{n}(\boldsymbol{r})\, |n_0\rangle = \frac{N}{N_L} \left|\psi_{0,0}(\boldsymbol{r})\right|^2. \tag{5.63}$$

Using this expression, the elastic cross section is

$$\frac{1}{a_s^2}\left(\frac{d\sigma}{d\Omega}\right)_{\text{el}} = \frac{N^2}{N_L^2} \left| \int d^3r \, e^{i\boldsymbol{\kappa}\cdot\boldsymbol{r}} \left|\psi_{0,0}(\boldsymbol{r})\right|^2 \right|^2. \tag{5.64}$$

Both the expression for the high energy probe cross section, (5.62), and for the elastic cross section, (5.64), contain a factor of the single particle elastic scattering cross section,

$$\frac{1}{a_s^2}\left(\frac{d\sigma}{d\Omega}\right)_{\text{1,el}} = \left| \int d^3r \, e^{i\boldsymbol{\kappa}\cdot\boldsymbol{r}} \left|\psi_{0,0}(\boldsymbol{r})\right|^2 \right|^2. \tag{5.65}$$

In the case of elastic scattering from the many body target, there will be peaks due to the Fourier transform of the lowest Bloch mode of the lattice, even for the single particle, $N = 1$ case. The high energy probe, in which inelastic scattering contributes with equal weight for all of the modes of the lowest band of the lattice, shows no peaked behavior when $N = 1$. The peaks in the first term of the high energy cross section are due to the interference of the elastically scattered waves from different atoms in the lattice. In addition to this elastic term, there is also a constant term equal to the number of target atoms, which is a background due to inelastic scattering.

5.6.2 Coherent State

It is convenient for large numbers of atoms in the lattice to treat the superfluid ground state as a product of coherent states at lattice sites. For the sake of completeness, we will consider the scattering cross section due to this approximate superfluid ground state. The operator which creates an atom at lattice site, $\boldsymbol{R}$, is $\hat{a}^\dagger_{\boldsymbol{R}} = \int d^3r\ w_0(\boldsymbol{r} - \boldsymbol{R})\,\hat{\psi}^\dagger(\boldsymbol{r})$. $w_0(\boldsymbol{r})$ is the Wannier function for the lowest band. We will treat the superfluid ground state as

$$|\mathrm{SF}\rangle = \prod_{\boldsymbol{R}} \exp\left(\sqrt{\frac{N}{N_L}}\hat{a}^\dagger_{\boldsymbol{R}}\right)|0\rangle\,. \tag{5.66}$$

As before, we must calculate the correlator, $\langle\hat{n}(\boldsymbol{r})\hat{n}(\boldsymbol{r}')\rangle$. It will be easiest to do this in the Wannier basis because the coherent state is an eigenstate of the on-site particle annihilation operator,

$$\hat{a}_{\boldsymbol{R}}\,|\mathrm{SF}\rangle = \sqrt{\bar{n}}\,|\mathrm{SF}\rangle\,, \tag{5.67}$$

where $\bar{n} = N/N_L$ is the average number of atoms per site. We expand the usual field operator formally in terms of the on-site field operators,

$$\hat{\psi}(\boldsymbol{r}) = \sum_{\boldsymbol{R}} w_0^*(\boldsymbol{r} - \boldsymbol{R})\,\hat{a}_{\boldsymbol{R}}. \tag{5.68}$$

Inserting this expansion into the correlator gives

$$\begin{aligned}\left\langle\hat{n}(\boldsymbol{r})\hat{n}(\boldsymbol{r}')\right\rangle = \sum_{\boldsymbol{R}_1,\ldots,\boldsymbol{R}_4} & w_0(\boldsymbol{r} - \boldsymbol{R}_1)\,w_0^*(\boldsymbol{r} - \boldsymbol{R}_2)\,w_0(\boldsymbol{r}' - \boldsymbol{R}_3)\,w_0^*(\boldsymbol{r}' - \boldsymbol{R}_4) \\ & \times \langle\mathrm{SF}|\,\hat{a}^\dagger_{\boldsymbol{R}_1}\hat{a}_{\boldsymbol{R}_2}\hat{a}^\dagger_{\boldsymbol{R}_3}\hat{a}_{\boldsymbol{R}_4}\,|\mathrm{SF}\rangle\,.\end{aligned} \tag{5.69}$$

The value of the matrix element, $\langle \mathrm{SF}| \hat{a}^\dagger_{R_1} \hat{a}_{R_2} \hat{a}^\dagger_{R_3} \hat{a}_{R_4} |\mathrm{SF}\rangle = \bar{n}(\bar{n} + \delta(\boldsymbol{R}_2, \boldsymbol{R}_3))$, is determined by applying the eigenvalue equation (5.68). Recall the relationship between the lowest energy Bloch wave and the Wannier function, $\psi_{0,0}(\boldsymbol{r}) = \sum_{\boldsymbol{R}} w_0(\boldsymbol{r} - \boldsymbol{R})$. These results allow us to simplify the expression for the correlator,

$$\left\langle \hat{n}(\boldsymbol{r})\hat{n}(\boldsymbol{r}')\right\rangle = \bar{n}^2 \left|\psi_{0,0}(\boldsymbol{r})\right|^2 \left|\psi_{0,0}(\boldsymbol{r}')\right|^2 + \bar{n}\, \psi_{0,0}(\boldsymbol{r})\psi^*_{0,0}(\boldsymbol{r}') \sum_{\boldsymbol{R}_2} w_0^*(\boldsymbol{r} - \boldsymbol{R}_2)\, w_0(\boldsymbol{r}' - \boldsymbol{R}_2) \quad (5.70)$$

The sum in the second term above may be addressed by using the completeness relation for the Wannier functions,

$$\sum_{n,\boldsymbol{R}} w_n^*(\boldsymbol{r} - \boldsymbol{R}) w_n(\boldsymbol{r}' - \boldsymbol{R}) = \delta(\boldsymbol{r} - \boldsymbol{r}'). \quad (5.71)$$

Although the sum in (5.70) is not over bands, n, we will write approximately

$$\left\langle \hat{n}(\boldsymbol{r})\hat{n}(\boldsymbol{r}')\right\rangle = \bar{n}^2 \left|\psi_{0,0}(\boldsymbol{r})\right|^2 \left|\psi_{0,0}(\boldsymbol{r}')\right|^2 + \bar{n}\, \left|\psi_{0,0}(\boldsymbol{r})\right|^2 \delta(\boldsymbol{r} - \boldsymbol{r}'). \quad (5.72)$$

We can insert this result for the correlator into the expression for the cross section, giving the final result for high energy scattering from the coherent state

$$\frac{1}{a^2}\frac{d\sigma}{d\Omega} = \frac{N^2}{N_L^2} \left| \int d^3r\; e^{-i\boldsymbol{\kappa}\cdot\boldsymbol{r}} \left|\psi_{0,0}(\boldsymbol{r})\right|^2 \right|^2 + N. \quad (5.73)$$

As the number of particles becomes large, such that $N \gg 1$, the expression for the cross section due to the exact ground state becomes equivalent to this result. When the total number of particles in the lattice is one, however, the exact ground state loses the structure due to the Fourier transform of the density (the Bragg peaks), and becomes uniform, $\frac{1}{a_s^2}\frac{d\sigma}{d\Omega} = 1$.

5.7 Inelastic Scattering Cross Sections at Arbitrary Probe Energy

We have shown that elastic scattering from the many body superfluid target gives rise to peaks due to the Fourier transform of the ground state Bloch wave in the lattice. Moreover, we have shown that, contrary to the expectations for a single target atom, the superfluid

ground state exhibits strong peaked behavior even when the probe energy is large and inelastic scattering occurs with equal weight into all of the modes of the lowest band of the lattice. The expression for the many body cross section produces the correct result for the case of a single target atom, in which the peaks are washed out, and only a smooth, inelastic background remains.

In this section, we return to the general expression for the many body cross section given in (5.47), and attempt to determine the cross section at arbitrary probe energy. This requires knowledge of the spectrum of the Bose Hubbard Hamiltonian. Deep in the superfluid regime, we may use the number of particles in each of the single particle Bloch modes of the lattice to specify the many body state. In the opposite case, when the interactions between the atoms in the lattice are strong, and the target is deep in the Mott insulating regime, the eigenstates of the Bose Hubbard Hamiltonian will be specified by the number of atoms at each lattice site.

We will find that the cross section of the target exhibits a strong dependence on the many body phase of the ground state. In particular, the superfluid cross section contains an inelastic background that scales as the number of target atoms. This background vanishes for the Mott insulator ground state when the probe energy is insufficient to overcome the insulator gap. Even for probes with energy exceeding the gap, the inelastic background of the Mott insulator is strongly suppressed.

5.7.1 Superfluid

We determined the following general expression for the cross section,

$$\frac{1}{a_s^2}\frac{d\sigma}{d\Omega} = \sum_n \sqrt{1 - \frac{E_n - E_0}{\hbar^2 k_0^2/2m}} \left| \int d^3r \; e^{i\boldsymbol{\kappa}\cdot\boldsymbol{r}} \left\langle n \right| \hat{n}(\boldsymbol{r}) \left| n_0 \right\rangle \right|^2 . \tag{5.74}$$

For very weak interactions, we may treat the target as a condensate in the lowest energy Bloch wave, $\psi_0(\boldsymbol{r})$, of the lowest band of the lattice. An eigenbasis for the many body states of the target in the non-interacting case is a designation of the number of atoms in each mode of the lowest band of the lattice. The cross section depends on the energy, E_n, of each many body state, both in the weighting factor that appears under the square root and also in the momentum, $\boldsymbol{\kappa} = \boldsymbol{k}_0 - k\hat{r}$, transferred to the lattice.

The sum over eigenstates of the lattice includes all possible distributions of the N target

atoms into the N_L Bloch modes of the lowest energy band. The sum can be dramatically simplified by noticing that the matrix element of the density, $\langle n|\,\hat{n}(\boldsymbol{r})\,|n_0\rangle$, is identically zero if more than one atom in the state, $|n\rangle$, is not in the ground state of the lattice. This is a consequence of the Born approximation that was made in deriving (5.74). Physically, in taking the Born approximation, we excluded processes in which the probe atom scatters from more than one target atom consecutively. As a result, the scattering solution was a sum of terms, each including an excitation of at most a single target atom out of the ground state.

Let us formally show which terms in the sum are non-zero. We use the abbreviated notation that the field operator for the Bloch mode in the lowest band with quasimomentum, $\boldsymbol{q}$, is

$$\hat{\psi}_{\boldsymbol{q}} = \int d^3r\, \psi^*_{\boldsymbol{q}}(\boldsymbol{r})\hat{\psi}(\boldsymbol{r}). \tag{5.75}$$

The superfluid ground state is

$$|n_0\rangle = \frac{1}{\sqrt{N!}}\left(\frac{\hat{\psi}_0^\dagger}{\sqrt{N_L}}\right)^N |0\rangle\,. \tag{5.76}$$

N_L is the number of lattice sites. Suppose we express $|n\rangle$ generically as an unknown $(N-1)$-particle state, $|\xi\rangle$, plus an atom in the mode of the lattice with quasimomentum, $\boldsymbol{q} \neq 0$,

$$|n\rangle = \frac{\hat{\psi}_{\boldsymbol{q}}^\dagger}{\sqrt{N_L}}\,|\xi\rangle\,, \tag{5.77}$$

The proper normalization of $|n\rangle$ depends on how many particles are already in the mode, $\boldsymbol{q}$. We will return to this point after we have determined the allowable states for $|\xi\rangle$. The matrix element is given by

$$\langle n|\,\hat{n}(\boldsymbol{r})\,|n_0\rangle = \langle\xi|\,\frac{\hat{\psi}_{\boldsymbol{q}}}{\sqrt{N_L}}\,\hat{\psi}^\dagger(\boldsymbol{r})\hat{\psi}(\boldsymbol{r})\frac{1}{\sqrt{N!}}\left(\frac{\hat{\psi}_0^\dagger}{\sqrt{N_L}}\right)^N |0\rangle\,. \tag{5.78}$$

We can simplify this using the identities:

$$\left[\hat{\psi}_{\boldsymbol{q}}, \hat{\psi}^{\dagger}(\boldsymbol{r})\right] = \psi^{*}_{\boldsymbol{q}}(\boldsymbol{r})$$

and

$$\hat{\psi}(\boldsymbol{r})\hat{\psi}_0^{\dagger\, N}\left|0\right\rangle = \psi_0(\boldsymbol{r}) N \hat{\psi}_0^{\dagger\,(N-1)}\left|0\right\rangle,$$

so that the matrix element is given by

$$\begin{aligned}\left\langle n\right|\hat{n}(\boldsymbol{r})\left|n_0\right\rangle &= \frac{\sqrt{N}}{N_L}\psi^{*}_{\boldsymbol{q}}(\boldsymbol{r})\psi_0(\boldsymbol{r})\ \left\langle \xi\right| \frac{1}{\sqrt{(N-1)!}}\left(\frac{\hat{\psi}_0^{\dagger}}{\sqrt{N_L}}\right)^{(N-1)}\left|0\right\rangle \qquad (5.79)\\ &= \frac{\sqrt{N}}{N_L}\psi^{*}_{\boldsymbol{q}}(\boldsymbol{r})\psi_0(\boldsymbol{r}).\end{aligned}$$

It is apparent from (5.79) that $\left|\xi\right\rangle$ must have $N-1$ particles in the single particle ground state in order for the matrix element of $\hat{n}(\boldsymbol{r})$ to be non-zero. The expression we used for $\left|n\right\rangle$ in (5.77) is, therefore, properly normalized. Notice that when $\left|n\right\rangle$ has only a single excitation, $E_n - E_0 = \varepsilon(\boldsymbol{q}) - \varepsilon(0)$, where $\varepsilon(\boldsymbol{q})$ is the energy of a single atom in the specified mode, corresponding to the excitation. The $\left|n\right\rangle = \left|n_0\right\rangle$ case must be handled separately. The result we obtain for the diagonal matrix element is

$$\left\langle n_0\right|\hat{n}(\boldsymbol{r})\left|n_0\right\rangle = \frac{N}{N_L}\left|\psi_0(\boldsymbol{r})\right|^2. \qquad (5.80)$$

We have determined the matrix elements of the density for all of the non-zero terms in the sum. We can express the sum equivalently by specifying the mode of the single excitation in the lattice for a particular choice of $\left|n\right\rangle$. We will separate the elastic term, $\left|n\right\rangle = \left|n_0\right\rangle$. The cross section can then be expressed as

$$\begin{aligned}\frac{1}{a_s^2}\frac{d\sigma}{d\Omega} = N^2\left|\int d^3r\ e^{i\boldsymbol{\kappa}\cdot\boldsymbol{r}}\frac{\left|\psi_0(\boldsymbol{r})\right|^2}{N_L}\right|^2 \\ + N\sum_{\boldsymbol{q}\neq 0}\sqrt{1-\frac{\varepsilon(\boldsymbol{q})-\varepsilon(0)}{\hbar^2k_0^2/2m}}\left|\int d^3r\ e^{i\boldsymbol{\kappa}\cdot\boldsymbol{r}}\frac{\psi^{*}_{\boldsymbol{q}}(\boldsymbol{r})\psi_0(\boldsymbol{r})}{N_L}\right|^2. \qquad (5.81)\end{aligned}$$

The first term in this expression is due solely to elastic scattering, and the second to inelastic scattering. We will mix the elastic and inelastic contributions to the cross section so that we can complete the sum over $\boldsymbol{q}$. This is accomplished by adding and subtracting the $\boldsymbol{q} = 0$

term. This gives

$$\frac{1}{a_s^2}\frac{d\sigma}{d\Omega} = N(N-1)\left|\langle\psi_0|\, e^{i\boldsymbol{\kappa}\cdot\hat{\boldsymbol{r}}_T}\,|\psi_0\rangle\right|^2 + N\sum_{\boldsymbol{q}}\sqrt{1-\frac{\varepsilon(\boldsymbol{q})-\varepsilon(0)}{\hbar^2k_0^2/2m}}\left|\langle\psi_{\boldsymbol{q}}|\, e^{i\boldsymbol{\kappa}\cdot\hat{\boldsymbol{r}}_T}\,|\psi_0\rangle\right|^2. \quad (5.82)$$

The $\boldsymbol{q}=0$ component of the cross section gives Bragg peaks due to the coherent overlap of elastically scattered waves from each individual lattice site. The scale of the elastic scattering that gives rise to the Bragg peaks can be determined by considering scattering in the forward direction ($\boldsymbol{\kappa}=0$). There we find that the central Bragg peak has a height $\frac{1}{a_s^2}\frac{d\sigma}{d\Omega} = N^2$.

The sum in the second term is over the modes of the lowest band of the lattice. This term is exactly N times the single target cross section. This includes the elastic single target channel, $\boldsymbol{q}=0$. We can estimate the scale of this term by considering the case in which the probe energy significantly exceeds the bandwidth of the lowest band, but is insufficient to excite atoms into higher bands. The energy of the probe and depth of the lattice are conveniently specified in units of the recoil energy, $E_r = \hbar^2k_L^2/(2m_T)$, for photons with wave number, k_L, and lattice atoms of mass, m_T. This condition is readily achieved for a typical lattice depth of $V_o = 15E_r$, in which the width of the lowest band is $0.03E_r$, and the band gap between the first and second bands is $6.28E_r$. When we approximate the final wave number of the probe to be equal to the initial wave number, the second term in (5.82) becomes Na_s^2.

There are two major features to the scattering from a superfluid: narrow elastic Bragg peaks that scale as N^2 and a superimposed inelastic background that scales as N. Fig. 5-8, which shows the differential cross sections for the superfluid (light gray) and the Mott insulator (dark gray), illustrates this behavior for a one-dimensional lattice arranged perpendicular to the incident probe wave vector. A diagram of the configuration is shown in Fig. 5-9. We consider the angle of deviation in the plane of the lattice. As the number of lattice sites increases, the width of the elastic peaks will become increasingly narrow. Away from the sharp Bragg peaks, the inelastic background is readily identifiable. This background emerges due to the availability of excited state modes to the condensate. The scattering behavior is qualitatively different when the interaction strength between atoms in the lattice becomes very large.

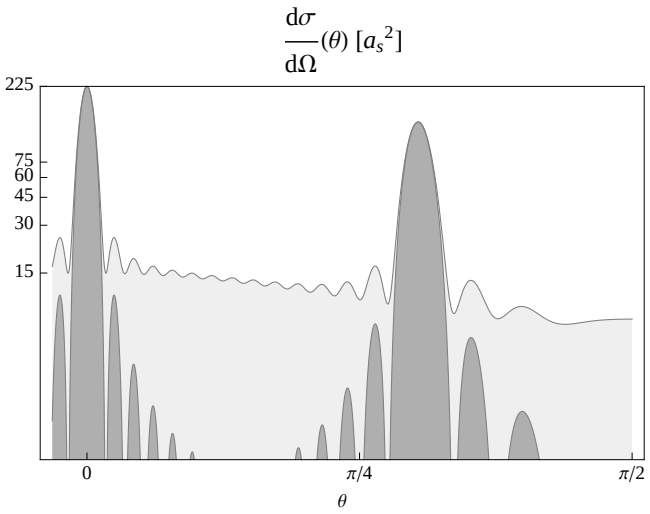

Figure 5-8: The analytic results for the superfluid (light gray) and Mott insulator (dark gray) differential cross sections for a sample lattice in 1D with 15 atoms and 15 sites. These are shown on a log scale in order to draw attention to the absence of inelastic scattering from the Mott insulator. The cross section is for a probe with energy $6E_r$ and a lattice depth of $V_o/E_r = 15$.

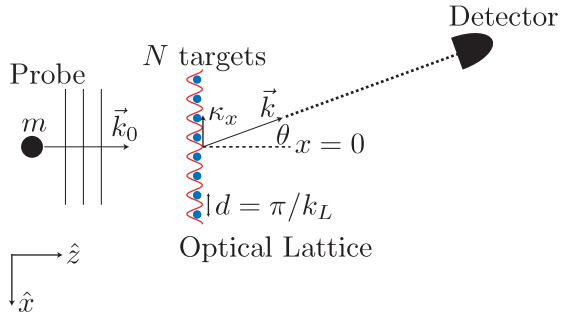

Figure 5-9: Diagram of the scattering configuration. The one-dimensional optical lattice, with N_L sites and N atoms, is arranged perpendicular to the incident probe wave vector. A detector is placed in the far-field to measure the scattering cross section at the angle, θ.

5.7.2 Mott Insulator

As the atoms in the lattice repel each other more strongly ($U/J \to \infty$), the superfluid fraction decreases, and the atoms become localized within individual wells of the lattice. For a sufficiently strong interaction, the Mott insulator state forms, and the ground state of the target can be represented by the number of atoms at each lattice site, $|n_o\rangle = \left|\bar{n}_{\boldsymbol{R}_1}, ..., \bar{n}_{\boldsymbol{R}_{N_L}}\right\rangle$. A uniform lattice will have $\bar{n} = N/N_L$ atoms per site for integer $\bar{n}$. We must determine the matrix element $\langle n|\,\hat{n}(\boldsymbol{r})\,|n_o\rangle$ for this ground state.

This is most easily done by expanding the density operator in a Wannier basis, using the Wannier function for the lowest band of the lattice, $w(\boldsymbol{r})$. Then $\hat{n}(\boldsymbol{r}) = \sum_{\boldsymbol{R}_1,\boldsymbol{R}_2} w^*(\boldsymbol{r} - \boldsymbol{R}_1)w(\boldsymbol{r} - \boldsymbol{R}_2)\hat{a}^\dagger_{\boldsymbol{R}_1}\hat{a}_{\boldsymbol{R}_2}$. Each term in the sum gives the contribution of the process in which a single target atom is scattered from one site to another by the probe. The $\boldsymbol{R}_1 = \boldsymbol{R}_2$ term is the elastic channel in which the state of the target is unchanged, $|n\rangle = |n_o\rangle$. Inelastic scattering corresponds to $\boldsymbol{R}_1 \neq \boldsymbol{R}_2$. The matrix element of the final state of the target, in which one atom has been displaced from $\boldsymbol{R'}$ to $\boldsymbol{R}$, is given by $\langle n|\,\hat{n}(\boldsymbol{r})\,|n_o\rangle = \sqrt{(\bar{n}+1)\bar{n}}\,w^*(\boldsymbol{r} - \boldsymbol{R})w(\boldsymbol{r} - \boldsymbol{R}')$. The energy cost associated with displacing one atom from the uniform ground state is the interaction strength, U, which is also the size of the Mott insulator gap. These results permit us to write the explicit expression for the scattering cross section of the Mott insulator target,

$$\frac{1}{a_s^2}\frac{d\sigma}{d\Omega} = \bar{n}^2\left|\sum_{\boldsymbol{R}} e^{i\boldsymbol{\kappa}\cdot\boldsymbol{R}}\right|^2 \times \left|\int d^3r\; e^{i\boldsymbol{\kappa}\cdot\boldsymbol{r}}\,|w(\boldsymbol{r})|^2\right|^2 + \bar{n}(\bar{n}+1)\sqrt{1 - \frac{U}{\hbar^2 k_o^2/2m}}\sum_{\boldsymbol{R}\neq\boldsymbol{R}'}\left|\int d^3r\; e^{i\boldsymbol{\kappa}\cdot\boldsymbol{r}} w^*(\boldsymbol{r} - \boldsymbol{R})w(\boldsymbol{r} - \boldsymbol{R}')\right|^2. \quad (5.83)$$

The sum over lattice sites in the first term takes a maximum value when the momentum transferred from the probe is a reciprocal lattice vector, with $\boldsymbol{\kappa}\cdot\boldsymbol{R}$ an integer multiple of 2π. As the number of lattice sites increases, the elastic Bragg peaks become increasingly sharp. In addition, there is an approximately Gaussian envelope due to the Fourier transform of the Wannier function.

We can examine the $\boldsymbol{\kappa} = 0$ case of forward scattering, as we did for the superfluid cross section. We see that the central peak has a height $\frac{1}{a_s^2}\frac{d\sigma}{d\Omega} = N^2$. The elastic scattering from the Mott insulator overlaps strongly with the elastic scattering given by the superfluid;

however, inelastic scattering from the Mott insulator phase is strongly suppressed (see Fig. 5-8). In particular, if the incident energy of the probe is less than the Mott insulator gap, the inelastic scattering vanishes completely. For probe energies exceeding the gap, the inelastic scattering is also negligible under the tight binding approximation. In that case, the integral in the inelastic part of the cross section in (5.83) is negligible when $\boldsymbol{R} \neq \boldsymbol{R'}$, so that we expect only elastic scattering from the Mott insulator.

We can estimate the scale of the Mott insulator's inelastic background more precisely by using the harmonic approximation of the Wannier function, in which we substitute the ground state of the harmonic approximation to the bottom of an individual well in the lattice. Using this approximation the cross section for a one-dimensional lattice is

$$\frac{1}{a_s^2}\frac{d\sigma}{d\Omega} = \exp\left(-\frac{\kappa_x^2}{2\pi^2\sqrt{s}}\right)\left(\left|\bar{n}\sum_j e^{i\kappa_x j}\right|^2 + \bar{n}(\bar{n}+1)\sqrt{1-\frac{U}{\hbar^2 k_0^2/2m}}\sum_{j\neq l}\exp\left(-\frac{\pi^2}{2}\sqrt{s}(j-l)^2\right)\right), \quad (5.84)$$

where j and l are positions of the lattice sites in units of the lattice spacing, so that $(j-l) \geq 1$. $s = V_0/E_r$ is the depth of the lattice.

Near to the central peak, the inelastic background decays exponentially with the lattice strength, as $\exp\left(-\frac{\pi^2}{2}\sqrt{\frac{V_o}{E_r}}(j-l)^2\right)$. For lattice depths in the typical range $V_o \leq 30E_r$, the inelastic contribution is strongly suppressed even for incident probe energies that exceed the gap energy. This contrasts markedly with the superfluid cross section, which carries a prominent inelastic background that scales as the number of atoms in the lattice. In the regions between the Bragg peaks, this background serves as an unambiguous indicator of the many body phase of the lattice.

5.7.3 Transition Between Superfluid and Mott Insulator

We have also examined the disappearance of the superfluid inelastic background as the interaction strength between the lattice atoms is increased. This required that we calculate scattering cross sections for arbitrary values of the parameter U/J. At intermediate values, this requires knowledge of the spectrum of the Bose Hubbard Hamiltonian. We calculated the matrix elements of the density operator by exactly diagonalizing the Bose Hubbard

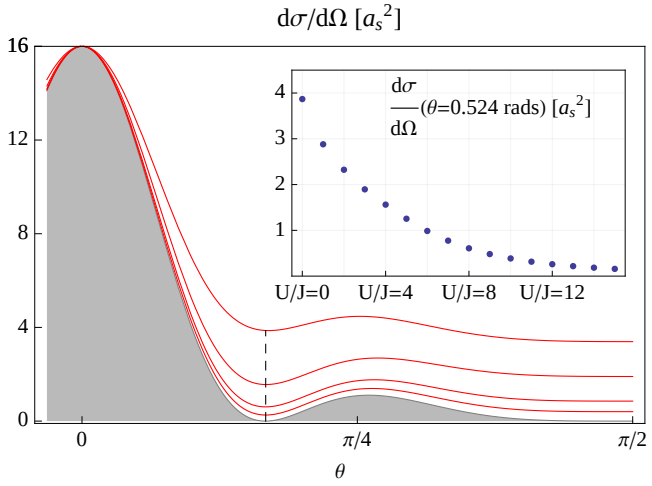

Figure 5-10: Cross sections for a probe with initial energy $(\hbar k_o)^2/(2m) = E_r$, a lattice of depth $V_o = 15E_r$, with 4 atoms and 4 sites, and $J = 0.002$. The values of U/J shown are: 0, 4, 8, and 16. The superfluid inelastic background ($U/J = 0$) scales as N. The analytic result for the Mott insulator ($U/J \to \infty$) background (filled in dark gray) is strongly suppressed. The inset shows the numerical cross section at the vertical dashed line as a function of U/J.

Hamiltonian for small lattices. Using these results, we have shown the angular cross section given in (5.74) for several values of U/J in Fig. 5-10. At $U/J = 0$ the numerical result coincides with the analytic result we presented. The inelastic background that scales as the number of atoms is present. This inelastic background decays to zero as the interaction strength is increased, and the cross section converges on the analytic result we gave for the Mott insulator. We note that the amplitude of the inelastic background has decayed by more than half at $U/J = 4$. For $U/J = 8$, the background is largely gone. This coincides with the range over which the superfluid fraction vanishes [46].

Our analytic results for the scattering cross section when the interaction strength dominates the tunneling matrix element ($U \gg J$) and vice versa show that the many body phase in the lattice strongly affects the scattering cross section of a low-energy matter wave probe. The periodic nature of the target gives rise in both many body phases to coherent Bragg peaks whose height scales as the square of the number of atoms in the lattice. In addition, an inelastic background determined by the excitation spectrum of the target serves as an indicator of the presence of superfluidity, and scales as the number of atoms in the target. This provides an easily identifiable signature of the many body phase.

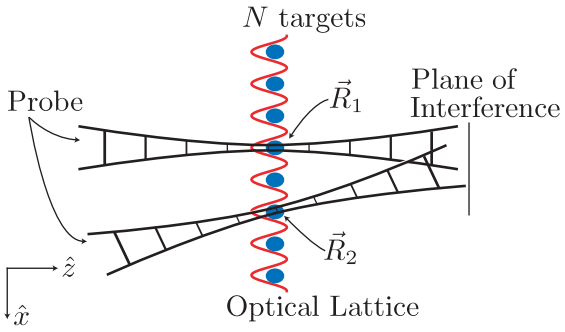

Figure 5-11: Diagram of the interference configuration. The probe matter wave is coherently split into two arms. The individual arms strike a one-dimensional lattice at the positions indicated. Downstream of the lattice, the arms overlap, and an interference pattern is formed.

5.8 Interference of Focused Beams Scattered from an Optical Lattice

We have shown above that the scattering cross section of an optical lattice for a matter wave exhibits strong dependence on the many body phase, due to the differing spectra of the superfluid and Mott insulator phases. The elastic scattering, which depends only on the density profile of the atoms in the lattice, is very similar for the two phases, especially in a deep lattice. Although the densities of the atoms in the superfluid and Mott insulator ground states resemble each other, the number statistics of these states are starkly different. In this section, we will move beyond the scattering cross section to illustrate a method by which these correlation properties can be probed by a matter wave.

We consider the arrangement, shown in Fig. 5-11, of a matter wave probe and lattice in which the probe is coherently split into two arms. When each arm is focused at a different point in a one-dimensional lattice, the interference between the scattered waves reveals density-density correlations of the lattice atoms. To obtain focusing in the probe, we allow it to be a superposition of plane waves. In order to apply the formalism of time-independent scattering theory, these plane waves must have the same wave number. The initial state of the probe and lattice can be expressed as,

$$|\phi\rangle = \sum_{\boldsymbol{k}_0} a_{\boldsymbol{k}_0} |\boldsymbol{k}_0, n_0\rangle \,, \tag{5.85}$$

where the sum is over vectors of length, k_0, and n_0 designates the ground state state of the lattice. $a_{\boldsymbol{k}_0}$ is a coefficient giving the amplitude of the contribution of the plane wave with wave vector, $\boldsymbol{k}_0$, to the initial probe state. The expression for the conditionally scattered probe was given in Eq. (5.28). Adjusting for the new initial probe wave function gives,

$$\psi_n(\boldsymbol{r}) = \phi(\boldsymbol{r})\,\delta_{n_0,n} - \frac{m}{2\pi\hbar^2}\frac{e^{ik_n r}}{r}(2\pi)^{3/2}\,\langle \boldsymbol{k}_n, n\,|V|\,\psi\rangle\,. \tag{5.86}$$

n is the final state of the lattice and $\phi(\boldsymbol{r})$ is the initial spatial wave function of the probe. k_n is the wave number of the scattered probe, whose energy is reduced by the corresponding excitation of the lattice energy,

$$\frac{\hbar^2 k_n^2}{2m} = (E_{n_0} - E_n) + \frac{\hbar^2 k_0^2}{2m}. \tag{5.87}$$

The outgoing wave vector of the probe is $\boldsymbol{k}_n = k_n\hat{r}$.

The appearance of $|\psi\rangle$ on the right-hand side of Eq. (5.86) motivates us to proceed in the first Born approximation. Replacing $|\psi\rangle$ with $|\phi\rangle$ simplifies the many-body matrix element of the interaction potential. The matrix element that we must evaluate reduces to

$$\langle \boldsymbol{k}_n, n\,|V|\,\psi\rangle \approx \sum_{\boldsymbol{k}_0} a_{\boldsymbol{k}_0}\,\langle \boldsymbol{k}_n, n\,|V|\,\boldsymbol{k}_0, n_0\rangle\,. \tag{5.88}$$

Whereas a probe initially in a plane wave state would require that we evaluate a single matrix element of the form, $\langle \boldsymbol{k}_n, n\,|V|\,\boldsymbol{k}_0, n_0\rangle$, we must now retain a collection of these corresponding to the various plane waves we superposed to obtain a focused probe. $V(\boldsymbol{r})$, the pair interaction between the projectile and a target at a separation $\boldsymbol{r}$, is $V(\boldsymbol{r}) = \frac{2\pi\hbar^2}{m}a_s\,\delta(\boldsymbol{r})$, with scattering length, a_s. Expanding the matrix element gives,

$$\langle \boldsymbol{k}_n, n\,|V|\,\boldsymbol{k}_0, n_0\rangle = \frac{2\pi\hbar^2}{(2\pi)^3 m}a_s\left\langle n\left|\sum_{j=1}^{N} e^{i(\boldsymbol{k}_0-\boldsymbol{k}_n)\cdot\hat{\boldsymbol{r}}_j}\right|n_0\right\rangle, \tag{5.89}$$

where N is the number of atoms in the lattice, and $\hat{\boldsymbol{r}}_j$ is the operator position of the j^{th} lattice atom. The sum over single body operators can be more conveniently expressed in second quantized notation, using the operator for the density, $\hat{n}(\boldsymbol{r})$, as we did in Sec. 5.5. Inserting the matrix element result given in Eq. (5.89) into Eq. (5.86) for the conditionally

scattered wave gives

$$\psi_n(\boldsymbol{r}) = \phi(\boldsymbol{r})\,\delta_{n_0,n} - a_s\frac{e^{ik_n r}}{r}\int d^3u\, e^{-i\boldsymbol{k}_n\cdot\boldsymbol{u}}\phi(\boldsymbol{u})\,\langle n\,|\hat{n}(\boldsymbol{u})|\,n_0\rangle\,. \tag{5.90}$$

In our discussion of the cross section, we considered an incident plane wave with wave vector, $\boldsymbol{k}_0$. Inserting this choice for $\phi(\boldsymbol{u})$ in Eq. (5.90) recovers our earlier expression, given for a general potential in Eq. (5.35), for the conditionally scattered probe wave function. In the case of a plane wave, the probe extends over the entire lattice, and the density at all points in the lattice contributes to the structure of the scattered wave. By focusing the incident probe wave function, we see that only those regions of the lattice in which the probe is appreciable will contribute to the scattering.

Let us now consider the situation in which $\phi(\boldsymbol{u})$ is comprised of two separated arms and determine the interference that results between the scattered arms. We may calculate the interference pattern of the scattered probe wave function from the expression, $I(\boldsymbol{r}) = \langle\psi|r\rangle\,\langle r|\psi\rangle$, in which we ignore the state of the lattice. The amplitude of the probe at the position $\boldsymbol{r}$ is given by $\langle r|\psi\rangle = \sum_n \psi_n(\boldsymbol{r})\,|n\rangle$. The interference pattern is then given by,

$$I(\boldsymbol{r}) = \sum_n |\psi_n(\boldsymbol{r})|^2\,. \tag{5.91}$$

The scattered probe is comprised of an incident wave plus a scattered wave, $\psi_n(\boldsymbol{r}) = \phi(\boldsymbol{r})\,\delta_{n_0,n} + \psi^{(\mathrm{sc})}(\boldsymbol{r})$. The part of the interference due to the scattered wave will have a dependence on the density-density correlations in the lattice. The contribution of the scattered wave to the interference pattern is

$$\sum_n \left|\psi_n^{(sc)}(\boldsymbol{r})\right|^2 = \frac{a_s^2}{r^2}\int d^3r_1\, d^3r_2\,\langle n_0|\,\phi^*(\boldsymbol{r}_2)\hat{n}(\boldsymbol{r}_2)e^{i\hat{\boldsymbol{k}}\cdot(\boldsymbol{r}_2-\boldsymbol{r}_1)}\phi(\boldsymbol{r}_1)\hat{n}(\boldsymbol{r}_1)\,|n_0\rangle\,. \tag{5.92}$$

$\hat{\boldsymbol{k}}$ is an operator whose eigenstates are the eigenstates of the lattice, $\hat{\boldsymbol{k}}\,|n\rangle = \boldsymbol{k}_n\,|n\rangle$. In order to evaluate this expression, we must make a specific choice for the incident probe wave function. In order to clarify the dependence of the interference pattern on the density-density correlations, we will choose the extreme case in which the probe wave function is very narrowly focused at two points in the lattice, $\boldsymbol{R}_1$ and $\boldsymbol{R}_2$, separated by a distance,

$d = |\boldsymbol{R}_1 - \boldsymbol{R}_2|$. Formally, let us treat the probe as a delta function at these positions,

$$\phi(\boldsymbol{r}) = A\left(\delta(\boldsymbol{r} - \boldsymbol{R}_1) + \delta(\boldsymbol{r} - \boldsymbol{R}_2)\right), \tag{5.93}$$

where A represents the amplitude of the probe wave function at the intercept with the lattice. $\boldsymbol{R}_1$ and $\boldsymbol{R}_2$ are directed along the axis of the optical lattice. We may replace $\hat{\boldsymbol{k}}$ with $k_0\hat{r}$ when the energy transferred to the lattice is small compared to the incident energy of the probe. Designating the angle of scattering, θ, from the forward direction (perpendicular to the lattice), we see that $\boldsymbol{k}_0 \cdot (\boldsymbol{R}_2 - \boldsymbol{R}_1) = k_0 d \sin(\theta)$. As a consequence, the contribution to the interference pattern simplifies to

$$\sum_n \left|\psi_n^{(sc)}(\boldsymbol{r})\right|^2 = \frac{a_s^2 |A|^2}{r^2}\left(\left\langle \hat{n}(\boldsymbol{R}_1)^2\right\rangle + \left\langle \hat{n}(\boldsymbol{R}_2)^2\right\rangle + 2\cos(k_0 d\sin(\theta))\left\langle \hat{n}(\boldsymbol{R}_2)\hat{n}(\boldsymbol{R}_1)\right\rangle\right). \tag{5.94}$$

The expectation values are taken in the ground state. We find that there is an incoherent background given by the second moment of the density fluctuations at the points at which the probe strikes the lattice. A term oscillating in the angle of scattering also appears, whose amplitude is twice the density-density correlator between the points at which the probe strikes the lattice.

The expectation values in Eq. (5.94) can be evaluated deep in the Mott insulator and superfluid phases. The density is $\hat{n}(\boldsymbol{R}) = \hat{\psi}^\dagger(\boldsymbol{R})\hat{\psi}(\boldsymbol{R})$. A formal expansion of the field operator in terms of the on-site field operators gives, $\hat{\psi}(\boldsymbol{R}) = \sum_{\boldsymbol{R}'} \hat{a}_{\boldsymbol{R}'} w(\boldsymbol{R} - \boldsymbol{R}')$. Let us specifically consider the case when $\boldsymbol{R}$ is a lattice site and we are in a deep lattice, $V_0 \sim 15E_r$. The contribution to the sum will be dominated by the $\boldsymbol{R}' = \boldsymbol{R}$ term, so that $\hat{\psi}(\boldsymbol{R}) \approx w(0)\hat{a}_{\boldsymbol{R}}$. Then we may expand the second moment of the density as

$$\left\langle \hat{n}(\boldsymbol{R})^2\right\rangle \approx |w(0)|^4\left(\left\langle \hat{a}^\dagger_{\boldsymbol{R}}\hat{a}^\dagger_{\boldsymbol{R}}\hat{a}_{\boldsymbol{R}}\hat{a}_{\boldsymbol{R}}\right\rangle + \left\langle \hat{a}^\dagger_{\boldsymbol{R}}\hat{a}_{\boldsymbol{R}}\right\rangle\right). \tag{5.95}$$

The expectation values of the on-site lattice field operators are readily evaluated. A lattice with an average number of particles per site, $\bar{n}$, in the insulating phase has $\left\langle \hat{n}(\boldsymbol{R})^2\right\rangle_{\mathrm{MI}} \approx |w(0)|^4 \bar{n}^2$. In the superfluid phase, we find $\left\langle \hat{n}(\boldsymbol{R})^2\right\rangle_{\mathrm{SF}} \approx |w(0)|^4(\bar{n}^2 + \bar{n})$. The density-density correlator is given by $\langle \hat{n}(\boldsymbol{R}_2)\hat{n}(\boldsymbol{R}_1)\rangle = |w(0)|^4 \bar{n}^2$ in either case.

The oscillating cosine varies between one and negative one, giving a maximum and minimum value of the fringes in Eq (5.94). In terms of this maximum and minimum, the

visibility of the interference due to the scattered part of the wave is [19]

$$C = \frac{I_{\max} - I_{\min}}{I_{\max} + I_{\min}}. \tag{5.96}$$

Inserting our results for the number statistics in the ground state, we find $C = 1$ for the Mott insulator, and $C = \bar{n}^2/(\bar{n}^2 + \bar{n})$ for the superfluid. In the case of unit filling, the superfluid contrast is reduced by the number fluctuations to one-half. As the number of atoms per lattice site increases, and the number fluctuations become small compared to the average number of atoms per site, the contrast of the superfluid goes to one.

Bibliography

[1] Jörg Schmiedmayer, Michael S. Chapman, Christopher R. Ekstrom, Troy D. Hammond, Stefan Wehinger, and David E. Pritchard. Index of refraction of various gases for sodium matter waves. *Phys. Rev. Lett.*, 74(7):1043–1047, Feb 1995.

[2] Enrico Fermi. *Nuclear Physics*, pages 201–202. University of Chicago Press, 1950.

[3] Melvin Lax. Multiple scattering of waves. *Rev. Mod. Phys.*, 23(4):287–310, Oct 1951.

[4] D. Jaksch, C. Bruder, J.I. Cirac, C.W. Gardiner, and P. Zoller. Cold bosonic atoms in optical lattices. *Phys. Rev. Lett.*, 81(15):3108–3111, Oct 1998.

[5] Markus Greiner, Olaf Mandel, Tilman Esslinger, Theodor W. Hansch, and Immanuel Bloch. Quantum phase transition from a superfluid to a mott insulator in a gas of ultracold atoms. *Nature*, 415(6867):39–44, 2002.

[6] J. J. Sakurai. *Modern Quantum Mechanics*, pages 379–386. Addison-Wesley, 1994.

[7] Leslie L. Foldy. The multiple scattering of waves. i. general theory of isotropic scattering by randomly distributed scatterers. *Phys. Rev.*, 67(3-4):107–119, Feb 1945.

[8] Richard L. Liboff. *Introductory Quantum Mechanics*. Addison Wesley Longman, Inc., third edition, 1997.

[9] Eugen Merzbacher. *Quantum Mechanics*, page 524. John Wiley and Sons, Inc., 1998.

[10] Richard L. Liboff. *Introductory Quantum Mechanics*, page 853. Addison Wesley Longman, Inc., third edition, 1997.

[11] Marvin L. Goldberger and Kenneth M. Watson. *Collision Theory*, chapter 3. John Wiley and Sons, Inc., 1964.

[12] Marvin L. Goldberger and Kenneth M. Watson. *Collision Theory*, chapter 3, page 48. John Wiley and Sons, Inc., 1964.

[13] Marvin L. Goldberger and Kenneth M. Watson. *Collision Theory*, chapter 3, pages 78–79. John Wiley and Sons, Inc., 1964.

[14] Marvin L. Goldberger and Kenneth M. Watson. *Collision Theory*, chapter 3, page 81. John Wiley and Sons, Inc., 1964.

[15] J. J. Sakurai. *Modern Quantum Mechanics*, pages 424–426. Addison-Wesley, 1994.

[16] Marvin L. Goldberger and Kenneth M. Watson. *Collision Theory*, chapter 3, pages 255–259. John Wiley and Sons, Inc., 1964.

[17] K. Wódkiewicz. Fermi pseudopotential in arbitrary dimensions. *Phys. Rev. A*, 43(1):68–76, Jan 1991.

[18] J. Y. Vaishnav, J. D. Walls, M. Apratim, and E. J. Heller. Matter-wave scattering and guiding by atomic arrays. *Physical Review A (Atomic, Molecular, and Optical Physics)*, 76(1):013620, 2007.

[19] Michael S. Chapman, Troy D. Hammond, Alan Lenef, Jörg Schmiedmayer, Richard A. Rubenstein, Edward Smith, and David E. Pritchard. Photon scattering from atoms in an atom interferometer: Coherence lost and regained. *Phys. Rev. Lett.*, 75(21):3783–3787, Nov 1995.

[20] Troy D. Hammond, Michael S. Chapman, Alan Lenef, Jörg Schmiedmayer, Edward T. Smith, Richard A. Rubenstein, David A. Kokorowski, and David E. Pritchard. Matter-wave index of refraction, intertial sensing, and quantum decoherence in an atom interferometer. *Brazilian Journal of Physics*, 27(2):193–213, Jun 1997.

[21] Paul R. Berman, editor. *Atom Interferometry*. Academic Press, 1997.

[22] S. M. Tan and D. F. Walls. Loss of coherence in interferometry. *Phys. Rev. A*, 47(6):4663–4676, Jun 1993.

[23] Hermann Uys, John D. Perreault, and Alexander D. Cronin. Matter-wave decoherence due to a gas environment in an atom interferometer. *Physical Review Letters*, 95(15):150403, 2005.

[24] Robert C. Forrey, Li You, Vasili Kharchenko, and Alex Dalgarno. Index of refraction of noble gases for sodium matter waves. *Phys. Rev. A*, 54(3):2180–2184, Sep 1996.

[25] V. Kharchenko and A. Dalgarno. Refractive index for matter waves in ultracold gases. *Phys. Rev. A*, 63(2):023615, Jan 2001.

[26] David A. Kokorowski, Alexander D. Cronin, Tony D. Roberts, and David E. Pritchard. From single- to multiple-photon decoherence in an atom interferometer. *Phys. Rev. Lett.*, 86(11):2191–2195, Mar 2001.

[27] Klaus Hornberger, Stefan Uttenthaler, Björn Brezger, Lucia Hackermüller, Markus Arndt, and Anton Zeilinger. Collisional decoherence observed in matter wave interferometry. *Phys. Rev. Lett.*, 90(16):160401, Apr 2003.

[28] Max Tegmark. Apparent wave function collapse caused by scattering. *Foundations of Physics Letters*, 6(6):571–589, 1993.

[29] Klaus Hornberger. Master equation for a quantum particle in a gas. *Physical Review Letters*, 97(6):060601, 2006.

[30] Marvin L. Goldberger and Kenneth M. Watson. *Collision Theory*, chapter 3, pages 80–82. John Wiley and Sons, Inc., 1964.

[31] J. J. Sakurai. *Modern Quantum Mechanics*, page 389. Addison-Wesley, 1994.

[32] Robert C. Forrey, Vasili Kharchenko, and Alex Dalgarno. On the statistical averaging procedure for the refractive index of matter waves. *J. Phys. B.: At. Mol. Opt. Phys.*, 35:L261–L264, Jun 2002.

[33] Marvin L. Goldberger and Kenneth M. Watson. *Collision Theory*, chapter 3, page 74. John Wiley and Sons, Inc., 1964.

[34] Immanuel Bloch, Jean Dalibard, and Wilhelm Zwerger. Many-body physics with ultracold gases. *Reviews of Modern Physics*, 80(3):885, 2008.

[35] Markus Greiner. *Ultracold quantum gases in three-dimensional optical lattice potentials*. PhD thesis, Ludwig-Maximilians-Universität München, 2003.

[36] Neil W. Ashcroft and David N. Mermin. *Solid state physics*. Holt, Rinehart and Winston, 1976.

[37] Charles Kittel. *Introduction to solid state physics*. J. Wiley, eigth edition, 2005.

[38] Richard L. Liboff. *Introductory Quantum Mechanics*, pages 302–315. Addison Wesley Longman, Inc., third edition, 1997.

[39] Gregory H. Wannier. The structure of electronic excitation levels in insulating crystals. *Phys. Rev.*, 52(3):191–197, Aug 1937.

[40] W. Kohn. Analytic properties of bloch waves and wannier functions. *Phys. Rev.*, 115(4):809–821, Aug 1959.

[41] Lixin He and David Vanderbilt. Exponential decay properties of wannier functions and related quantities. *Phys. Rev. Lett.*, 86(23):5341–5344, Jun 2001.

[42] J. C. Slater. A soluble problem in energy bands. *Phys. Rev.*, 87(5):807–835, Sep 1952.

[43] Milton Abramowitz and Irene A. Stegun. *Handbook of Mathematical Functions*. Dover Publications, Inc., 1972.

[44] Yvan Castin and Jean Dalibard. Relative phase of two bose-einstein condensates. *Phys. Rev. A*, 55(6):4330–4337, Jun 1997.

[45] Simon Fölling, Fabrice Gerbier, Artur Widera, Olaf Mandel, Tatjana Gericke, and Immanuel Bloch. Spatial quantum noise interferometry in expanding ultracold atom clouds. *Nature*, 434:481, 2005.

[46] Robert Roth and Keith Burnett. Phase diagram of bosonic atoms in two-color superlattices. *Phys. Rev. A*, 68(2):023604, Aug 2003.

[47] R. Roth and K. Burnett. Superfluidity and interference pattern of ultracold bosons in optical lattices. *Phys. Rev. A*, 67(3):031602, Mar 2003.

[48] E. L. Pollock and D. M. Ceperley. Path-integral computation of superfluid densities. *Phys. Rev. B*, 36(16):8343–8352, Dec 1987.

[49] V.I. Yukalov. Cold bosons in optical lattices. *Laser Physics*, 19(1):1–110, 2009.

[50] Eugen Merzbacher. *Quantum Mechanics*. John Wiley and Sons, Inc., 1998.

[51] Léon Van Hove. Correlations in space and time and born approximation scattering in systems of interacting particles. *Phys. Rev.*, 95(1):249–262, July 1954.